การสังเคราะห์นาโนคอมโพสิทของพอลิเอทิลีนความหนาแน่นต่ำแบบโซ่ตรงกับไทเทเนีย
ด้วยตัวเร่งปฏิกิริยาเซอร์โคโนซีนโดยการพอลิเมอร์ไรเซชันแบบอินซิตูของเอทิลีนกับหนึ่งเฮกซีน

นายวทัญญ โอ้วประดิษฐ์

SYNTHESIS OF LINEAR LOW DENSITY POLYETHYLENE/TITANIA NANOCOMPOSITES
WITH ZIRCONOCENE CATALYST BY *IN SITU* POLYMERIZATION OF
ETHYLENE/1-HEXENE

Mr. Wathanyoo Owpradit

A Thesis Submitted in Partial Fulfillment of the Requirements

for the Degree of Master of Engineering Program in Chemical Engineering

Department of Chemical Engineering

Faculty of Engineering

Chulalongkorn University

Academic Year 2007

Thesis Title   SYNTHESIS OF LINEAR LOW DENSITY
                  POLYETHYLENE/TITANIA NANOCOMPOSITES WITH
                  ZIRCONOCENE CATALYST BY *IN SITU* POLYMERIZATION
                  OF ETHYLENE/1-HEXENE
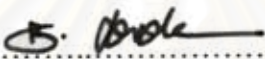
By   Mr. Wathanyoo Owpradit
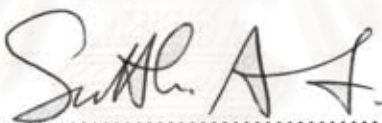Field of Study   Chemical Engineering
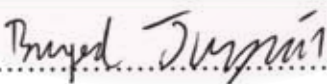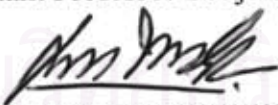Thesis Advisor   Assistant Professor Bunjerd Jongsomjit, Ph.D.

Accepted by the Faculty of Engineering, Chulalongkorn University in Partial
Fulfillment of the Requirements for the Master's Degree
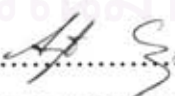
.... Dean of the Faculty of Engineering
(Associate Professor Boonsom Lerdhirunwong, Dr.Ing.)
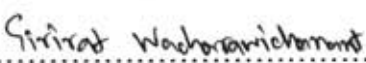
THESIS COMMITTEE

.... Chairman
(Associate Professor Suttichai Assabumrungrat, Ph.D.)

.... Thesis Advisor
(Assistant Professor Bunjerd Jongsomjit, Ph.D.)

.... Member
(Associate Professor ML. Supakanok Thongyai, Ph.D.)

.... Member
(Anongnat Somwangthanaroj, Ph.D.)

.... External Member
(Assistant Professor Sirirat Wacharawichanant, D.Eng.)

วทัญญู โอ้วประดิษฐ์ : การสังเคราะห์นาโนคอมโพสิทของพอลิเอทิลีนความหนาแน่นต่ำแบบ
โซ่ตรงกับไทเทเนียด้วยตัวเร่งปฏิกิริยาเซอร์โคโนซีนโดยการพอลิเมอร์ไรเซชันแบบอินซิตู
ของเอทิลีนกับหนึ่งเฮกซีน. (SYNTHESIS OF LINEAR LOW DENSITY
POLYETHYLENE/TITANIA NANOCOMPOSITES WITH ZIRCONOCENE
CATALYST BY *IN SITU* POLYMERIZATION OF ETHYLENE/1-HEXENE)
อาจารย์ที่ปรึกษา: ผศ. ดร. บรรเจิด จงสมจิตร, 97 หน้า.

เนื่องจากตัวเร่งปฏิกิริยาเมทัลโลซีนกำลังได้รับความสนใจในธุรกิจเชิงพาณิชย์สำหรับในการ
พอลิเมอร์ไรเซชันของโอเลฟิน จึงทำให้ตัวเร่งปฏิกิริยาเมทัลโลซีนถูกนำไปศึกษาอย่างแพร่หลายเพื่อ
ทำให้ตัวเร่งปฏิกิริยานี้มีประสิทธิภาพมากที่สุด ซึ่งเป็นที่รู้กันว่าพอลิเอทิลีนความหนาแน่นต่ำแบบโซ่
สามารถสังเคราะห์ได้จากการโคพอลิเมอร์เซชันของเอทิลีนกับหนึ่งโอเลฟินโดยใช้ตัวเร่งปฏิกิริยา
เมทัลโลซีน แต่ถึงอย่างไรก็ตามการสังเคราะห์พอลิเมอร์ชนิดดังกล่าวโดยตัวเร่งปฏิกิริยาเมทัลโลซีนใน
ระบบที่ไม่มีตัวรองรับยังคงมีข้อเสียอยู่ 2 ข้อ คือไม่สามารถควบคุมโครงสร้างสัณฐานของพอลิเมอร์ที่
ผลิตได้และเกิดสิ่งสกปรกติดที่เครื่องปฏิกรณ์ ดังนั้นตัวเร่งปฏิกิริยาในระบบที่มีตัวรองรับจึงถูก
นำมาใช้เพื่อแก้ไขปัญหาดังกล่าว พอลิเมอร์ที่ถูกเติมด้วยอนุภาคในระดับนาโนเมตรของสารอนินทรีย์
(หรือสารเติมแต่งในระดับนาโนเมตร) ถูกเรียกว่าพอลิเมอร์นาโนคอมโพสิท ซึ่งพอลิเมอร์นาโนคอม
โพสิทนี้สามารถผลิตได้จากการพอลิเมอร์ไรเซชันแบบอินซิตูด้วยการใส่สารเติมแต่งในระดับนาโนใน
ระหว่างการสังเคราะห์โดยใช้เป็นตัวรองรับของตัวเร่งปฏิกิริยา และผลของสารเติมแต่งในระดับนาโน
ที่ต่างชนิดกันทำให้สมบัติของพอลิเมอร์ที่ได้แตกต่างกันด้วย ซึ่งทั่วไปสารเติมแต่งที่นำมาใช้เพื่อศึกษา
ส่วนใหญ่ ได้แก่ ซิลิกา ไทเทเนีย อะลูมินา และเซอร์โคเนีย โดยในหลายวิธีการที่ถูกใช้เพื่อเตรียมพอลิ
เมอร์นาโนคอมโพสิท วิธีอินซิตูพอลิเมอร์ไรเซชันได้รับการยอมรับว่าเป็นวิธีการเตรียมพอลิเมอร์นา
โนคอมโพสิทที่ช่วยทำให้สารเติมแต่งในระดับนาโนเมตรที่ใส่ลงไปมีการกระจายตัวได้เป็นอย่างดี
ทั้งนี้เนื่องมาจากการเกิดพันธะกันโดยตรงระหว่างตัวเร่งปฏิกิริยากับพื้นผิวของสารเติมแต่งในระดับนา
โนเมตร ดังนั้นในระหว่างขั้นตอนการสังเคราะห์พอลิเมอร์ดังกล่าวจะต้องมีการตรึงตัวเร่งปฏิกิริยาที่ใช้
ไว้บนพื้นผิวของสารเติมแต่งในระดับนาโนเมตร ในการศึกษานี้จะสังเคราะห์พอลิเมอร์นาโนคอมโพ
สิทโดยวิธีอินซิตูพอลิเมอร์ไรเซชันโดยใช้เซอร์โคโนซีนเป็นตัวเร่งปฏิกิริยาและเมทิลอะลูมินอกเซน
เป็นตัวเร่งปฏิกิริยาร่วม ซึ่งสารเติมแต่งในระดับนาโนเมตรที่นำมาใช้คือไทเทเนียที่มีเฟสต่างกัน และ
อนุภาคในระดับนาโนเมตรที่ถูกนำมาใช้รวมทั้งพอลิเมอร์นาโนคอมโพสิทที่สังเคราะห์ได้จะถูกนำไป
ทดสอบสมบัติด้วยเทคนิคต่างๆ ต่อไป

ภาควิชา	วิศวกรรมเคมี	ลายมือชื่อนิสิต	
สาขาวิชา	วิศวกรรมเคมี	ลายมือชื่ออาจารย์ที่ปรึกษา	
ปีการศึกษา	2550		

4970543921: MAJOR CHEMICAL ENGINEERING
KEY WORD: ZIRCONOCENE CATALYST/TITANIA/LLDPE
/SUPPORTED CATALYST/POLYMER NANOCOMPOSITES

WATHANYOO OWPRADIT: SYNTHESIS OF LINEAR LOW DENSITY POLYETHYLENE/TITANIA NANOCOMPOSITES WITH ZIRCONOCENE CATALYST BY *IN SITU* POLYMERIZATION OF ETHYLENE/1-HEXENE. THESIS ADVISOR: ASST. PROF. BUNJERD JONGSOMJIT, Ph.D., 97 pp.

Because of the commercial interest of using metallocene catalysts for olefin polymerization, it has led to an extensive effort for utilizing metallocene catalysts more efficiently. It is known that linear low-density polyethylene (LLDPE) can be synthesized by copolymerization of ethylene and 1-olefins using metallocene catalysts. However, it was found that homogenization of metallocene has two major disadvantages; the lack of morphology control of polymers produced and reactor fouling. Therefore, heterogenization of metallocene was brought to solve these problems. Polymers filled with inorganic nanoparticles as nanofillers are recognized as polymer nanocomposites. It can be produced via the *in situ* polymerization with the presence of nanofillers added during synthesis by the application of supported metallocene catalysts. The effects of different nanofillers on the properties of polymers are different. The most commonly used nanofillers such as SiO_2, TiO_2, Al_2O_3, and ZrO_2 were studied. Among the methods to produce polymer nanocomposites, the *in situ* polymerization is perhaps the most promising method to produce LLDPE-nanocomposite with an exceptional dispersion of nanofillers throughout the polymer matrix. This is due to the direct linkage of active centers to the surface of nanoparticles. Therefore, it is necessary to immobilize the active centers onto nanofiller surface. In this present study, LLDPE/TiO_2 nanocomposites were synthesized by the *in situ* polymerization with dried modified methylaluminoxane (dMMAO)/zirconocene catalyst. The TiO_2 nanofillers having different phases were employed. All nanoparticles and the obtained LLDPE/TiO_2 nanocomposites were further characterized using various techniques.

Department	Chemical Engineering	Student's signature	Wathanyoo Owpradit
Field of study	Chemical Engineering	Advisor's signature	Bunjerd Jongsomjit
Academic Year	2007		

ACKNOWLEDGEMENTS

CONTENTS

LIST OF TABLES

LIST OF FIGURES

Figure   **Page**

Figure	**Page**

CHAPTER I

INTRODUCTION

The development of metallocene technologies has led to the synthesis of new polymers with different structures and properties to feed up the progressive demand of modern industry. According to the olefin polymerization, metallocences are crucial since they can control the properties of polyolefins. Metallocene catalysts are often used in the heterogeneous form based on the most existent technologies such as gas phase and slurry polymerization. Therefore, they are supported on an insoluble carrier prior to the polymerization. The reasons for the heterogenization of the metallocene are to slower the deactivation of the metallocene, employ less cocatalyst required, protect the reactor fouling, control the polymer morphologies and fulfil the requirements of the commercial polymerization processes [1-3]. It has been known that polyethylene such as linear low-density polyethylene (LLDPE) is obtained via the copolymerization of ethylene with various alpha olefins. They have grown in importance because of the specific properties that can be obtained by varying comonomer content and polymerization condition.

Recently, polymer nanocomposites have attracted a great deal of interest from material scientists since their applications have dramatically improved material properties in engineering plastics. These characteristics usually resulted from the synergistic effect arising from the addition of the nanofillers. Depending on the composition and microstructure, the effects of different nanoparticles on the properties of polymers are different. The most commonly used inorganic nanoparticles are SiO_2 [4-5], TiO_2 [6-8], Al_2O_3 [9], and ZrO_2 [10]. In addition, TiO_2 nanoparticles were used as fillers in order to produce new materials. Due to many interesting properties of TiO_2 such as anti-bacterial with photocatalysis technique (when exposed to light radiation, the pairs of electron-cavity are formed on TiO_2, and consequently the oxygen and water absorbed in the surface of TiO_2 are radicalized). Hydroxyl (OH) excited by light plays an important role in catalysis reaction. It attacks the microorganisms and makes them lose activity [7] and optical properties

(absorption of UV light up to the proximity of visible wavelengths, transparency at visible wavelengths, and very high refractive index) [6]. In general, polymer nanocomposites can be prepared by three methods, such as, i) a melt mixing [11-13], ii) a solution blending [14] and iii) *in situ* polymerization [15-17]. Due to the direct synthesis via polymerization along with the presence of fillers, the *in situ* polymerization is perhaps considered the most promising technique to produce polymer nanocomposites with homogeneous distribution of the nanoparticles inside the polymer matrix. Although LLDPE/TiO$_2$ nanocomposites have been investigated by some authors [6-7], only the melt mixing or solution blending processes were employed to synthesize those polymer samples.

This present work focused on the synthesis of LLDPE/TiO$_2$ nanocomposites by *in situ* polymerization of ethylene/1-hexene with zirconocene/dMMAO catalyst. The effects of the TiO$_2$ nanofillers having different phases such as, the anatase titania nanoparticles [TiO$_2$ (A)] and the rutile titania nanoparticles [TiO$_2$ (R)] employed along with different ratios of [Al]$_{dMMAO}$/[Zr]$_{cat}$ on the LLDPE/TiO$_2$ nanocomposites. And the various TiO$_2$ nanofillers were employed. In general, they had different phases and crystallite sizes. The catalytic activity and properties of polymer nanocomposites obtained were further investigated and discussed in more details.

1.1 The objectives of this thesis

1.1.1 To synthesize and characterize the LLDPE/TiO$_2$ nanocomposites obtained by *in situ* polymerization of ethylene/1-hexene using zirconocene/dMMAO catalyst.

1.1.2 To study effect of the TiO$_2$ nanofillers on properties of LLDPE/TiO$_2$ nanocomposites obtained.

1.2 The scopes of this thesis

1.2.1 Synthesize LLDPE/TiO$_2$ nanocomposites with *rac*-Et(Ind)$_2$ZrCl$_2$/dMMAO catalysts by *in situ* polymerization of ethylene/1-hexene.

1.2.2 Vary amounts and phases of the TiO$_2$ nanofillers.

1.2.3 Characterize the TiO$_2$ nanofillers and catalyst precursors with scanning electron microscopy (SEM), energy dispersive X-ray spectroscopy (EDX), X-ray diffraction (XRD), transmission electron microscopy (TEM) and thermal gravimetric analysis (TGA).

1.2.4 Characterize LLDPE/TiO$_2$ nanocomposites with scanning electron microscopy (SEM), energy dispersive X-ray spectroscopy (EDX), transmission electron microscopy (TEM), differential scanning calorimetry (DSC) and ^{13}C nuclear magnetic resonance spectrometer (^{13}C NMR).

CHAPTER II

LITERATURE REVIEW

2.1 Evolution of polyolefin catalysts

In 1953 Karl Ziegler, who succeeded in polymerizing ethylene into high-density polyethylene (HDPE) at standard pressure and room temperature, discovered of catalysts based on titanium trichloride and diethylaluminum chloride as cocatalyst, at the Max-Planck-Institute in Mulheim. A little later, Natta, at the Polytechnical Institute of Milan, was able to indicate that an appropriate catalyst system was capable of polymerizing propene into semi-crystalline polypropene. Ziegler and Natta shared a Nobel Prize for Chemistry in 1963 for their work [18]. With this so-called Ziegler-Natta catalyst.

Ziegler-Natta catalyst has been widely used in olefin polymerization; the coordination polymerization allows the catalyst geometry around the metal center to control the polymer structure. In homogeneous polymerization, the ligand of catalyst largely controls the geometry of an active metal center on which the polymerization reaction occurs. However, the conventional Ziegler-Natta catalysts the molecular structure of the polymers cannot be controlled well the molecular structure of the polymers because these catalysts have different nature types of catalytic sites.

In the last two decade Kaminsky and Sinn [19, 20] discovered the metallocene and other transition metal complexes activated by methylaluminoxane are highly active catalysts for the polymerization of olefin, diene, and styrene; they have proven to be a major breakthrough for the polyolefin industry. Contrast to Phillips and Ziegler-Natta catalysts that have been used already commercially to produce polyolefins, the metallocene catalysts are single site catalysts. Therefore, these catalysts produce a very uniform polymer, having a narrow molecular weight distribution (Mw/Mn = 2). Since the defined ligand sphere greatly influences the properties of the catalysts and that way the polymer, it is possible to tailor the ligand

environment according to need (their structure can be easily changed). The metallocence catalysts allow control of molecular weight, incorporation of comonomer, and in the case of polypropylene, the isotaticity and the amount of misinsertions [20]. Furthermore, they are soluble in hydrocarbons or liquid propene. In addition, their catalytic activity is 10-100 times higher than that of the classical Ziegler-Natta catalysts.

The evolution of the metallocene catalysts structures for olefin polymerization is shown in Table 2.1. [21]

Table 2.1 Timetable and historical development of metallocene research

1952	Development of the structure of metallocenes (ferrocene) by Fischer and Wilkinson
1955	Metallocene as component of Ziegler-Natta catalysts, low activity with common aluminum alkyls.
1973	Addition of small amount of water to increase the activity (Al:H_2O = 1:0.05 up to 1:0.3) (Reichert, Meyer and Breslow)
1975	Unusual increase in activity by adding water at the ratio Al:H_2O = 1:2 (Kaminsky, Sinn and Motweiler)
1977	Using separately prepared methylaluminoxane (MAO) as Cocatalyst for olefin polymerization. (Kaminsky and Sinn)
1982	Synthesis of *ansa* metalocenes with C_2 symmetry (Brintzinger)
1984	Polymerization of propylene using a *rac/meso* mixture of *ansa* titanocenes lead to partially isotactic polypropylene. (Ewen)
1984	Chiral ansa zirconocenes produce highly isotactic polypropylene (Kaminsky and Brintzinger)

Initially, it was found that using simple group 4 metallocenes like bis(cyclopentadienyl)titanium dichloride together with a cocatalyst like diethylaluminium chloride for the polymerization of ethylene lead to a catalyst system that showed initial fair activity which then rapidly decreased, due to factors like alkyl exchange reactions, hydrogen transfer and reduction of the transition metal species.

Reichart and Meyer [22] found a remarkable increase in activity (20-100 times better) by adding small amounts of water to the system $Cp_2TiCl_2/C_2H_5AlCl_2$. An enormous increase in activity was found in 1975 (up to 1 million times better) when water was added in a far greater amount, and, in 1977, when MAO was used with titanocenes and zirconocenes [23, 24]. Thereafter the next important step was using *ansa* metallocenes synthesized by Brintzinger *et al* in 1982 [25]. This allowed stereospecific polymerization of propylene. Ewen synthesized a C_s symmetric zirconocene ($[Me_2C(Flu)(Cp)]ZrCl_2$) in 1988 which allowed for the production of syndiotactic polypropylene in high quantities [26]. Since 1985, a rapid world-wide industrial and academic development began in the field of metallocene catalysts which continues today.

2.2 Metallocene catalysts

Metallocene catalysts are organometallic coordination compounds in which one or two π-carbocylic ligands such as cyclopentadienyl ring, substituted cyclopentadienyl ring, or derivative of cyclopentadienyl ring (such as fluorenyl, indenyl etc.) are chained to a metal central transition atom. The typical chemical structure of a metallocene catalyst is represented by Figure 2.1.
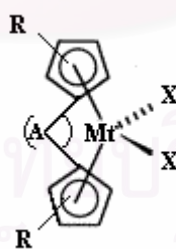
Figure 2.1 Typical chemical structure of a metallocene catalyst [27]

where Mt = Group 4, 5, or 6 transition metal (e.g. Zr, Ti or Hf)

        A = an optional bridging unit consisting of 1-3 atoms in the backbone

        R = hydrocarbyl substituents or fused ring systems (indenyl, fluorenyl and

           substituted derivatives)

        X = chlorine or other halogens from group 7 or an alkyl group

Single site catalysts can be separated into five main symmetry group, which influence on the polymer architectures as shown in Figure 2.2. It is assumed that the polymer rapidly equilibrates with the available coordination site for the purposes of assigning symmetry. Catalysts exhibiting C_{2v} symmetry typically produce atactic polymers or moderately stereoregular polymers by chain-end control mechanisms. C_s-symmetric catalysts that have mirror planes containing the two-diastereotopic coordination sites behave similarly. However, C_s-symmetric catalysts that have a mirror plane reflecting two enantiotopic coordination sites frequently produce syndiotactic polymers. C_2-symmetric complexes, both racemic mixtures and enantiomerically pure ones, typically produce isotactic polymers via a site-control mechanism. Stereoselectivities of asymmetric (C_1) complexes are unpredictable and have been reported to produce polymer architectures ranging from highly isotactic, to atactic, including isotactic-atactic stereoblock and hemiisotactic. Polymer architectures relevant to this modification of ligands are shown in Figure 2.3.
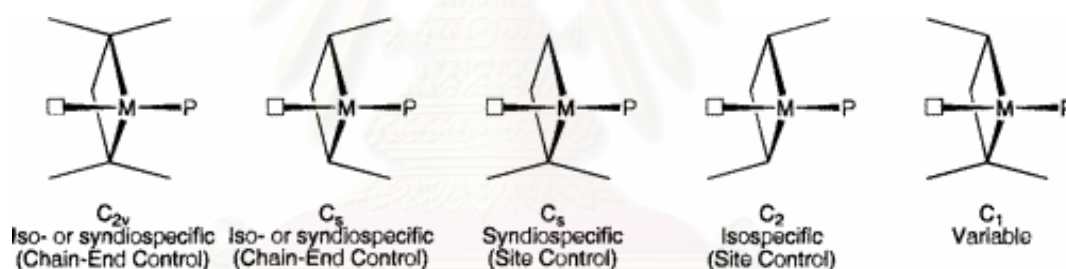
Figure 2.2 General symmetry classifications, based on ligand geometries, of catalysts and their stereoselectivities for polyolefin synthesis [28]
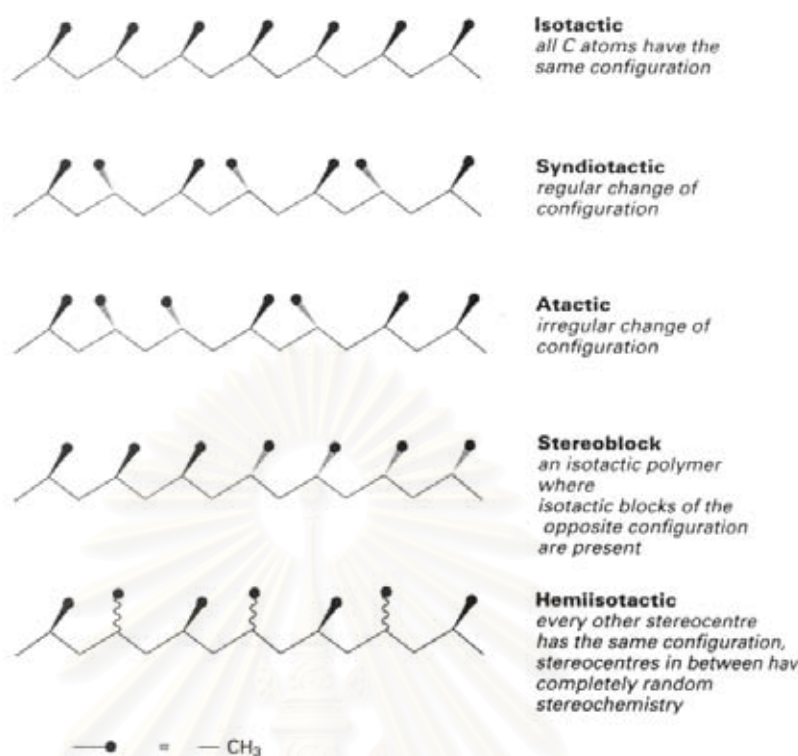
Figure 2.3 Different types of polymer tacticity [29]

Representative examples of each category of metallocenes and some of zirconocene catalysts are shown in Table 2.2 and Figure 2.4, respectively.

Table 2.2 Representative examples of metallocenes [30]

Category of Metallocenes	Metallocene Catalysts
[A] Nonstereorigid metallocenes	1) Cp_2MCl_2 (M = Ti, Zr, Hf) 2) Cp_2ZrR_2 (M = Me, Ph, CH_2Ph, CH_2SiMe_3) 3) $(Ind)_2ZrMe_2$
[B] Nonstereorigid ring-substituted metallocenes	1) $(Me_5C_5)_2MCl_2$ (M = Ti, Zr, Hf) 2) $(Me_3SiCp)_2ZrCl_2$
[C] Stereorigid metallocenes	1) $Et(Ind)_2ZrCl_2$ 2) $Et(Ind)_2ZrMe_2$ 3) $Et(IndH4)_2ZrCl_2$
[D] Cationic metallocenes	1) $Cp_2MR(L)+[BPh_4]^-$ (M = Ti, Zr) 2) $[Et(Ind)_2ZrMe]+[B(C_6F_5)4]^-$ 3) $[Cp_2ZrMe]+[(C_2B_9H_{11})_2M]^-$ (M = Co)
[E] Supported metallocenes	1) Al_2O_3-$Et(IndH_4)_2ZrCl_2$ 2) $MgCl_2$-Cp_2ZrCl_2 3) SiO_2-$Et(Ind)_2ZrCl_2$
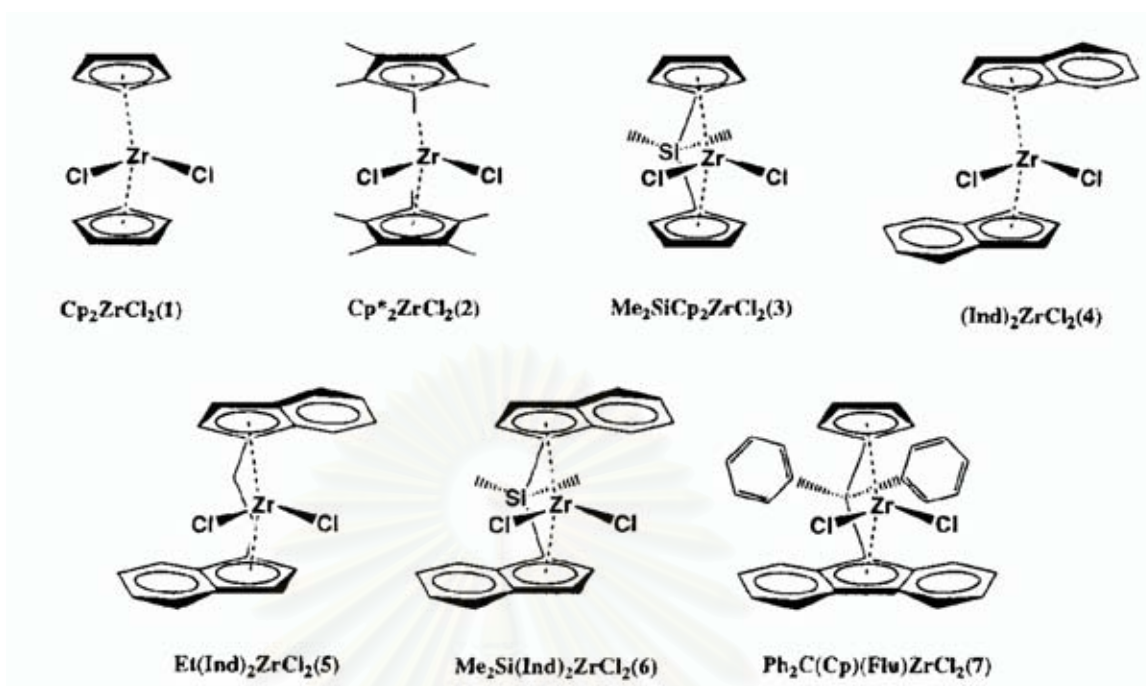
Figure 2.4 Some of zirconocene catalysts structure [31]

2.3 Cocatalysts or activators

The metallocene catalysts took their road success only after the right cocatalysts had been developed. Aluminoxane, especially methylaluminoxane (MAO) plays the very important role to activate the metallocene catalysts. Before the MAO was discovered, in Ziegler-Natta catalyst alkylaluminumchloride was used to activate Cp_2TiCl_2 but it exhibited the very low activity. Using of MAO as cocatalyst can promote the productivity of polymerization by several order of magnitude. Otherwise using of MAO, the other aluminoxanes such as ethylaluminoxane (EAO) or isobuthylaluminoxane (iBAO) or modified methylaluminoxane was employed to use as cocatalyst too. (Structure of MAO, EAO, iBAO and MMAO was shown in Figure 2.5).

$$\underline{\hspace{1cm}}(\!\!-\text{Al}\underline{\hspace{0.3cm}}\text{O}\underline{\hspace{0.3cm}})_n\underline{\hspace{1cm}}$$
$$|$$
$$\textbf{Me}$$

MAO

$$\underline{\hspace{1cm}}(\!\!-\text{Al}\underline{\hspace{0.3cm}}\text{O}\underline{\hspace{0.3cm}})_n\underline{\hspace{1cm}}$$
$$|$$
$$\textbf{Et}$$

EAO

$$\underline{\hspace{1cm}}(\!\!-\text{Al}\underline{\hspace{0.3cm}}\text{O}\underline{\hspace{0.3cm}})_n\underline{\hspace{1cm}}$$
$$|$$
$$\textbf{i-Bu}$$

iBAO

$$\underline{\hspace{1cm}}(\!\!-\text{Al}\underline{\hspace{0.3cm}}\text{O}\underline{\hspace{0.3cm}})_n(\text{Al}\underline{\hspace{0.3cm}}\text{O}\underline{\hspace{0.3cm}})_m\underline{\hspace{1cm}}$$
$$\hspace{2cm}|\hspace{3cm}|$$
$$\hspace{2cm}\textbf{Me}\hspace{2.5cm}\textbf{i-Bu}$$

MMAO
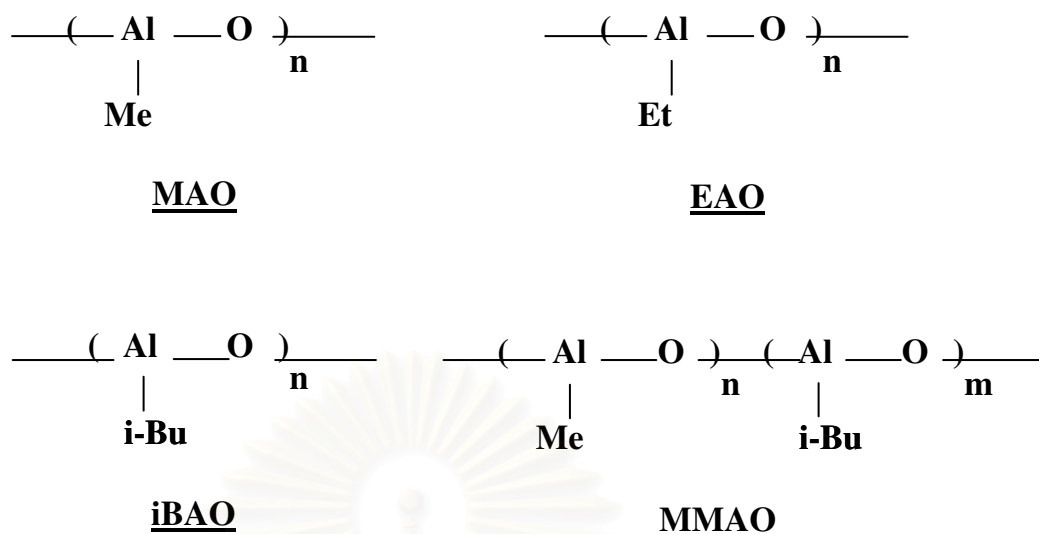
Figure 2.5 Several kinds of MAO

A metallocene catalyst precursor can be activated with organoalumoxanes, especially methylaluminoxane (MAO), which provides maximum activity. Methylaluminoxane is a compound in which aluminum and oxygen atoms are arranged alternately and free valances are saturated by methyl substitutions. It is prepared by carefully controlled partial hydrolysis of trimethylaluminum (TMA) and according to investigations [32]. The hydrolysis of AlR_3 (R = Me, Et, iBu) has been shown to proceed via the formation of an alkylaluminum water complex shown in Equation 1 [33], which subsequently eliminates an alkane to form a dialkylaluminum hydroxide complex. This rapidly associates to give dimers or larger oligomers in solution as shown in Equation 2.

$$AlR_3 + H_2O \longrightarrow AlR_3(H_2O) \tag{1}$$

$$AlR_3(H_2O) \longrightarrow 1/n \, [R_2Al(OH)]_n + RH \tag{2}$$
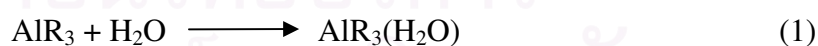
This new compound cannot be described as single molecule but as a mixture of chains and rings that consist of the repeating unit ($-O-Al(CH_3)-$) as shown in Figure 2.6.
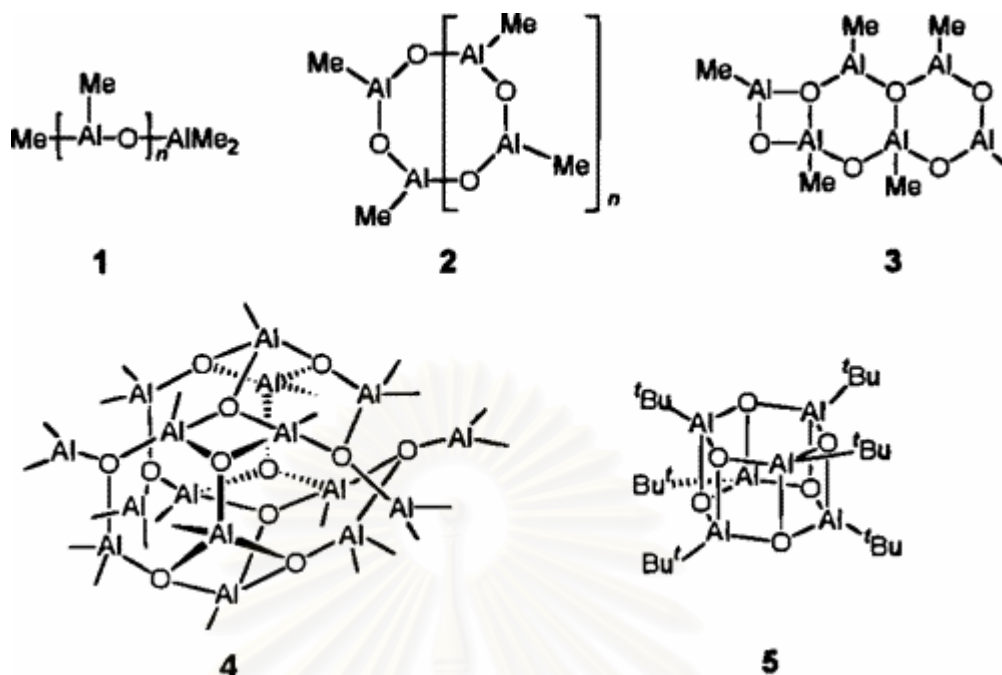
Figure 2.6 Include: (1) one-dimensional linear chains; (2) cyclic rings, which contain threecoordinate Al centers; (3) two-dimensional structures and (4) three dimensionalclusters is based on structural similarities with *tert*-butylaluminoxanes, which form isoluable and X-ray crystallographically characterizable cage structures

It is believed that MAO alkylates the metallocene and then abstracts one of methyl groups to generate the catalytically active species: a metallocenium cation (Equation 3.)

(3)
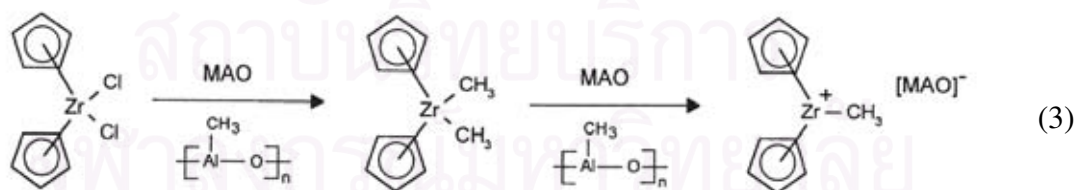
The balance of the three properties: as an alkylating agent for the generation of transition metal-alkyl adduct; as a Lewis acid for anion abstraction from the complex generating an electrophilic species; and as a scavenger for removal of impurities, particularly water in the olefin and solvent., made MAO a unique tool and a cocatalyst of choice in metallocene activation.

In the case of rac-Et(Ind)$_2$ZrMe$_2$ as precursor, the extracted methyl ligands do not yield any modification in the structure and reactivity of the MAO counter-anion, thus allowing zirconium coordination site available for olefin that presented in Figure 2.7 [34].

Figure 2.7 Representation of MAO showing the substitution of one bridging methyl group by X ligand extracted from racEt(Ind)$_2$ZrCl$_2$ (X = Cl, NMe$_2$, CH$_2$Ph) [34].

Cam and Giannini [35] investigated the role of TMA present in MAO by a direct analysis of Cp$_2$ZrCl$_2$/MAO solution in toluene-d$_8$ using ^{1}H-NMR. Their observation indicated that TMA might be the major alkylating agent and that MAO acted mainly as a polarization agent. However, in general it is believed that MAO is the key cocatalyst in polymerizations involving metallocene catalysts. The role of MAO included 1) alkylation of metallocene, thus forming catalyst active species, 2) scavenging impurities, 3) stabilizing the cationic center by ion-pair interaction and 4) preventing bimetallic deactivation of the active species.

The homogeneous metallocene catalyst cannot be activated by common trialkylaluminum only. However, Soga *et al*. [36] were able to produce polyethylene with modified homogeneous Cp$_2$ZrCl$_2$ activated by common trialkylaluminum in the presence of Si(CH$_3$)$_3$OH. Their results show that for an "optimum" yield aging of the catalyst and Si(CH$_3$)$_3$OH mixture for four hours is required. However, MWD of the produced polymers is bimodal although the polymers obtained in the presence of MAO have narrow MWD.

Ethylene/α-olefins copolymers with bimodal CCD were produced with homogeneous Cp_2ZrCl_2 with different cocatalysts such as MAO and mixture of TEA/borate or TIBA/borate [37]. It seemed that the active species generated with different cocatalysts have different activities and produce polymers with different molecular weights.

2.4 Polymerization mechanism

The mechanism of catalyst activation is not clearly understood. However, alkylation and reduction of the metal site by a cocatalyst (generally alkyl aluminum or alkyl aluminoxane) is believed to generate the cationic active catalyst species.

First, in the polymerization, the initial mechanism started with formation of cationic species catalyst that is shown below.

Initiation

$$Et(Ind)_2ZrCl_2 + Al(CH_3)_3 \longrightarrow Et(Ind)_2ZrClMe + Al(CH_3)_2Cl$$
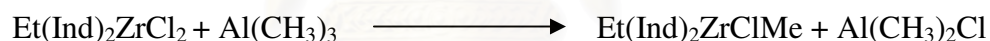
Propagation proceeds by coordination and insertion of new monomer unit in the metal carbon bond. Cossee mechanism is still one of the most generally accepted polymerization mechanism (Figure 2.8) [38]. In the first step, monomer forms a complex with the vacant coordination site at the active catalyst center. Then through a four-centered transition state, bond between monomer and metal center and between monomer and polymer chain are formed, increasing the length of the polymer chain by one monomer unit and generating another vacant site.
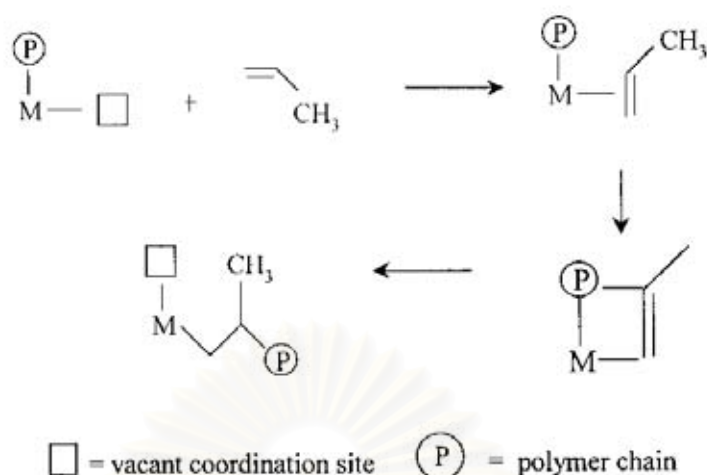
Figure 2.8 Cossee mechanism for Ziegler-Natta olefin polymerization [38].

The trigger mechanism has been proposed for the polymerization of α-olefin with Ziegler-Natta catalysts [39]. In this mechanism, two monomers interact with one active catalytic center in the transition state. A second monomer is required to form a new complex with the existing catalyst-monomer complex, thus trigger a chain propagation step. No vacant site is involved in this model. The trigger mechanism has been used to explain the rate enhancement effect observed when ethylene is copolymerized with α-olefins.
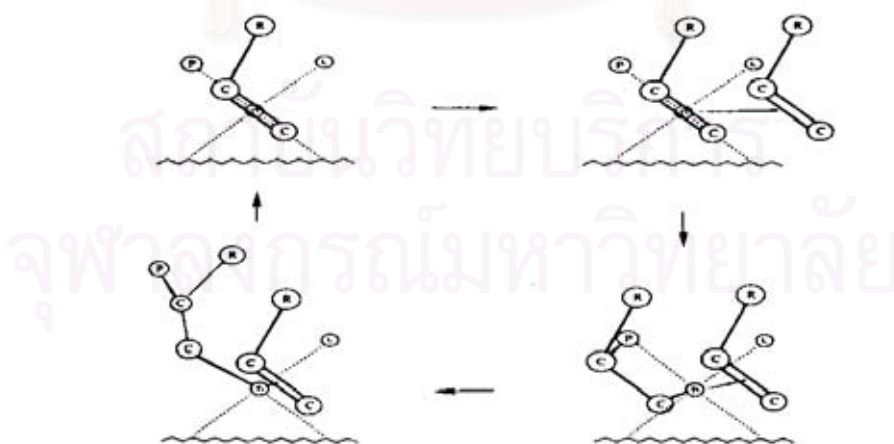
Figure 2.9 The propagation step according to the trigger mechanism [39].

After that, the propagation mechanism in polymerization shown in Figure 2.10.

Propagation

Figure 2.10 Propagation mechanism in polymerization

Finally, the termination of polymer chains can be formed by 1) chain transfer via β-H elimination, 2) chain transfer via β-Me elimination, 3) chain transfer to aluminum, 4) chain transfer to monomer, and 5) chain transfer to hydrogen (Figure 2.11-2.15) [40]. The first two transfer reactions form the polymer chains containing terminal double bonds.

Figure 2.11 Chain transfer via β-H elimination [40]

Figure 2.12 Chain transfer via β-CH$_3$ elimination [40]
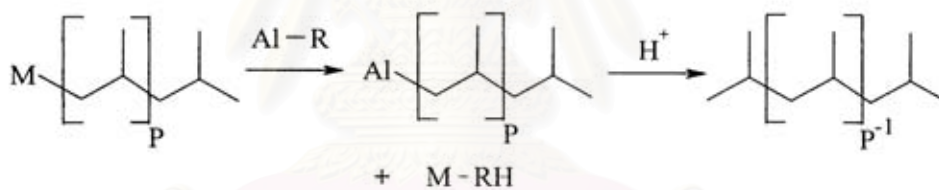
Figure 2.13 Chain transfer to aluminum [40]
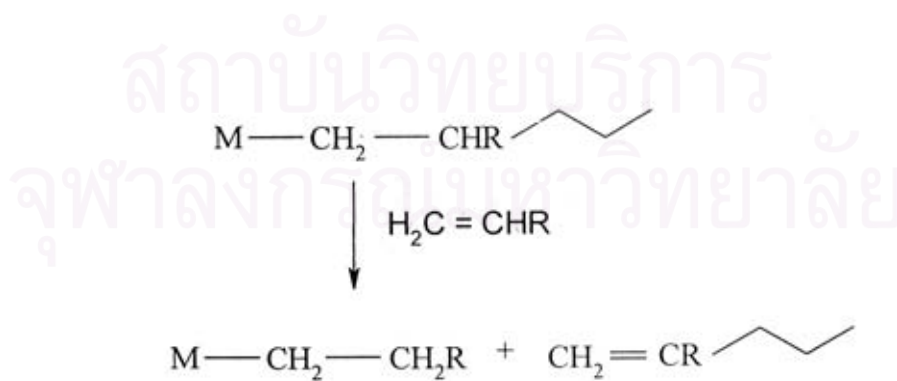
Figure 2.14 Chain transfer to monomer [40]
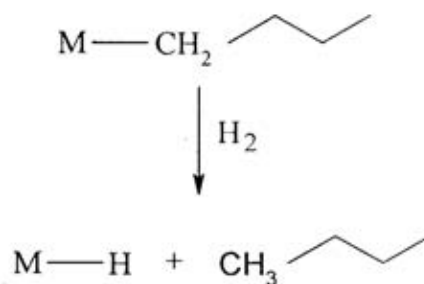
Figure 2.15 Chain transfer to hydrogen [40]

2.5 Catalyst activity

The ethylene polymerization rate of the copolymerization reaction with the catalyst system SiO_2/MAO/rac-Me_2Si [2-Me-4-Ph-lnd]$_2$ZrCl$_2$ was studied by Fink *et al.* [41]. The temperature was varied from 40 to 57°C. Small amount of hexene in the reaction solution increased the polymerization rate. The extent of the "comonomer effect" depended on the polymerization temperature. At 57°C the maximum activity of the ethylene/hexene copolymerization was 8 times higher than the homopolymerization under the same conditions. At 40°C the highest reaction rate for the copolymerization is only 5 times higher than that for the ethylene homopolymerization. For the polymer properties of the ethylene/α-olefin copolymerization, the molecular weights of the polymers decreased with increasing comonomer incorporation. Ethylene/hexene copolymers produced by a metallocene catalyst also have the same melting point and glass transition temperature.

Series of ethylene copolymerization with 1-hexene or 1-hexadecene over four different siloxy-substituted ansa-metallocene/methylaluminoxane (MAO) catalyst systems were studied by Seppala *et al.* [42]. Metallocene catalysts rac-Et[2-(t-BuMe$_2$SiO)Ind]$_2$ZrCl$_2$ (1), rac-Et[1-(t-BuMe$_2$SiO)Ind]$_2$ZrCl$_2$ (2), rac-Et[2-(i-Pr$_3$SiO)Ind]$_2$ZrCl$_2$ (3) and rac-Et[1-(i-Pr$_3$SiO)Ind]$_2$ZrCl$_2$ (4) were used. The effects of minor changes in the catalyst structure, more precisely changes in the ligand substitution pattern were studied. They found that series of polymerization with siloxy-substituted bis(indenyl) ansa-metallocene are highly active catalyst precursors

for ethylene-α-olefins copolymerizations. The comonomer response of all four catalyst precursors was good. Under the same conditions the order of copolymerization ability of the catalyst was rac- Et[2-(i-Pr$_3$SiO)Ind]$_2$ZrCl$_2$ > rac-Et[2-(t-BuMe$_2$SiO)Ind]$_2$ZrCl$_2$ and rac-Et[1-(i-Pr$_3$SiO)Ind]$_2$ZrCl$_2$ > rac-Et[1-(t-BuMe$_2$SiO)Ind]$_2$ZrCl$_2$. These catalysts are able to produce high molecular weight copolymers.

2.6 Copolymerization

By adding a small amount of comonomer to the polymerization reactor, the final polymer characteristics can be dramatically changed. For example, the Unipol process for linear low density polyethylene (LLDPE) uses hexene and the British Petroleum process (BP) uses 4-methylpentene to produce high-performance copolymers [43]. The comonomer can be affected the overall crystallinity, melting point, softening range, transparency and also structural, thermochemical, and rheological properties of the formed polymer. Copolymers can also be used to enhance mechanical properties by improving the miscibility in polymer blending [44].

Ethylene is copolymerized with α-olefin to produce polymers with lower densities. It is commonly observed that the addition of a comonomer generally increases the polymerization rate significantly. This comonomer effect is sometimes linked to the reduction of diffusion limitations by producing a lower crystallinity polymer or to the activation of catalytic sites by the comonomer. The polymer molecular weight often decreases with comonomer addition, possibly because of a transfer to comonomer reactions. Heterogeneous polymerization tends to be less sensitive to changes in the aluminum/transition metal ratio. Chain transfer to aluminum is also favored at high aluminum concentrations. This increase in chain transfer would presumably produce a lower molecular weight polymer. In addition, some researchers observed the decrease, and some observed no change in the molecular weight with increasing aluminum concentration [45].

The effect of polymerization conditions and molecular structure of the catalyst on ethylene/α-olefin copolymerization have been investigated extensively. Pietikainen

and Seppala [46] investigated the effect of polymerization temperature on catalyst activity and viscosity average molecular weights for low molecular weight ethylene/propylene copolymers produced with homogeneous Cp_2ZrCl_2. Soga and Kaminaka [47] compared copolymerizations (ethylene/propylene, ethylene/1-hexene, and propylene/l-hexene) with $Et(H_4Ind)_2ZrC1_2$ supported on SiO_2, Al_2O_3 or $MgCl_2$. Broadness of MWD was found to be related to the combination of support types and types of monomers. The effect of silica and magnesium supports on copolymerization characteristics was also investigated by Nowlin *et al.* [48]. Their results indicated that comonomer incorporation was significantly affected by the way that support was treated based on the reactivity ratio estimation calculated with simplified Finemann Ross method. However, it should be noted that Finemann Ross method could be misleading due to linear estimation of nonlinear system.

Copolymer based on ethylene with different incorporation of 1-hexene, 1-octene, and 1-decene were investigated by Quijada [49]. The type and the concentration of the comonomer in the feed do not have a strong influence on the catalytic activity of the system, but the presence of the comonomer increases the activity compared with that in the absence of it. From ^{13}C-NMR it was found that the size of the lateral chain influences the percentage of comonomer incorporated, 1-hexene being the highest one incorporated. The molecular weight of the copolymers obtained was found to be dependent on the comonomer concentration in the feed, showing that there is a transfer reaction with the comonomer. The polydispersity (Mw/Mn) of the copolymers is rather narrow and dependent on the concentration of the comonomer incorporation.

Soga et al. [50] noted that some metallocene catalysts produce two-different types of copolymers in terms of crystallinity. They copolymerized ethylene and 1-alkenes using 6 different catalysts such as Cp_2ZrCl_2, Cp_2TiCl_2, Cp_2HfCl_2, $Cp_2Zr(CH_3)_2$, $Et(Ind\ H_4)_2ZrCl_2$ and $i-Pr(Cp)(Flu)ZrCl_2$. Polymers with bimodal crystallinity distribution (as measured by TREF-GPC analysis) were produced with some catalytic systems. Only Cp_2TiCl_2-MAO and $Et(H_4Ind)_2ZrCl_2$-MAO produced polymers that have unimodal crystallinity distribution. The results seem to indicate that more than one active site types are present in some of these catalysts. However, it

is also possible that unsteady-state polymerization conditions might have caused the broad distributions since the polymerization times were very short (5 minutes for most cases).

Marques *et al.* [51] investigated copolymerization of ethylene and 1-octene by using the homogeneous catalyst system based on Et(Flu)$_2$ZrCl$_2$/MAO. A study was performed to compare this system with that of Cp$_2$ZrCl$_2$/MAO. The influence of different support materials for the Cp$_2$ZrCl$_2$ was also evaluated, using silica, MgCl$_2$, and the zeolite sodic mordenite NaM. The copolymer produced by the Et(Ind)$_2$ZrCl$_2$/MAO system showed higher molecular weight and narrower molecular weight distribution, compared with that produced by Cp$_2$ZrCl$_2$/MAO system. Because of the extremely congested environment of the fluorenyl rings surrounding the transition metal, which hinders the beta hydrogen interaction, and therefore, the chain transference. Moreover, the mostactive catalyst was the one supported on SiO$_2$, whereas the zeolite sodic mordenite support resulted in a catalyst that produced copolymer with higher molecular weight and narrower molecular weight distribution. Both homogeneous catalytic systems showed the comonomer effect, considering that a significant increase was observed in the activity with the addition of a larger comonomer in the reaction medium.

The effect of different catalyst support treatments in the 1-hexene/ethylene copolymerization with supported metallocene catalyst was investigated by Soares *et al.* [52]. The catalysts in the study were supported catalysts containing SiO$_2$, commercial MAO supported on silica (SMAO) and MAO pretreated silica(MAO/silica) with Cp$_2$HfCl$_2$, Et(Ind)$_2$HfCl$_2$, Cp$_2$ZrCl$_2$ and Et(Ind)$_2$ZrCl$_2$. All the investigated supported catalysts showed good activities for the ethylene polymerization (400-3000 kgpolymer/mol metal.h). Non-bridged catalysts tend to produce polymers with higher molecular weight when supported on to SMAO and narrow polydispersity. The polymer produced with Cp$_2$HfCl$_2$ supported on silica has only a single low crystallinity peak. On the other hand, Cp$_2$HfCl$_2$ supported on SMAO and MAO/silica produced ethylene/1-hexene copolymers having bimodal CCDs. For the case of Cp$_2$ZrCl$_2$ and Et(Ind)$_2$ZrCl$_2$, only unimodal CCDs were

obtained. It seems that silica-MAO-metallocene and silicametallocene site differ slightly in their ability to incorporate comonomer into the growing polymer chain, but not enough to form bimodals CCDs.

Soares *et al.* [53] studied copolymerization of ethylene and 1-hexene. It was carried out with different catalyst systems (homogeneous $Et(Ind)_2ZrCl_2$, supported $Et(Ind)_2ZrCl_2$ and in-situ supported $Et(Ind)_2ZrCl_2$). Supported $Et(Ind)_2ZrCl_2$: an $Et(Ind)_2ZrCl_2$ solution was supported on SMAO. It was used for polymerization of ethylene and 1-hexene. In-situ supported $Et(Ind)_2ZrCl_2$: an $Et(Ind)_2ZrCl_2$ solution was directly added to SMAO in the polymerization reactor, in the absence of soluble MAO. Homogeneous $Et(Ind)_2ZrCl_2$ showed higher catalytic activity than the corresponding supported and in-situ supported metallocene catalysts. The relative reactivity of 1-hexene increased in the following order: supported metallocene ≈ in situ supported metallocene < homogeneous metallocene catalysts. The MWD and short chain branching distribution (SCBD) of the copolymer made with the in-situ supported metallocene were broader than those made with homogeneous and supported metallocene catalysts. They concluded that there are at least two different active species on the in-situ supported metallocene catalyst for the copolymerization of ethylene and 1-hexene.

Soares *et al.* [54] investigated copolymerization of ethylene and 1-hexene with different catalysts: homogeneous $Et(Ind)_2ZrCl_2$, Cp_2HfCl_2 an $[(C_5Me_4)SiMe_2N(tert-Bu)]TiCl_2$, the corresponding in-situ supported metallocene and combined in-situ supported metallocene catalyst (mixture of $Et(Ind)_2ZrCl_2$ and Cp_2HfCl_2 and mixture of $[(C_5Me_4)SiMe_2N(tert-Bu)]TiCl_2$. They studied properties of copolymers by using ^{13}C NMR, gel permeation chromatography (GPC) and crystallization analysis fractionation (CRYSTAF) and compared with the corresponding homogeneous metallocene. The in-situ supported metallocene produced polymers having different 1-hexene fractions, SCBD and MDW. It was also demonstrated that polymers with broader MWD and SCBD can be produced by combining two different in-situ supported metallocenes.

In addition, Soares *et al.* [55] studied copolymerization of ethylene and 1-hexene with an in-situ supported metallocene catalysts. Copolymer was produced with alkylaluminum activator and effect on MWD and SCBD was examined. They found that TMA exhibited the highest activity while TEA and TIBA had significantly lower activities. Molecular weight distributions of copolymers produced by using the different activator types were unimodal and narrow, however, short chain branching distributions were very different. Each activator exhibited unique comonomer incorporation characteristics that can produce bimodal SCBD with the use of a single activator. They used individual and mixed activator system for controlling the SCBDs of the resulting copolymers while maintaining narrow MWDs.

2.7 Heterogenous metallocene catalysts

The development of metallocene technologies has led to the synthesis of new polymers with different structures and properties to feed up the progressive demand of modern industry. According to the olefin polymerization, metallocences are crucial since they can control the properties of polyolefins. Metallocene catalysts are often used in the heterogeneous form based on the most existent technologies such as gas phase and slurry polymerization. Therefore, they are supported on an insoluble carrier prior to the polymerization. The reasons for the heterogenization of the metallocene are to slower the deactivation of the metallocene, employ less cocatalyst required, protect the reactor fouling, control the polymer morphologies and fulfil the requirements of the commercial polymerization processes [2-3].

2.7.1 Supported metallocene catalysts method [2]

The main preparatory routes reported in the literature for metallocene immobilization on these supports can be classified according to three main methodologies, as follows:

1. The first method involves direct impregnation of metallocene on the support (modified by previous treatment or not). This can be done either (a) with mild

impregnation conditions or (b) at high temperatures and long impregnation times (refined route).

2. The second method involves immobilization of MAO on the support followed by reaction with the metallocene compound. A modified version of this method involves the replacement of MAO by an aluminum alkyl.

3. The third method involves immobilization of aryl ligands on the support followed by addition of a metal salt such as zirconium halide; recently, titanium and neodymium halides have also been used to form the attached metallocene.

Method 1 involves physical mixing of metallocene and support, and it was one of the first preparatory routes used. In this method, the dry support is reacted first with the metallocene compound in a solvent such as toluene. The solid part is then recovered by filtration and washed with a hydrocarbon. The mixing temperature and the contact time are important parameters since they influence both the catalytic performances and the final properties of the polymer, as will be further discussed.

In 1991, Kaminaka and Soga used this impregnation method, at very mild conditions (room temperature and impregnation time) 10 min), to prepare and compare the performances of different supported systems. Later on, Kaminsky and Renner (1993) used a refined route (method 1b) for the preparation of silica-supported ansa-metallocene catalysts. This method involves direct reaction of metallocene with SiO_2 at high temperature (T = 70 °C) and for a long period of time (16 h). The traces of the remaining highly active homogeneous catalyst were carefully extracted from the solid catalyst, to prevent the formation of low-melting and low-molecular-weight polypropylene.

The second and third methods have been mostly used for the preparation of silica-supported metallocenes. Silica is one of the most frequently used carriers, since it leads to good morphological features for polymer particles.

In method 2, silica is first pretreated with a small amount of MAO under mild conditions (room temperature, 30 min). After filtration and washing with toluene, the

MAO-modified SiO_2 support is then mixed with the metallocene and treated as described in method 1. The supported zirconocenes obtained in this way can be activated by MAO [56-58] or by common alkylaluminum [59-61].

Method 3 deals with the synthesis of catalysts where metallocene ligands are chemically bonded to the support (mainly modified SiO_2). It involves four steps:

Step 1 is the modification of the silica surface by addition of compounds such as $SiCl_4$, $C_2H_2Br_4$, $SOCl_2$, or $MeSiCl_2$. Typical conditions are reaction in toluene at reflux for 48 h.

Step 2 is the reaction of modified SiO_2 with the lithium salt of the aryl derivatives to be immobilized (indenyllithium, cyclopentadienyllithium, fluorenyllithium, etc.). This step is generally achieved in THF at relatively low temperatures.

Step 3 is the treatment of the resulting aryl-grafted silica gel with a solution of butyllithium in hexane (at room temperature) to form new aryllithium derivatives.

Step 4 is the reaction of the latter system with zirconium, titanium [62] or neodymium [63] halides to yields supported metallocenes.

After each modification step, the silica is filtered and washed with large quantities of THF and finally evaporated to dryness under vacuum. These supported metallocenes can be used with either MAO or a common trialkylaluminum as the cocatalyst. A typical catalyst preparation according to this procedure, as well as the structure of the species formed.

2.8 Polymer/inorganic or/and organic nanocomposites

From the many previous study results, they reported that different composite systems can lead to very different results. One important observation is that composites with nano-sized inclusions generally have different properties than composites with larger scale inclusions [64]. The specific reasons why the polymer matrix composites with nano-sized reinforcement have different properties than composites with micron-sized reinforcement are not fully understood, but several theories have been introduced to explain some of the changes in material morphology

and behavior that are seen at the nano-scale. It is important to point out, however, that most of these theories were developed to explain particular results and, therefore, are not necessarily applicable to a large number of polymer nanocomposites.

Kontou and Niaounakis [4] studied thermo-mechanical properties of LLDPE/SiO$_2$ nanocomposites. Linear low-density polyethylene (LLDPE)/SiO$_2$ nanocomposites were prepared by two types of catalysts, one prepared by metallocene (mLLDPE) and the other by traditional Ziegler–Natta (zLLDPE) catalysts, and silica nanoparticles surface treated with dimethyldichlorosilane. The silica nanonparticles used have an average diameter of 16 nm., and their weight fraction varied from 2 up to 10%. The structure and thermal-mechanical features of the nanocomposites were characterized by scanning electron microscopy (SEM), differential scanning calorimetry (DSC), dynamic mechanical spectroscopy (DMA) as well as tensile tests. The effect of nanoparticles on crystallinity, and hence to the morphology of the materials was studied. The secondary transitions were also affected by the filler presence, while the tensile properties were reinforced with varying the nanoparticle weight fraction. The addition of the nanofillers brought up an increase in the elastic modulus and the tensile strength of mLLDPE accompanied by an unusual dramatic increase in the elongation at break. The same trend, although to a lesser extent, was observed for the zLLDPE/SiO$_2$ composites. The increment of the elastic modulus of the composites with increasing filler content was simulated with three micromechanical models developed in previous works. The model which assumes an effective interface between the matrix and the nanoparticles provided the best fitting with the experimental data of mLLDPE/SiO$_2$.

Cheng et al. [15] prepared SiO$_2$/polyacrylamide (PAM) composite via the polymerization of acrylamide in the presence of silica sol in water/hexane emulsion, and pure SiO$_2$ was also prepared without the use of acrylamide in the same way. Field emission scanning electron micrographs (FESEM) showed that PAM covered the silica nanoparticles to form SiO$_2$/PAM nanospheres, which loosely agglomerated to form SiO$_2$/PAM secondary particles, while SiO$_2$ secondary particles were made up of tightly agglomerated silica nanoparticles. Metallocene catalyst was then immobilized over SiO$_2$ and SiO$_2$/PAM respectively to prepare supported metallocene catalyst for

ethylene polymerization. Transmission electron micrographs (TEM) showed that support particles broke up to smaller particles and even nanoparticles in polyethylene (PE) matrix when the support particles were the fragile SiO_2/PAM secondary particles, which shows a novel way to prepare silica/polyacrylamide/polyethylene nanocomposite.

Li et al. [5] investigated nano-sized and micro-sized silica particles. The particles were used to support Cp_2ZrCl_2/MAO catalyst for ethylene polymerization. Nano-sized catalyst exhibited much better ethylene polymerization activity than micro-sized catalyst. At the optimum temperature of 60 $^{\circ}$C, nano-sized catalyst's activity was 4.35 times the micro-sized catalyst's activity, which was attributed to the large specific external surface area, the absence of internal diffusion resistance, and the better active site dispersion for the nano-sized catalyst. Polymers produced were characterized with SEM, XRD, DSC, and densimeter. SEM indicated that the resulting polymer morphology contained discrete tiny particles and thin long fiberous interlamellar links.

Kuo et al. [9] studied the poly(ether-ether-ketone) (PEEK) polymer filled with nano-sized silica or alumina measuring 15-30 nm to 2.5-10 wt.% are fabricated by vacuum hot press molding at 400 $^{\circ}$C. The resulting nanocomposites with 5-7.5 wt.% SiO_2 or Al_2O_3 nanoparticles exhibit the optimum improvement of hardness, elastic modulus, and tensile strength by 20-50%, with the sacrifice of tensile ductility. With no surface modification for the inorganic nanoparticles, the spatial distribution of the nanoparticles appears to be reasonably uniform. There seems no apparent chemical reaction or new phase formation between the nanoparticle and matrix interface. The crystallinity degree and thermal stability of the PEEK resin with the addition of nanoparticles are examined by X-ray diffraction, differential scanning calorimetry, and thermogravity analyzer, and it is found that a higher crystallinity fraction and degradation temperature would result in the composites as compared with the unfilled PEEK.

2.9 Polymer/Titania (TiO$_2$) nanocomposites

Although the high amount of nanocomposite researches have done, there still have the low amount of them dealing with the nano-sized titania were used as fillers. The adequately experimental made by some researches include here.

Nussbaumer et al. [6] prepared colloids of TiO$_2$, where rutile was the only crystal modification which could be detected, with ca. 2.5 nm. average particle diameter were synthesized by hydrolysis of TiCl$_4$ in acidic solutions. The as-prepared particles were incorporated in polymers such as poly(vinyl alcohol) (PVAL), partially hydrolyzed poly(vinyl acetate) (PVAC88), polyvinylpyrrolidone, and poly(4-vinylpyridine). Nanocomposites transparent in the visible range were obtained. The highest TiO$_2$ contents in such materials were achieved with PVAL and PVAC88, with TiO$_2$ contents of ca. 35 wt.% (i.e.10.5 vol.-%). In particular, the nanocomposites withTiO$_2$ contents above 24 wt.% acted as efficient UV filters for radiation up to ca. 360 nm. At very low TiO$_2$ contents, an absorption maximum of the embedded TiO$_2$ particles was observed at 225 nm. with an extinction coefficient of 140 000 cm^{-1} and a full width at half maximum of 45 nm., i.e. not only the absorption at the maximum at 225 nm. but also at the flank of this band contributed significantly to the broadband UV absorption in the nanocomposites at higher TiO$_2$ fractions. The incorporation of TiO$_2$ enhanced the refractive index of the nanocomposites: for instance a refractive index of 1.609 was measured for a nanocomposite comprising 10.5 vol.% TiO$_2$ in PVAL, compared with 1.521 for the pristine polymer.

Wang et al. [7] studied dispersion behavior of TiO$_2$ nanoparticles in LLDPE/LDPE/TiO$_2$ nanocomposites where TiO$_2$ was pre-dispersed in LDPE by melt compounding. The dispersion behavior of TiO$_2$ nanoparticles was investigated by field-emission scanning electron microscopy (FE-SEM). The rheology results show that the viscosity of LDPE/TiO$_2$ master batch is lower than that of LLDPE/LDPE composites. Energy dispersive x-ray spectrometer (EDS) composition distribution map indicates that TiO$_2$ nanoparticles were dispersed randomly in the master batch. Scanning electron microscopy (SEM) images show that LDPE/TiO$_2$ master batch is crushed into micron scale dispersed phases due to the shear stress during the blow-

forming process. Subsequently, TiO$_2$ nanoparticles in the dispersed phases are released into the ambient matrix and form a wide ring composed of monodispersed particles. The sizes of spherical crystals decrease due to the presence of TiO$_2$ nanoparticles in LLDPE/LDPE/TiO$_2$ nanocomposites. The transparency of LLDPE/LDPE/TiO$_2$ composite films decreases little compared to that of LLDPE/LDPE composite films.

Su et al. [65] prepared and characterized the TiO$_2$/polymer complex nanomaterial. It was successfully synthesized through a simple procedure and characterized by the methods of TEM, XRD, UV-Vis, IR, and XPS. Results showed that the TiO$_2$/P complex particles were nano-sized and the average size was about 30 nm. Treated at the same temperature, TiO$_2$ of the complex particles was crystalline and of Anatase while pure polymer (P) was amorphous. P was a conjugated polymer with active groups and was linked together with TiO$_2$ by Ti-O-C bond. Photocatalytic experiments showed that the nanoparticles had extremely high photocatalytic activity for the decolorizations of dyes MB and AO. The role of the polymer on the photocatalytic decolorization of dyes and other influence factors were also discussed.

Ma et al. [66] studied effect of titania nanoparticles on the morphology of LDPE. The role of TiO$_2$ nanoparticle surfaces in affecting the crystalline structure of LDPE has been investigated by varying the nanoparticle surface from hydrophilic (as-received) to less hydrophilic (dried) or more hydrophilic (polar silane treated). Differential scanning calorimetry (DSC) and wide-angle X-ray diffraction (WXRD) were used to determine the degree of crystallinity and crystalline structure. The impact of nanoparticle aggregates on the nanometer to micrometer organization of LDPE crystals was studied with atomic force microscopy (AFM) and small-angle light scattering (SALS). This characterization showed that the presence of the TiO$_2$ nanoparticles, with the various different surface conditions investigated, did not alter the degree of LDPE crystallinity, the unit cell dimensions, the average lamellar thickness, or the average spherulite size. However, the nanoparticles did affect the internal arrangement of intraspherulitic crystalline aggregates by decreasing the relative optic axis orientation of these crystals, usually referred to as internal spherulite disorder. The LDPE filled with the nanoparticles treated with a polar silane

(N-(2-aminoethyl) 3-aminopropyl-trimethoxysilane (AEAPS)) showed the highest internal spherulitic disorder and exhibited the most poorly developed spherulite structure. The combination of SALS with AFM has allowed a detailed characterization of the morphology of the semicrystalline polymer nanocomposites. Information on the internal organization of the spherulites, the size of the nanoparticle aggregates, and the location of the nanoparticle aggregates can be uniquely obtained when both techniques are used.

Liu et al. [67] investigated effect of nanoscale SiO_2 and TiO_2 as the fillers on the mechanical properties and aging behavior of LLDPE/LDPE blends. LLDPE was blended with LDPE at a fixed ratio (80 wt LLDPE and 20 wt %LDPE) and filled with nanoparticles of SiO_2 and TiO_2 at a ratio up to wt 5%, so as to develop the polymeric composites suitable to preparing the agricultural micro-irrigation pipes having good environmental adaptability. These compounds were blended using calcium stearate, polyethylene wax, and titanate coupling agent as the auxiliary dispersants, and ethylene-vinyl acetate copolymer (EVA) as the toughness improver. The LLDPE/LDPE composites filled with the nanoparticles were extruded and injected to prepare the composites specimens for the performance evaluations and micro-irrigation pipe field test. The mechanical properties, thermostability, and processibility of the injected composites were investigated. The effect of heating in an oven and irradiating by ultraviolet on the mechanical properties of the composites was explored. The environmental adaptability of the micro-irrigation pipes made of the filled LLDPE/LDPE composites was evaluated making use of long-term outdoor field test in northwest China where the arid and harsh natural conditions are of great concerns. It was found that the LLDPE/LDPE blend with the LLDPE mass fraction fixed as 80% showed balanced mechanical and thermal properties and flexibility, and was suitable to be used as the basic resin matrix. The incorporation of nano-TiO_2 contributed to effectively improving the resistance to heating and ultraviolet irradiation of the composites. The composite made from 91% basic resin matrix, 6% EVA, and 3% mixed nano-SiO_2 and TiO_2, showed balanced comprehensive properties. The micro-irrigation pipes made of this filled LLDPE/LDPE composite had good environmental adaptability and service behavior in a three-year field test and were suitable to be used in arid area.

Chau et al. [68] prepared acetic acid-modified TiO_2 nanoparticles by sol–gel synthesis method. The nanoparticles can be incorporated directly into the polymer matrix to form transparent high refractive index nanocomposite thin films. The result shows that increasing the titania content in the hybrid nanocomposite thin films can significantly increase the refractive index. Hybrid nanocomposite thin film with refractive index value of 2.38 had been prepared. All prepared films also exhibit excellent optical transparency in the visible region.

Nakayama et al. [69] studied novel of nanocomposite films of TiO_2 nanoparticles and hydrophobic polymers having polar groups, poly(bisphenol-A and epicholohydrin) or copolymer of styrene and maleic anhydride, with high refractive indices, high transparency, no color, solvent-resistance, good thermal stability, mechanical properties were prepared by incorporating surface-modified TiO_2 nanoparticles into polymer matrices. In the process of preparing colloidal solution of TiO_2 nanoparticles, severe aggregation of particles can be reduced by surface modification using carboxylic acids and long chain alkyl amines. These TiO_2 nanoparticles dispersed in solvent were found not to aggregate after mixing with polymer solutions. Transparent colorless free-standing films were obtained by drying a mixture of TiO_2 nanoparticles colloidal solution and polymer solution in vacuum. Transmission electronic microscopic studied of the films suggest that the TiO_2 nanoparticles of 3-6 nm in diameter were dispersed in polymer matrices while maintaining their original size. Thermogravimetric analysis results indicate that the nanocomposite film has good thermal stability and the weight fraction of observed TiO_2 nanoparticles in the film is in good accordance with that of theoretical calculations. The refractive index of nanocomposite films of TiO_2 and poly(bisphenol-A and epichlorohydrin) was in the range of 1.58-1.81 at 589 nm, which linearly increased with the content of TiO_2 nanoparticles from 0 to 80 wt%.

CHAPTER III

EXPERIMENTAL

Research Methodology

Research Methodology of flow diagram is shown in Figure 3.1.

All reactions were conducted under argon atmosphere using Schlenk techniques and glove box.

Part 1 **(TiO$_2$ different phases** **and ratios of [Al]$_{dMMAO}$/[Zr]$_{cat}$)**	**Part 2** **(TiO$_2$ different phases** **at same ratios of [Al]$_{dMMAO}$/[Zr]$_{cat}$)**
Vacuum heat TiO$_2$ (A) and TiO$_2$ (R) At 673 K, 6 h	Vacuum heat TiO$_2$ (A), TiO$_2$ (R) (from part 1), TiO$_2$ (J), and TiO$_2$ (D) At 673 K, 6 h

Preparation of dMMAO

Impregnation of dMMAO onto the TiO$_2$ nanofillers

Characterization of the TiO$_2$ nanofillers before and after impregnation with dMMAO using XRD, TGA, SEM/EDX and TEM	Characterization of the TiO$_2$ nanofillers before and after impregnation with dMMAO using XRD, TGA, SEM/EDX and TEM

Copolymerization of ethylene with 1-hexene reaction
At T = 343 K, [Al/Zr] = 1135, 2270 and 3405
[initiated copolymerization by introducing ethylene gas
(at 6 psi consumption and total pressure 50 psi)]

LLDPE/TiO$_2$ nanocomposites

Characterization of LLDPE/ TiO$_2$ nanocomposites using SEM/EDX, TEM, DSC and ^{13}C-NMR

Discussion and conclusion

Figure 3.1 Flow diagram of research methodology

Experimental Section

The experimental was divided into four major parts:

(i)   Chemicals and equipments,

(ii)   Impregnation procedure,

(iii)   Ethylene and 1-hexene copolymerization procedure,

(iv)   Characterization of filler before and after impregnation with dMMAO and polymer nanocomposites.

The details of the experiments are explained as follows

3.1 Chemicals and equipments

3.1.1 Chemicals

The chemicals used in these experiments are analytical grade, but only major materials are specified as follows:

1. Ethylene gas (99.96%) was devoted from National Petrochemical Co., Ltd., Thailand and used as received.

2. 1-Hexene (99+%) was purchased from Aldrich Chemical Company, Inc. and purified by distilling over sodium under argon atmosphere before use.

3. 1-Hexane (95%) was donated from Shell (Public) Company, Inc. and purified by distilling over sodium under argon atmosphere before use.

4. 1-Heptane ($\geq$ 97%) was purchased from Fluka Chemie A.G. Switzerland and purified by distilling over sodium under argon atmosphere before used.

5. Toluene was devoted from EXXON Chemical Ltd., Thailand. This solvent was dried over dehydrated $CaCl_2$ and distilled over sodium/benzophenone under argon atmosphere before use.

6. Modified Methylaluminoxane (MMAO) 1.86 M in hexane was donated from Tosoh Akso, Japan and used without further purification.

7. Trimethylaluminum (TMA) 2.0 M in toluene was supplied from Nippon aluminum Alkyls Ltd., Japan and used without further purification.

8. Rac-ethylenebis(indenyl)zirconiumn dichloride ($Et(Ind)_2ZrCl_2$) was suppleid from Aldrich Chemical Company, Inc. and used without further purification.

9. Titanium (IV) oxide nanopowder (100 % anatase, TiO_2 (A)) was purchased from Aldrich Chemical Company, Inc. was vacuum heated at 673 K for 6 h.

10. Titanium (IV) oxide nanopowder (100 % rutile, TiO_2 (R)) was purchased from Aldrich Chemical Company, Inc. was vacuum heated at 673 K for 6 h.

11. Titanium (IV) oxide nanopowder (80% anatase : 20% rutile, TiO_2 (J)) was obtained from Ishihara Sangyo, Japan was vacuum heated at 673 K for 6 h.

12. Titanium (IV) oxide nanopowder (90% anatase : 10% rutile, TiO_2 (D)) was obtained from Degussa was vacuum heated at 673 K for 6 h.

13. Hydrochloric acid (Fuming 36.7%) was supplied from Sigma and used as received.

14. Methanol (Commercial grade) was purchased from SR lab and used as received.

15. Sodium (99%) was purchased from Aldrich Chemical Company, Inc. and used as received.

16. Benzophenone (99%) was purchased from Fluka Chemie A.G. Switzerland and used as received.

17. Calciumhydride (99%) was purchased from Fluka Chemie A.G. Switzerland and used as received.

18. Ultra high purity argon gas (99.999%) was purchased from Thai Industrial Gas Co., Ltd., and further purified by passing through columns packed with molecular sieve 3A, BASF Catalyst R3-11G, sodium hydroxide (NaOH) and phosphorus pentaoxide (P_2O_5) to remove traces of oxygen and moisture.

3.1.2 Equipments

Due to the metallocene system is extremely sensitive to the oxygen and moisture. Thus, the special equipments were required to handle while the preparation and polymerization process. For example, glove box: equipped with the oxygen and moisture protection system was used to produce the inert atmosphere. Schlenk

techniques (Vacuum and Purge with inert gas) are the others set of the equipment used to handle air-sensitive product.

3.1.2.1 Cooling system

The cooling system was in the solvent distillation in order to condense the freshly evaporated solvent.

3.1.2.2 Inert gas supply

The inert gas (argon) was passed through columns of BASF catalyst R3-11G as oxygen scavenger, molecular sieve 3×10^{-10} m to remove moisture. The BASF catalyst was regenerated by treatment with hydrogen at 573 K overnight before flowing the argon gas through all the above columns. The inert gas supply system can be shown in Figure 3.2.

Figure 3.2 Inert gas supply system

3.1.2.3 Magnetic stirrer and heater

The magnetic stirrer and heater model RTC basis from IKA Labortechnik were used.

3.1.2.4 Reactor

The autoclave is made of stainless steel with a volume of 100 mL and 3 cm inside diameter. This autoclave was used as polymerization reactor.

3.1.2.5 Schlenk line

Schlenk line consists of vacuum and argon lines. The vacuum line was equipped with the solvent trap and vacuum pump, respectively. The argon line was connected with the trap and the mercury bubbler that was a manometer tube and contains enough mercury to provide a seal from the atmosphere when argon line was evacuated. The schlenk line was shown in Figure 3.3.
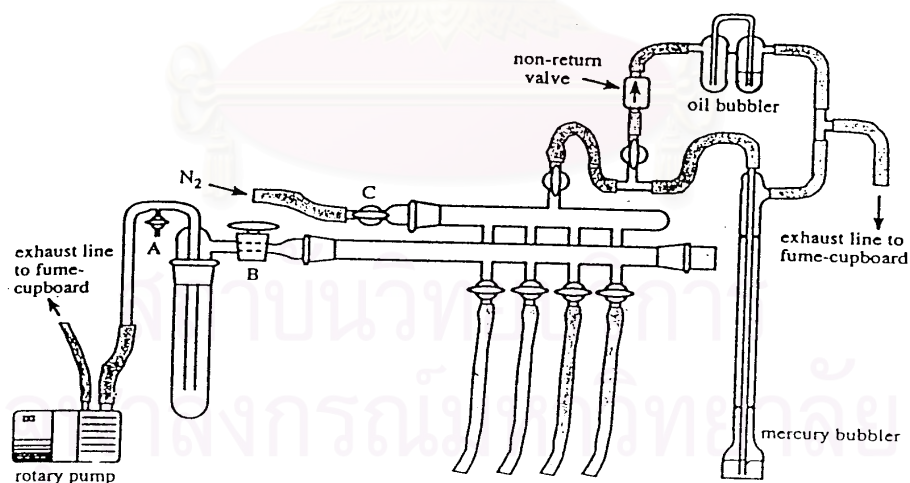
Figure 3.3 Schlenk line

3.1.2.6 Schlenk tube

A tube with a ground glass joint and side arm, which was three-way glass valve. Sizes of Schlenk tubes were 50, 100 and 200 mL used to prepare catalyst and store materials which are sensitive to oxygen and moisture. The Schlenk tube picture was shown in Figure 3.4.
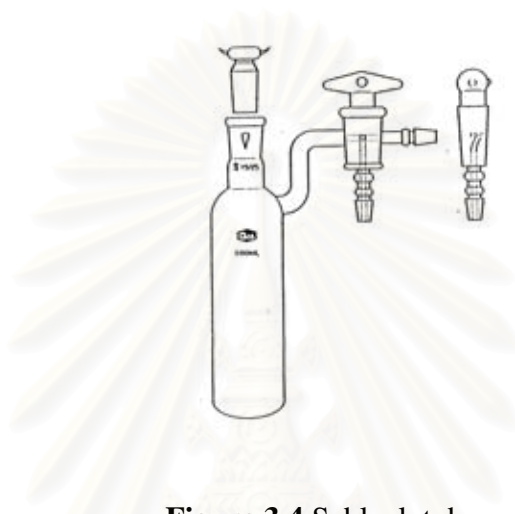
Figure 3.4 Schlenk tube

3.1.2.7 Vacuum pump

The vacuum pump model 195 from Labconco Corporation was used. A pressure of 10^{-1} to 10^{-3} mmHg was adequate for the vacuum supply to the vacuum line in the Schlenk line. The vacuum pump is shown in Figure 3.5.
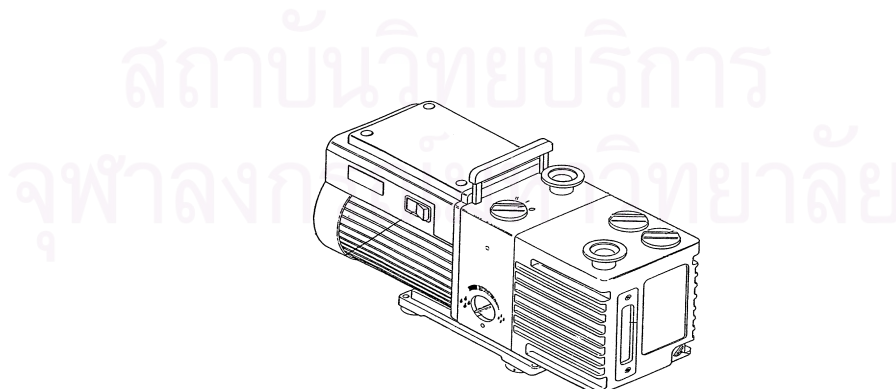
Figure 3.5 Vacuum pump

3.1.2.8 Polymerization line
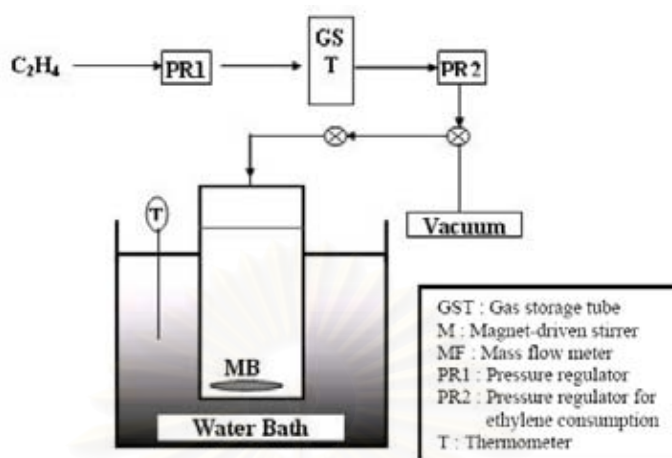
Figure 3.6 Diagram of system in slurry phase polymerization.

3.2 Impregnation procedure

3.2.1 Preparation of dried MMAO (dMMAO)

Removal of TMA from MMAO was carried out according to the reported procedure [70]. The toluene solution of MMAO was dried under vacuum for 6 h at room temperature to evaporate the solvent, TMA and TIBA. Then, continue to dissolve with 100 mL of heptane and the solution was evaporated under vacuum to remove the remaining TMA and TIBA. This procedure was repeated four times and the white powder of dried MMAO (dMMAO) was obtained.

3.2.2 Preparation of dMMAO impregnated on TiO₂ nanofillers (dMMAO/TiO₂)

The dMMAO (concentration of Al = 5.6 %wt, 1.00 g or 16.3 mmol) was impregnated on TiO$_2$ (1.30 g or 12.5 mmol) in 20 mL of toluene at room temperature. The mixture was stirred for 30 min. The solvent was then removed from the mixture by evacuated. This procedure was done only once with toluene (20 mL x 1) and three

times with hexane (20 mL x 3). Then, the solid part was evaporated and dried under vacuum at room temperature. The gray powder of dMMAO/TiO$_2$ was then obtained.

3.3 Polymerization reaction

The copolymerization of ethylene/1-hexene was carried out in a 100 mL semi-batch stainless steel autoclave reactor equipped with magnetic stirrer. In the glove box, the desired amount of *rac*-Et[Ind]$_2$ZrCl$_2$ and TMA was mixed and stirred for 5 min aging to affect alkylation of the zirconocene catalyst. Then, toluene (to make a total volume of 30 ml) and 0.2, 0.4, and 0.6 g of dMMAO/TiO$_2$ corresponding to the [Al]$_{dMMAO}$/[Zr]$_{cat}$ ratios of 1135, 2270, and 3405, respectively, were introduced into the reactor for each run. After that, the mixture of *rac*-Et[Ind]$_2$ZrCl$_2$ and TMA was injected into the reactor. The reactor was frozen in liquid nitrogen to stop reaction and then 0.018 mol of 1-hexene was injected into the reactor. The autoclave was evacuated to remove the argon. Then, the reactor was heated up to polymerization temperature (343 K) and the polymerization was started by feeding ethylene gas (total pressure 50 psi in the reactor) until the consumption of ethylene at 0.018 mol (decreased ethylene pressure of 6 psi was observed) was reached. The reaction of polymerization was terminated by addition of acidic methanol (0.1% HCl in methanol). The reaction time was recorded for purpose of calculating the activity. The precipitated polymer was washed with methanol and dried at room temperature.

3.4 Characterization procedures

3.4.1 Characterization of TiO$_2$ nanofillers

3.4.1.1 X-ray diffraction (XRD)

X-ray diffraction: XRD was performed to determine the bulk crystalline phases of samples. It was conducted using a SIEMEN D-5000 X-ray diffractometer with CuK$_\alpha$ (λ = 1.54439 Å). The spectra were scanned at a rate of 2.4 $^\circ$/min in the range 2θ = 10-80°.

3.4.1.2 Transmission electron microscopy (TEM)

Transmission electron microscopy: TEM was used to determine the shape and size of TiO_2 nanofillers. The sample was dispersed in ethanol before using TEM (JEOL JEM-2010) for microstructural characterization.

3.4.1.3 Thermal gravimetric analysis (TGA)

Thermal gravimetric analysis: TGA was performed using a TA Instruments SDT Q-600 analyzer. The samples of 10-20 mg and a temperature ramping from 298 to 873 K at 2 K/min were used in the operation. The carrier gas was N_2 UHP.

3.4.1.4 Scanning electron microscopy (SEM) and energy dispersive X-ray spectroscopy (EDX)

Scanning electron microscopy and energy dispersive X-ray spectroscopy: SEM and EDX were used to investigate the sample morphologies and elemental distribution throughout the nanofillers. The SEM of JEOL mode JSM-5800 LV scanning microscope was employed. EDX was further performed using Link Isis series 300 program.

3.4.2 Characterization of polymer

3.4.2.1 Scanning electron microscopy (SEM) and energy dispersive X-ray spectroscopy (EDX)

Scanning electron microscopy and energy dispersive X-ray spectroscopy: SEM and EDX were performed to study the morphologies of polymer and elemental distribution within polymer matrix. The same equipment as mentioned above was employed

3.4.2.2 Transmission electron microscopy (TEM)

Transmission electron microscopy: TEM was used to determine the dispersion of TiO_2 nanofillers in LLDPE. The same equipment as mentioned above was employed.

3.4.2.3 Differential scanning calorimetry (DSC)

Differential scanning calorimetry: the melting temperature of ethylene/1-hexene copolymer products was determined with a Perkin-Elmer diamond DSC. The analyses were performed at the heating rate of 10 K/min in the temperature range of 283-423 K. The heating cycle was run twice. In the first scan, sample was heated and cooled to 283 K. In the second scan, sample was reheated at the same rate, but only the result of the second scan was reported because the first scan was influenced by the mechanical and thermal history of sample.

3.4.2.4 Nuclear magnetic resonance (NMR)

^{13}C NMR spectroscopy: ^{13}C NMR spectroscopy was used to determine the 1-hexene incorporation and copolymer microstructure. Chemical shifts were referenced internally to the $CDCl_3$ and calculated according to the method described by Randall [71]. Each sample solution was prepared by dissolving 50 mg of copolymer in 1,2 dicholobenzene and $CDCl_3$. The ^{13}C NMR spectra were taken at 373 K using a BRUKER AVANCE II 400 operating at 100 MHz with an acquisition time of 1.5 s and delay time of 4 s.

CHAPTER IV

RESULTS AND DISCUSSIONS

In this present study, results and discussions were divided into two sections. In the first section, the investigate and characterize effects of the TiO_2 nanofillers having different phases and ratios of $[Al]_{dMMAO}/[Zr]_{cat}$ on the catalyst activity and properties of LLDPE/TiO_2 nanocomposites. And the second section, the study and characterize effect of different TiO_2 nanofillers when the $[Al]_{dMMAO}/[Zr]_{cat}$ ratio was fixed at 2270 on the catalyst activity and properties of LLDPE/TiO_2 nanocomposites. All fillers and dMMAO/fillers were also investigated to make better understanding about polymerization results.

4.1 Effects of the TiO_2 nanofillers having different phases and ratios of $[Al]_{dMMAO}/[Zr]_{cat}$ on the catalyst activity and properties of LLDPE/TiO_2 nanocomposites.

In this section, the synthesis of LLDPE/TiO_2 nanocomposites using the TiO_2 nanofillers having different phases [TiO_2 (A) and TiO_2 (R)] and ratios of $[Al]_{dMMAO}/[Zr]_{cat}$ = 1135, 2270, and 3405 with zirconocene/dMMAO catalyst was investigated.

4.1.1 Characterization of fillers and dMMAO/fillers with X-ray diffraction (XRD).

The XRD patterns of fillers and dMMAO/fillers are shown in Figure 4.1 indicating the characteristic peaks for the anatase form of TiO_2 (A) at 25° (major), 38°, 48°, 55°, and 63° and the rutile form of TiO_2 (R) at 27° (major), 36°, 41°, and 54°. Average crystallite sizes for both TiO_2 (A) and TiO_2 (R) was calculated from the major peaks obtained from XRD using Sherrer's equation. It was found that the average crystallite sizes of TiO_2 (A) and TiO_2 (R) were 6.1 and 6.9 nm, respectively. After impregnation with dMMAO the XRD patterns for both samples exhibited the

similar patterns. No peaks of dMMAO were detected. This was suggested that the dMMAO was in the highly dispersed form on the TiO_2 nanofillers.
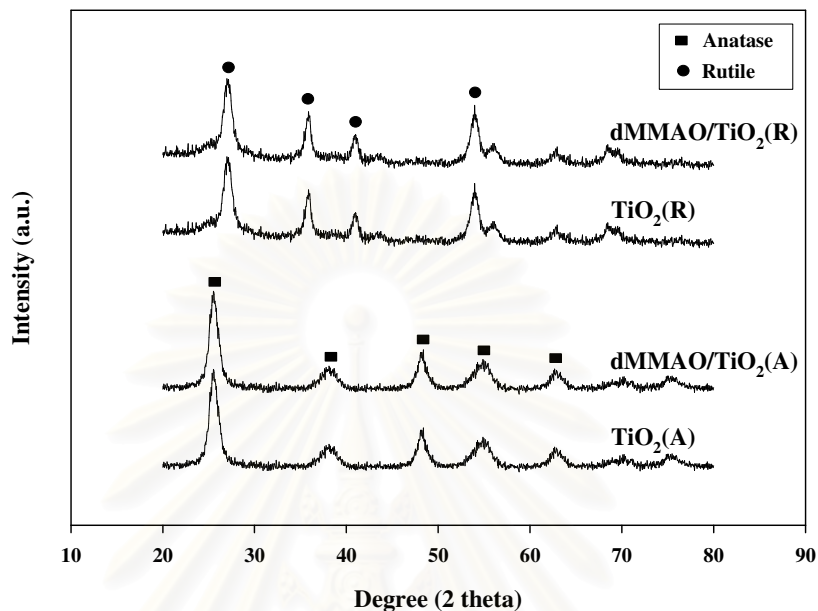
Figure 4.1 XRD patterns of different TiO_2 nanofillers before and after impregnation with dMMAO.

4.1.2 Characterization of dMMAO/fillers with Scanning electron microscopy (SEM) and energy dispersive X-ray spectroscopy (EDX).

The SEM micrographs and EDX mapping for the dMMAO/TiO_2 are shown in Figure 4.2. Both samples apparently exhibited the similar morphologies. It can be observed that the dMMAO was well distributed all over the TiO_2 granules as seen by the EDX mapping. Based on the EDX measurement, the amounts of $[Al]_{dMMAO}$ present on the TiO_2 samples can be determined. They were in the range of 12.5 and 10.2 wt% for TiO_2 (A) and TiO_2 (R), respectively. The larger amount of $[Al]_{dMMAO}$ present in the TiO_2 (A) can be attributed to larger surface area for the TiO_2 (A).
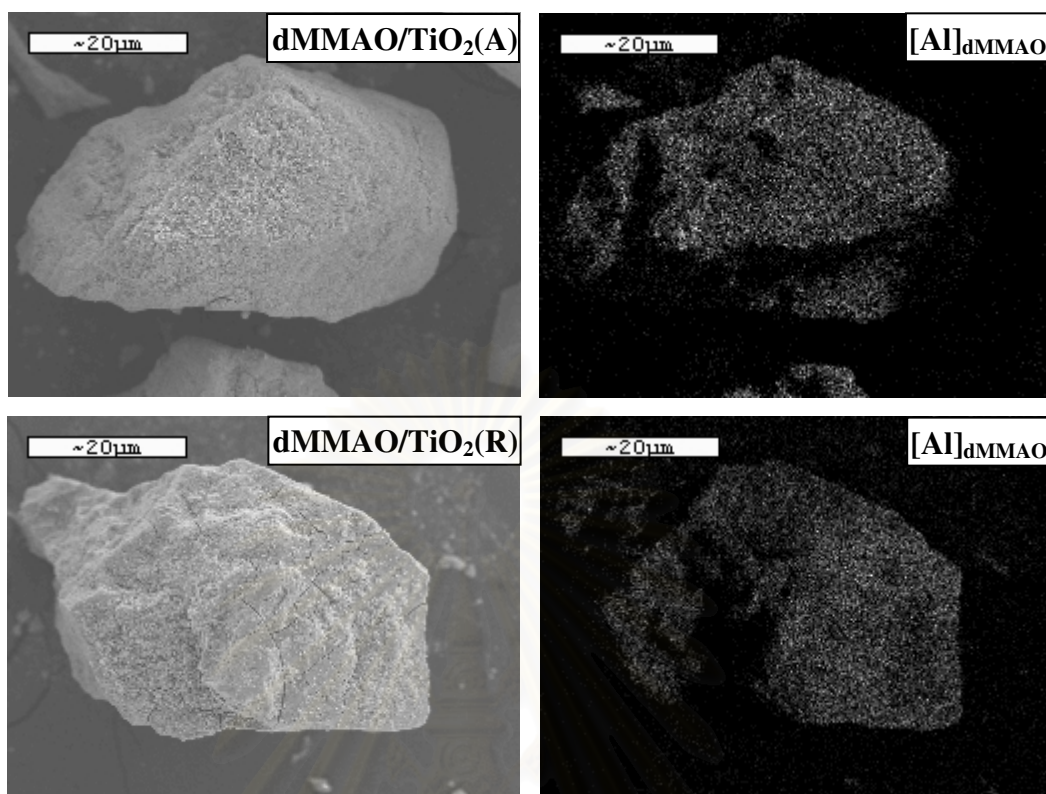
Figure 4.2 SEM micrographs and EDX mapping for different dMMAO/TiO$_2$ nanofillers.

4.1.3 Characterization of fillers and dMMAO/fillers with Transmission electron microscope (TEM).

The TEM micrographs of both TiO$_2$ nanofillers before and after impregnation with dMMAO are also shown in Figure 4.3. It indicated that the TiO$_2$ (A) crystals appeared in the spherical-like shape, whereas the TiO$_2$ (R) crystals were in the needle-like shape. It appeared that the crystal size of primary particle obtained from the TEM measurement was below 50 nm for both samples, as seen in Figure 4.3. In addition, the crystal sizes for both TiO$_2$ samples became larger after impregnation with dMMAO due to the deposition of dMMAO on the TiO$_2$ nanofillers.
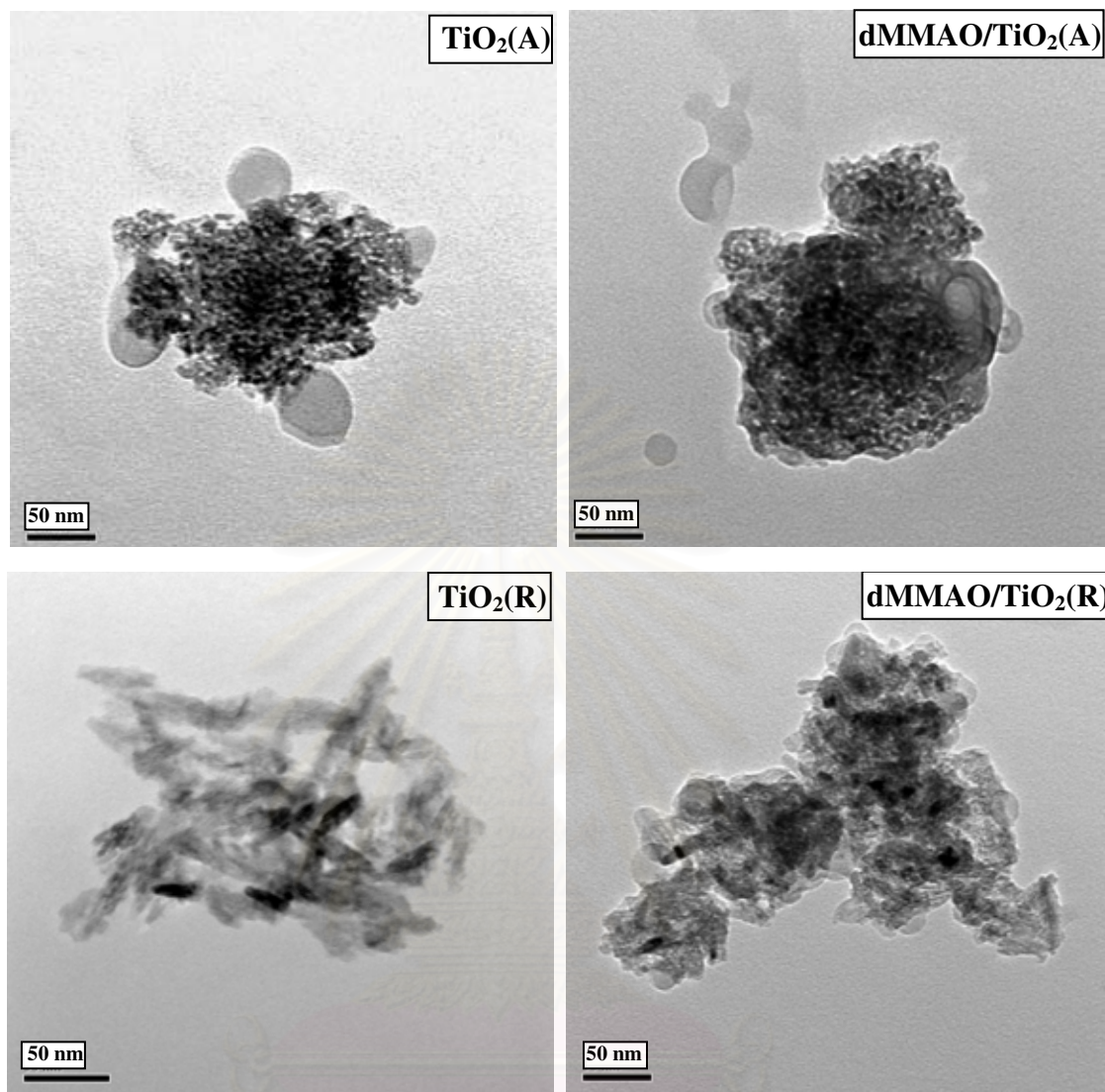
Figure 4.3 TEM micrographs of different TiO$_2$ nanofillers before and after impregnation with dMMAO.

4.1.4 Effect of the TiO$_2$ nanofillers having different phases and ratios of [Al]$_{dMMAO}$/[Zr]$_{cat}$ on the catalyst activity of LLDPE/TiO$_2$ nanocomposites.

After impregnation with dMMAO to obtain the dMMAO/TiO$_2$, the *in situ* polymerization of ethylene/1-hexene was performed with the presence of dMMAO/TiO$_2$ using zircocene catalyst in order to produce the LLDPE/TiO$_2$ nanocomposites. The amounts of dMMAO/TiO$_2$ were varied in the range of 0.1, 0.2, and 0.3 g with corresponding to the [Al]$_{dMMAO}$/[Zr]$_{cat}$ ratios of 1135, 2270 and 3405, respectively. The resulted polymerization activities obtained from both dMMAO/TiO$_2$

(A) and dMMAO/TiO$_2$ (R) with different ratios of [Al]$_{dMMAO}$/[Zr]$_{cat}$ are summarized in Table 4.1. It was found that the polymerization activities obtained from the dMMAO/TiO$_2$ (A) exhibited pronouncedly higher activities than those from the dMMAO/TiO$_2$ (R) at the same [Al]$_{dMMAO}$/[Zr]$_{cat}$ ratios. Increased [Al]$_{dMMAO}$/[Zr]$_{cat}$ ratios apparently resulted in increased activities for both dMMAO/TiO$_2$ (A) and dMMAO/TiO$_2$ (R). This indicated that the greater amounts of dMMAO resulted in more active species being present during polymerization. It was proposed that the dMMAO possibly had many functions, such as an alkylating agent, a stabilizer for a cationic metallocene alkyl and/or counter-ion, an ionizing and/or reducing agent for the transition element, and a scavenger for the metallocene catalytic system. However, one of the most important roles of this alkylaluminoxane is apparently to prevent the formation of ZrCH$_2$CH$_2$Zr species, which is formed via a bimolecular process [72]. Therefore, the polymerization activities obtained from the dMMAO/TiO$_2$ (A) were higher due to the larger amount of [Al]$_{dMMAO}$ being present (based on the EDX measurement as mentioned before).

Table 4.1 Polymerization activities of LLDPE/TiO$_2$ nanocomposites synthesized by *in situ* polymerization with *rac*-Et(Ind)$_2$ZrCl$_2$/dMMAO catalysts.

Types of filler	[Al]$_{dMMAO}$/[Zr]$_{cat}$	Time [a] (s)	Polymer yield [b] (g)	Catalytic activity (kg polymer/mol Zr.h)
TiO$_2$(A)	1135	229	0.91	9564
	2270	171	1.01	14123
	3405	133	1.13	20403
TiO$_2$(R)	1135	345	0.30	2098
	2270	266	0.41	3667
	3405	234	0.59	6100

[a] A period of time used for the total 0.018 mol of ethylene to be consumed.

[b] Measurement at polymerization temperature of 343 K, [Ethylene] = 0.018 mol, [Al]$_{TMA}$/[Zr]$_{cat}$ = 2500, in toluene with total volume = 30 mL, and [Zr]$_{cat}$ = 5 x 10^{-5} M.

Besides the concentration of $[Al]_{dMMAO}$ being present on the TiO_2 nanofillers, the interactions between the $[Al]_{dMMAO}$ and TiO_2 nanofillers were also important to consider. In fact, the strong interaction of the active species with TiO_2 nanofillers employed in this study was essentially referred to the interactions between the TiO_2 nanofillers and the dMMAO cocatalyst. Based on this study, the dMMAO was impregnated onto the TiO_2 nanofillers prior to polymerization. The degree of interactions between the TiO_2 nanoparticles and dMMAO can be determined by the TGA measurement. In order to give a better understanding, we propose the interactions of TiO_2 nanofillers and dMMAO based on the review paper by Severn et al. [73]. They explained that the connection of the TiO_2 nanofillers and cocatalyst occurred via the $O_{filler}–Al_{cocatalyst}$ linkage. In particular, the TGA can only provide useful information on the degree of interactions for the dMMAO bound to the TiO_2 nanofillers in terms of the weight loss and removal temperature. The stronger interaction can result in it being more difficult for the dMMAO bound to the TiO_2 nanofillers to react with Zr-complex during activation processes, leading to lower catalytic activity for polymerization [74]. The TGA measurement was performed in order to prove the interaction between the $[Al]_{dMMAO}$ and TiO_2 nanofillers. The TGA profiles of both dMMAO/TiO_2 samples are given in Figure 4.4. The weight loss of $[Al]_{dMMAO}$ present on TiO_2 nanofillers was in the order of TiO_2 (A) (20.0%) > TiO_2 (R) (18.8%) indicating stronger interaction for the dMMAO/TiO_2 (R) sample. Thus, the higher polymerization activity obtained from dMMAO/TiO_2 (A) can be attributed to both larger amount of dMMAO present coupled with weaker interaction between the dMMAO and the TiO_2 nanofillers.
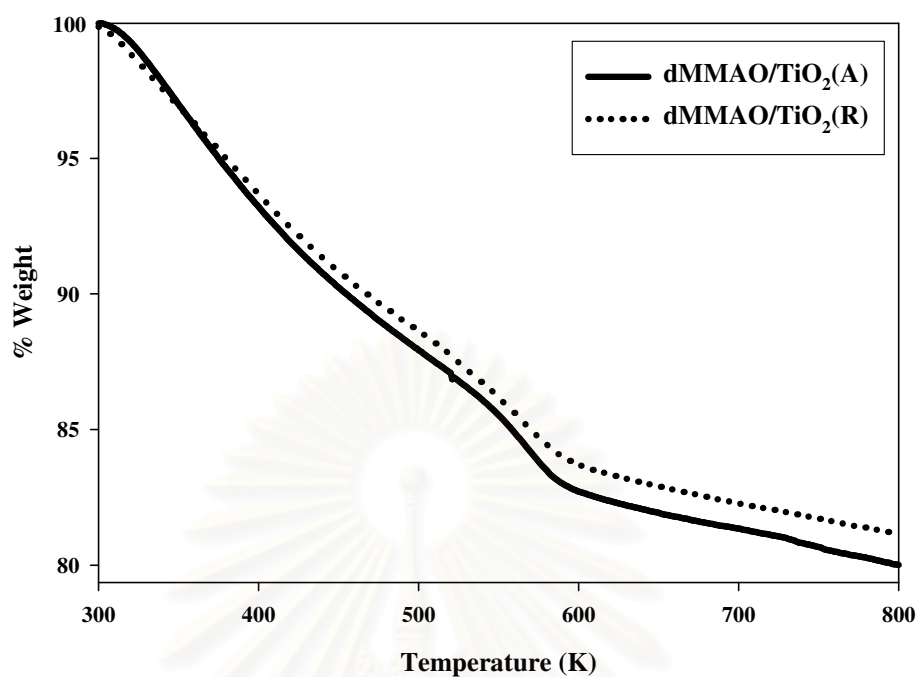
Figure 4.4 TGA profiles of [Al]$_{dMMAO}$ on different TiO$_2$ nanofillers.

4.1.5 Effect of the TiO$_2$ nanofillers having different phases and ratios of [Al]$_{dMMAO}$/[Zr]$_{cat}$ on the incorporation of LLDPE/TiO$_2$ nanocomposites.

Table 4.2

Triad distribution of LLDPE/TiO$_2$ nanocomposites obtained from ^{13}C NMR analysis.

Types of filler	[Al]$_{dMMAO}$/ [Zr]$_{cat}$	EEE	HEE	HEH	EHE	EHH	HHH	1-hexene incorporation (%)
	1135	0.504	0.194	0.034	0.116	0.151	0.000	26.8
TiO$_2$(A)	2270	0.438	0.174	0.053	0.120	0.215	0.000	33.5
	3405	0.388	0.201	0.041	0.124	0.246	0.000	37.0
	1135	0.759	0.110	0.000	0.051	0.080	0.000	13.1
TiO$_2$(R)	2270	0.674	0.152	0.006	0.071	0.097	0.000	16.8
	3405	0.667	0.140	0.005	0.069	0.119	0.000	18.8

E refers to ethylene and **H** refers to 1-hexene.

The ^{13}C NMR is one of the most powerful techniques used to identify the polymer microstructure, especially for polyolefins. The resulted ^{13}C NMR spectra (see Appendix B) for all samples were assigned typically to the LLDPE obtained from copolymerization of ethylene/1-hexene. The triad distribution was identified based on the method described by Randall [71]. It can be observed that the LLDPE/TiO$_2$ (A) and LLDPE/TiO$_2$ (R) nanocomposites exhibited similar ^{13}C NMR patterns indicating similar molecular structure of polymer. Based on calculations described by Galland [75], the triad distribution of monomer and 1-hexene incorporation is listed in Table 4.2. It indicated that all LLDPE/TiO$_2$ nanocomposites were random copolymer with the difference in 1-hexene incorporation. It was found that 1-hexene incorporation of LLDPE/TiO$_2$ (A) nanocomposites were higher than that of LLDPE/TiO$_2$ (R) nanocomposites probably due to less steric hindrance. Increased [Al]$_{dMMAO}$/[Zr]$_{cat}$ ratios also resulted in a slight increase in 1-hexene incorporation for both LLDPE/TiO$_2$ (A) and LLDPE/TiO$_2$ (R) nanocomposites.

4.1.6 Effect of the TiO$_2$ nanofillers having different phases and ratios of [Al]$_{dMMAO}$/[Zr]$_{cat}$ on the melting temperature of LLDPE/TiO$_2$ nanocomposites.

Table 4.3

Thermal properties of LLDPE/TiO$_2$ nanocomposites obtained from DSC measurement.

Types of filler	[Al]$_{dMMAO}$/[Zr]$_{cat}$	T$_m$(K)	ΔH$_m$ (J/g)	Crystallinity (%)
TiO$_2$(A)	1135	355.9	4.30	1.5
	2270	-[a]	-[a]	-[a]
	3405	-[a]	-[a]	-[a]
TiO$_2$(R)	1135	368.5	25.29	8.8
	2270	354.9	17.98	6.3
	3405	364.4	12.84	4.5

[a] Value not be detected from the measurement.

The DSC analysis was used to measure the thermal properties of LLDPE/TiO$_2$ nanocomposites obtained. The DSC results are shown in Table 4.3. It was found that increased 1-hexene incorporation dramatically decreased the crystallinity of samples. This was in agreement with the results obtained from ^{13}C NMR as mentioned before. Thus, the higher crystallinity for the LLDPE/TiO$_2$ (R) nanocomposites was evident. The less crystallinity of LLDPE can be decreased with a higher degree of 1-olefin (1-hexene) [76-78] along with the larger amount of TiO$_2$ being present [79-80]. However, when the larger amounts of the TiO$_2$ nanoparticles are employed, they may locate themselves in the interlamellar spaces, which leave little room for additional crystallization. So, the presence of these nanoparticles may even inhibit crystallization.

4.1.7 Characterization of LLDPE/TiO$_2$ nanocomposites with Scanning electron microscopy (SEM) and energy dispersive X-ray spectroscopy (EDX).

In order to study the morphologies and TiO$_2$ distribution inside the polymer matrix of LLDPE/TiO$_2$ nanocomposites, SEM/EDX was performed. The SEM micrographs and EDX mapping for Ti are shown in Figures 4.5 and 4.6 for the LLDPE/TiO$_2$ (A) and LLDPE/TiO$_2$ (R) nanocomposites, respectively. There was no significant change in morphologies for both LLDPE/TiO$_2$ (A) and LLDPE/TiO$_2$ (R) nanocomposites upon the similar amount of TiO$_2$ employed. Based on the EDX mapping, it revealed good distribution of the TiO$_2$ nanoparticles inside the polymer matrix.
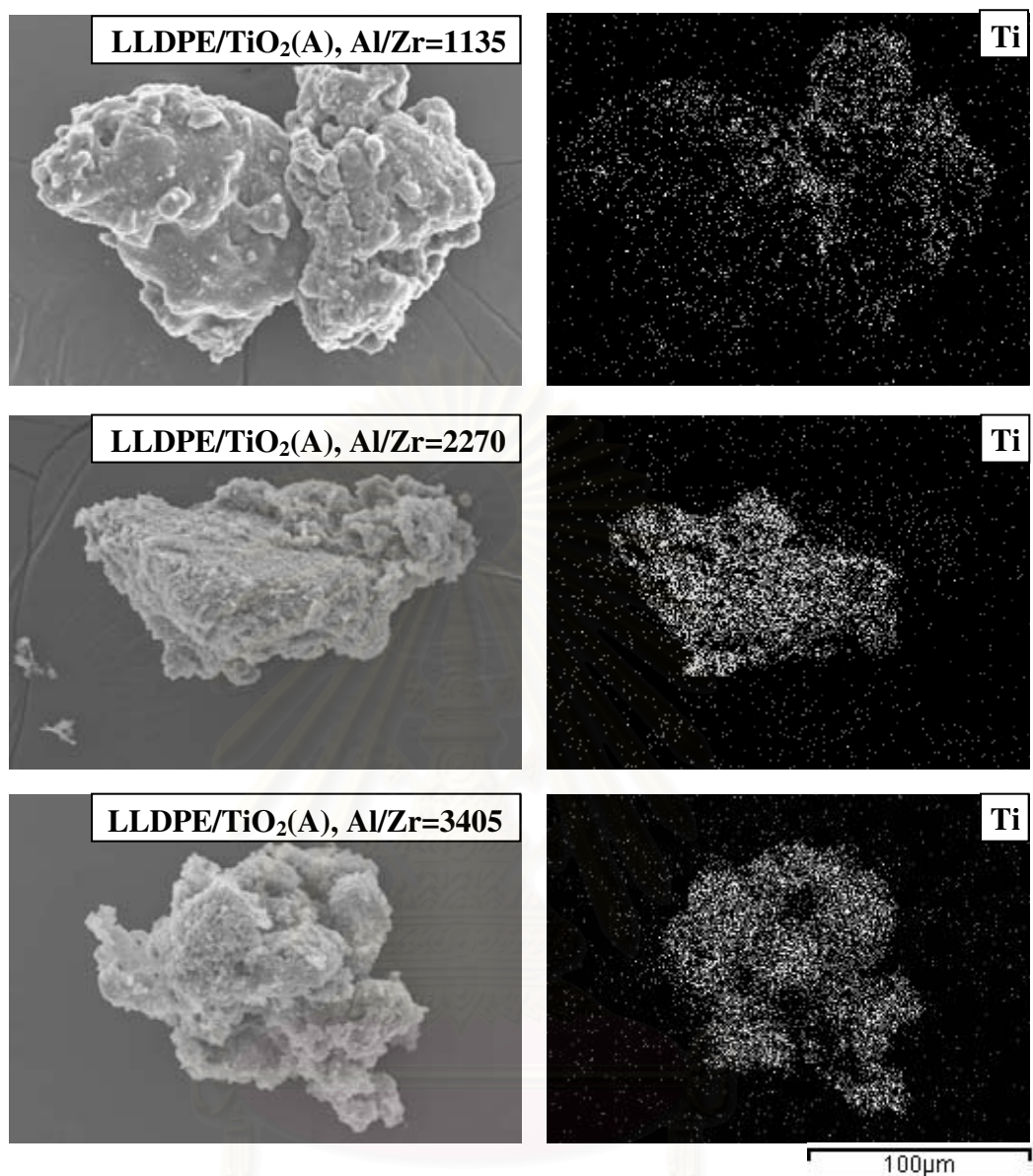
Figure 4.5 SEM micrographs of LLDPE/TiO$_2$ (A) nancomposites and Ti distribution obtained from EDX upon different [Al]$_{dMMAO}$/[Zr]$_{cat}$ ratios.
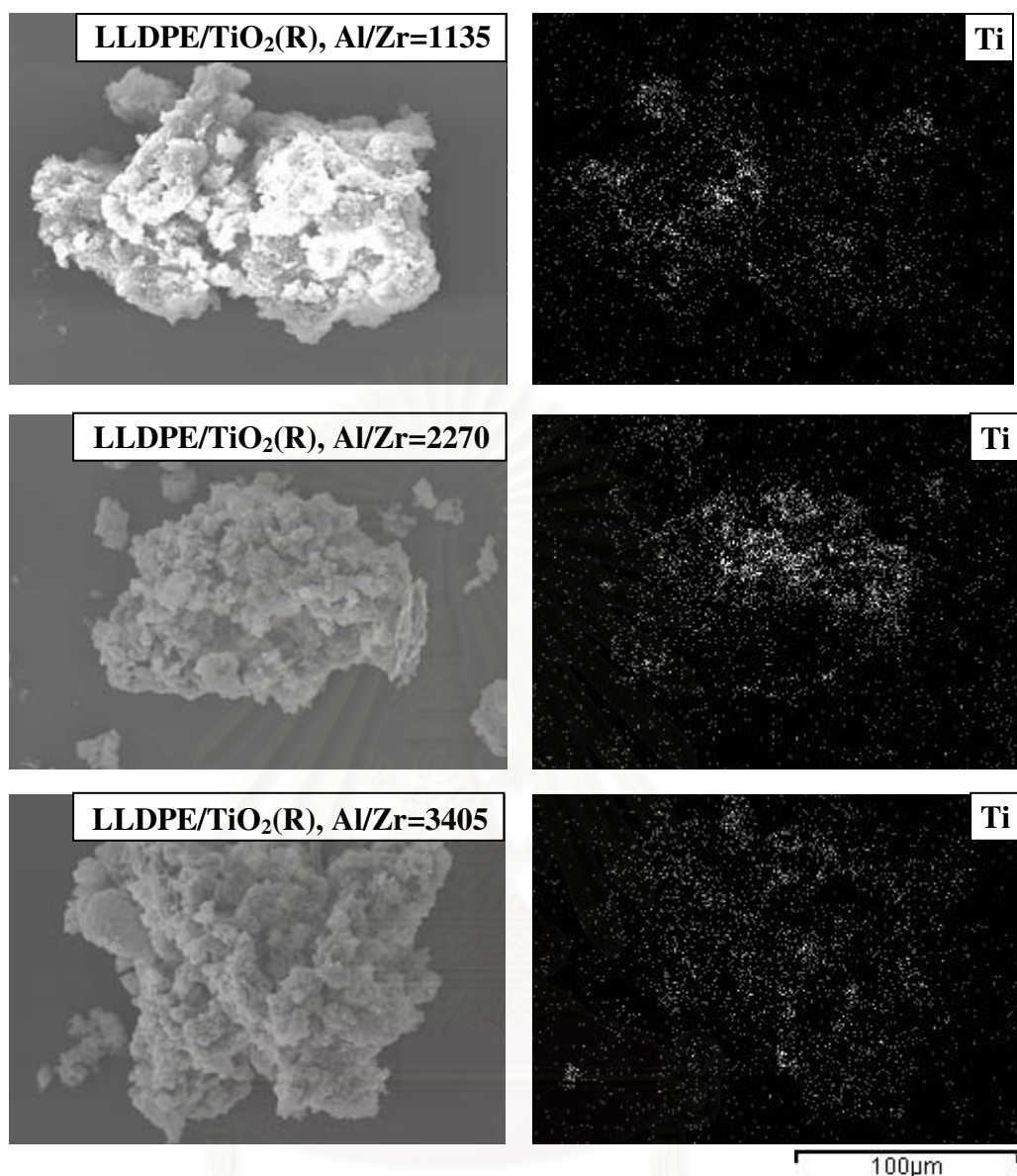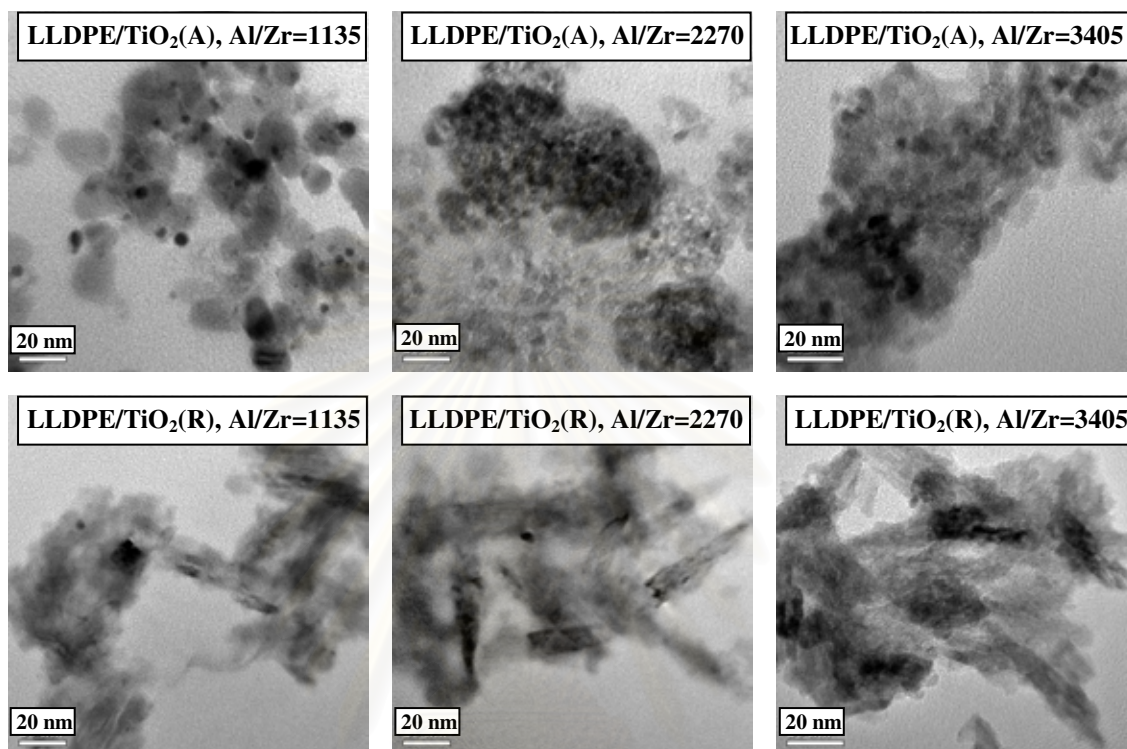
Figure 4.6 SEM micrographs of LLDPE/TiO$_2$ (R) nancomposites and Ti distribution obtained from EDX having different [Al]$_{dMMAO}$/[Zr]$_{cat}$ ratios.

4.1.8 Characterization of LLDPE/TiO$_2$ nanocomposites with Transmission electron microscope (TEM).

As known, the images from high-resolution transmission electron microscopy (TEM) are essential components of nanoscience and nanotechnology, therefore TEM was performed in order to determine the dispersion of TiO$_2$ nanofillers inside the polymer matrix. The TEM micrographs for the dispersion of TiO$_2$ in the LLDPE/TiO$_2$ (A) and LLDPE/TiO$_2$ (R) nanocomposites having different [Al]$_{dMMAO}$/[Zr]$_{cat}$ ratios

are shown in Figure 4.7. In general, both TiO_2 (A) and TiO_2 (R) nanofillers apparently exhibited good dispersion inside the polymer matrix without any changes in crystal morphologies.

**Figure 4.7** TEM micrographs of both LLDPE/TiO_2 (A) and LLDPE/TiO_2 (R) nancomposites having different $[Al]_{dMMAO}/[Zr]_{cat}$ ratios.

4.2 Effect of different TiO_2 nanofillers when the $[Al]_{dMMAO}/[Zr]_{cat}$ ratio was fixed at 2270 on the catalyst activity and properties of LLDPE/TiO_2 nanocomposites.

In this section, the different TiO_2 nanofillers [TiO_2 (A), TiO_2 (J), TiO_2 (D), and TiO_2 (R) as listed in Table 4.4 having different phase compositions and crystallite sizes] as filler of LLDPE/TiO_2 nanocomposites synthesized by *in situ* polymerization with same ratio of $[Al]_{dMMAO}/[Zr]_{cat}$ was also reported in this study.

4.2.1 Characterization of fillers and dMMAO/fillers with X-ray diffraction (XRD).

The XRD patterns of TiO_2 nanofillers before and after impregnation with dMMAO are shown in Figure 4.8 indicating the characteristic peaks for the anatase form of TiO_2 (A) at 25° (major) and the rutile form of TiO_2 (R) at 27° (major). The average crystallite sizes for the TiO_2 (A) and TiO_2 (R) calculated from the Sherrer's equation were 6.1 and 6.9 nm, respectively. The XRD patterns for the TiO_2 (J) and TiO_2 (D) revealed the mixed phases of anatase and rutile having the crystallite sizes of 23.1 and 21.2 nm, respectively. No significant changes were observed upon the dMMAO impregnation onto the TiO_2 nanofillers suggesting well dispersion of dMMAO. More details of the characteristics of different TiO_2 nanofillers are also listed in Table 4.4.
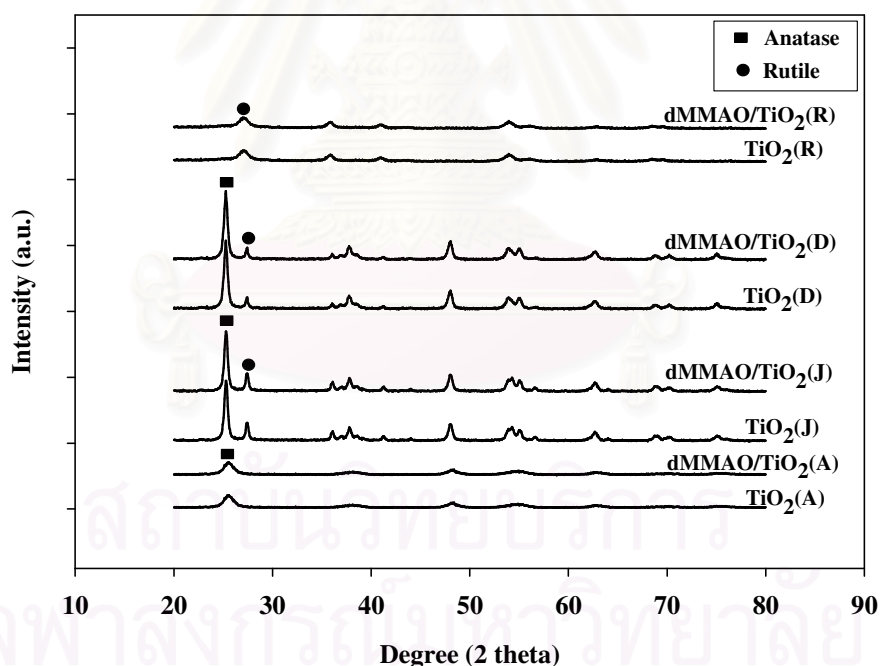
**Figure 4.8** XRD patterns of different TiO_2 nanofillers before and after impregnation with dMMAO.

Table 4.4

Characteristics of different TiO_2 nanofillers.

Types of filler	Surface area (m²/g)	Crystallize size[a] (nm)	% Anatase [b]	% Rutile[b]
$TiO_2(A)$	240	6.1	100	0
TiO_2 (J)	50	23.1	80.4	19.6
$TiO_2(D)$	47	21.2	90.7	9.3
$TiO_2(R)$	160	6.9	0	100

[a] Based on XRD measurement.

[b] Calculated from equation based on ref. [81].

4.2.2 Characterization of dMMAO/fillers with Scanning electron microscopy (SEM) and energy dispersive X-ray spectroscopy (EDX).

SEM and EDX were performed in order to study the morphologies and distribution of dMMAO onto the different TiO_2 nanfillers, respectively. The SEM micrographs and EDX mapping for the dMMAO/TiO_2 samples are shown in Figure 4.9. All samples apparently exhibited the similar morphologies. It can be observed that the dMMAO was well distributed all over the TiO_2 granules as seen by the EDX mapping. Based on the EDX measurement, the amounts of $[Al]_{dMMAO}$ present on the TiO_2 samples can be also determined. They were in the range of 12.5, 11.8, 10.4, and 10.2 wt% for TiO_2 (A), TiO_2 (J), TiO_2 (D), and TiO_2 (R), respectively. The largest amount of $[Al]_{dMMAO}$ present in the TiO_2 (A) can be attributed to largest surface area for the TiO_2 (A) coupled with the absence of rutile phase. It can be also observed that the presence of rutile phase apparently resulted in decreased amounts of $[Al]_{dMMAO}$ being present on the TiO_2 nanofillers.
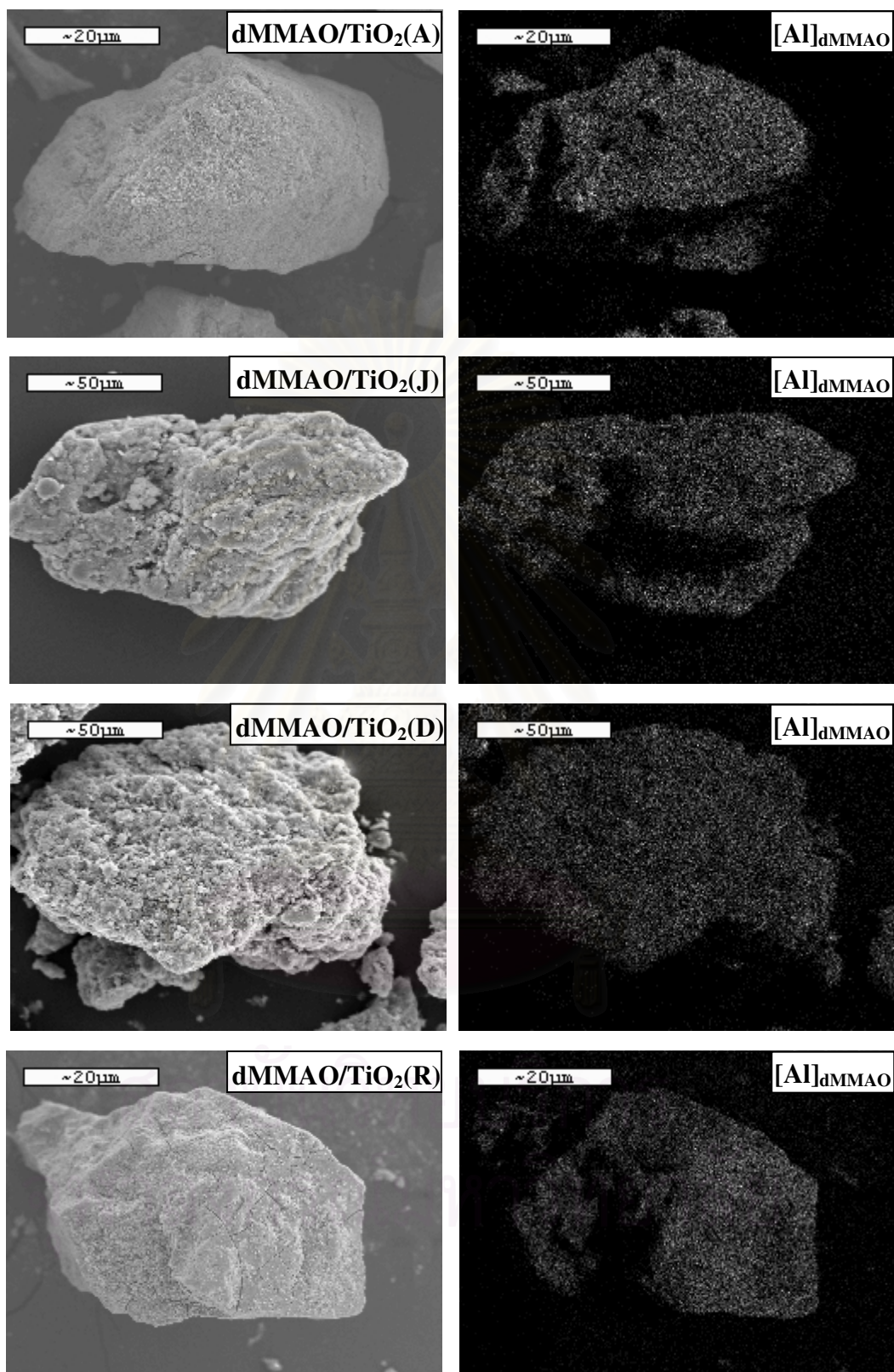
Figure 4.9 SEM micrographs and EDX mapping for different dMMAO/TiO$_2$ nanofillers.

4.2.3 Characterization of fillers and dMMAO/fillers with Transmission electron microscope (TEM).

In order to determine the dispersion of TiO_2 before and after dMMAO impregnation, a more powerful technique such as TEM was applied to all samples. The TEM micrographs of all TiO_2 nanofillers before and after impregnation with dMMAO are shown in Figure 4.10. It indicated that the TiO_2 (A), TiO_2 (J), and TiO_2 (D) crystals appeared in the spherical-like shape, whereas the TiO_2 (R) crystals were in the needle-like shape. It appeared that the crystal size of primary particle obtained from the TEM measurement was below 50 nm for all samples. However, only the TiO_2 (A) and TiO_2 (R) exhibited the sizes below 20 nm.
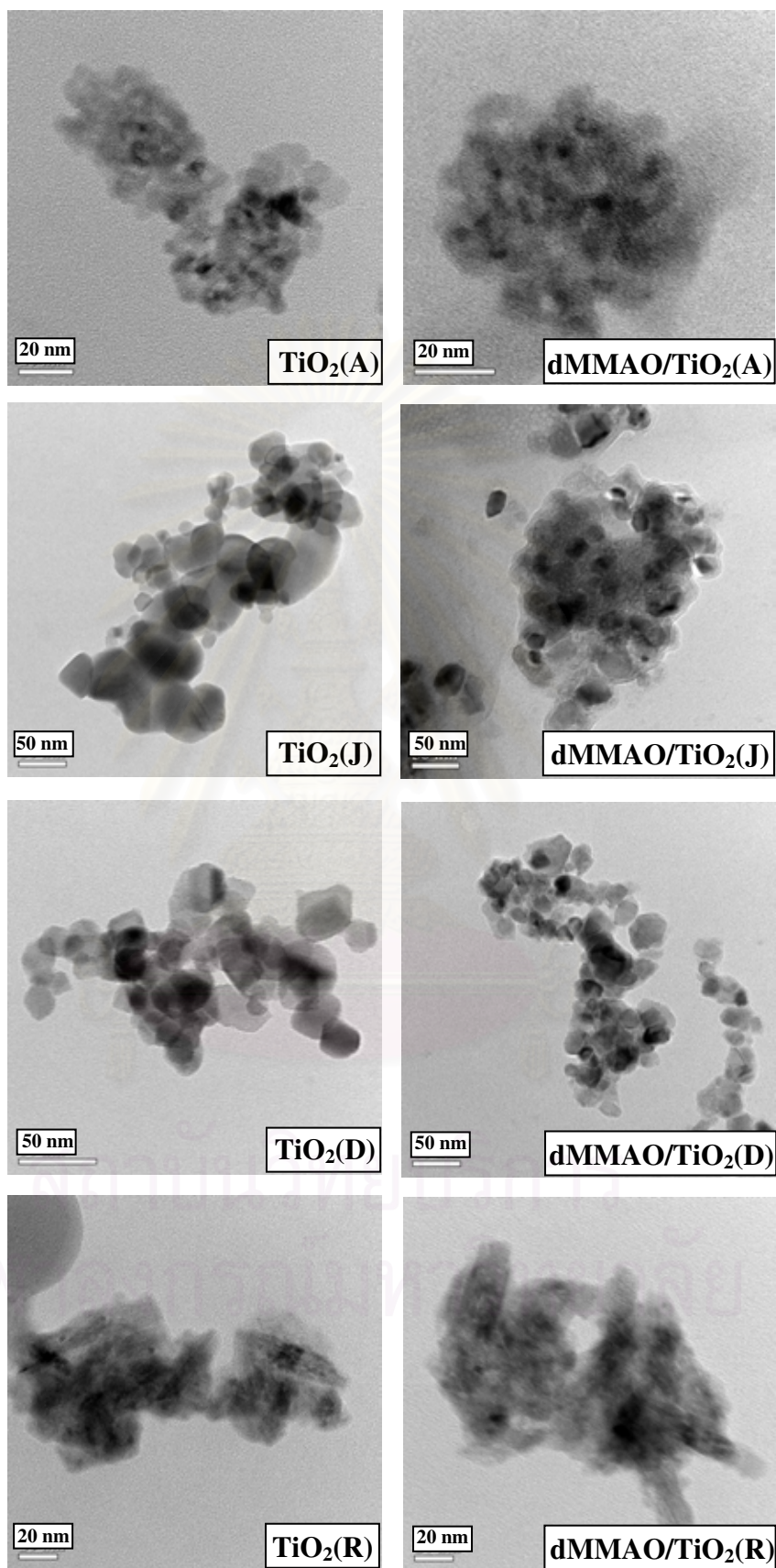
Figure 4.10 TEM micrographs of different TiO$_2$ nanofillers before and after impregnation with dMMAO

4.2.4 Effects of the different TiO$_2$ nanofillers when the [Al]$_{dMMAO}$/[Zr]$_{cat}$ ratios was fixed at 2270 on the catalyst activity of LLDPE/TiO$_2$ nanocomposites.

The resulted polymerization activities obtained from dMMAO/TiO$_2$ (A), dMMAO/TiO$_2$ (J), dMMAO/TiO$_2$ (D) and, dMMAO/TiO$_2$ (R) with same ratio of [Al]$_{dMMAO}$/[Zr]$_{cat}$ are summarized in Table 4.5. It was found that the polymerization activities obtained from the dMMAO/TiO$_2$ (A) exhibited pronouncedly highest activities among those from the dMMAO/TiO$_2$ (J), dMMAO/TiO$_2$ (D), and dMMAO/TiO$_2$ (R). This indicated that the largest amounts of dMMAO present (12.5 wt%) on TiO$_2$ (A) resulted in highest amount of active species being present during polymerization. Therefore, the polymerization activities obtained from the dMMAO/TiO$_2$ (A) were the highest due to the largest amount of [Al]$_{dMMAO}$ being present (based on the EDX measurement as mentioned before). Besides the concentration of [Al]$_{dMMAO}$ being present on the TiO$_2$ nanofillers, the interactions between the [Al]$_{dMMAO}$ and TiO$_2$ nanofillers were also important to consider. The TGA measurement was performed in order to prove the interaction between the [Al]$_{dMMAO}$ and TiO$_2$ nanofillers. The TGA profiles of all dMMAO/TiO$_2$ samples are given in Figure 4.11. The weight loss of [Al]$_{dMMAO}$ present on TiO$_2$ nanofillers was in the order of TiO$_2$ (J) (26.6%) > TiO$_2$ (A) (20.0%) > TiO$_2$ (R) (18.8%) > TiO$_2$ (D) (18.1%). Thus, the highest polymerization activity obtained from dMMAO/TiO$_2$ (A) can be attributed to both largest amount of dMMAO present coupled with weak interactions between the dMMAO and the TiO$_2$ nanofillers compared with those TiO$_2$ (R) (18.8%) and TiO$_2$ (D) (18.1%). Although the TiO$_2$ (J) had the weakest interactions, it exhibited the moderate activity due to moderate amount of dMMAO being present.
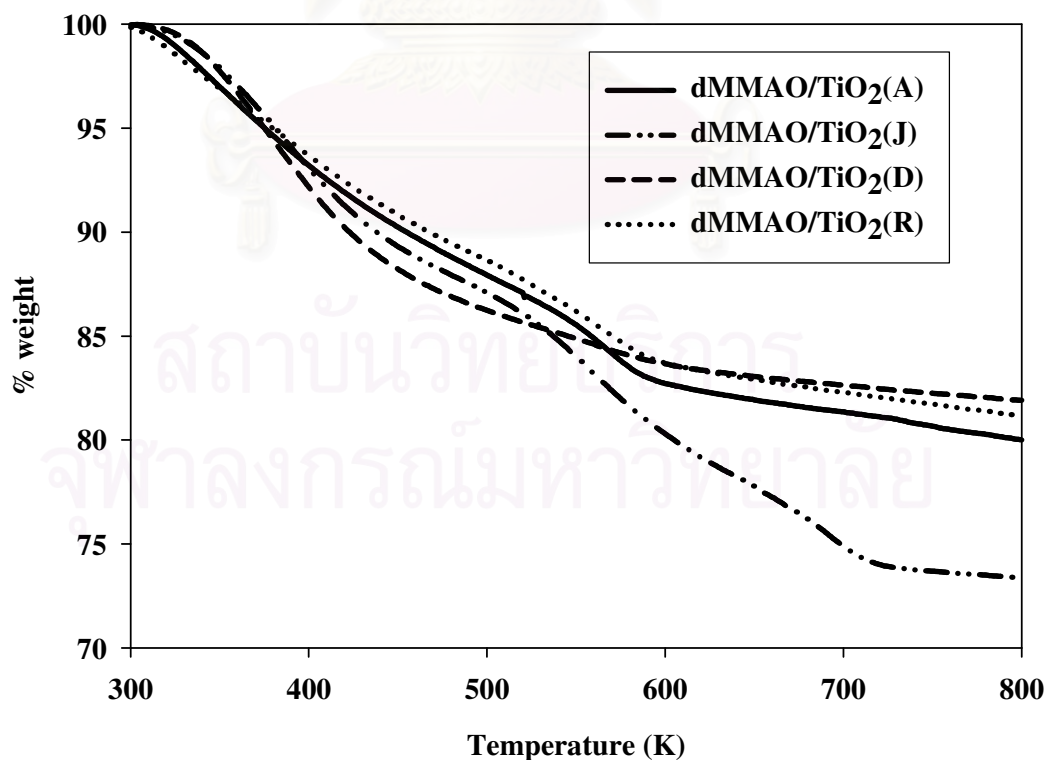
Table 4.5

Polymerization activities of LLDPE/TiO$_2$ nanocomposites synthesized by *in situ* polymerization with *rac*-Et(Ind)$_2$ZrCl$_2$/dMMAO catalysts.

Types of filler	Time [a] (s)	Polymer yield [b] (g)	Catalytic activity (kg polymer/mol Zr.h)
TiO$_2$(A)	171	1.01	14123
TiO$_2$ (J)	242	0.70	6905
TiO$_2$(D)	204	0.39	4596
TiO$_2$(R)	266	0.41	3667

[a] A period of time used for the total 0.018 mol of ethylene to be consumed.

[b] Measurement at polymerization temperature of 343 K, [Ethylene] = 0.018 mol, [Al]$_{dMMAO}$/[Zr]$_{cat}$ = 2270, [Al]$_{TMA}$/[Zr]$_{cat}$ = 2500, in toluene with total volume = 30 mL, and [Zr]$_{cat}$ = 5 x 10^{-5} M.

Figure 4.11 TGA profiles of [Al]$_{dMMAO}$ on different TiO$_2$ nanofiller.

4.2.5 Effects of the different TiO$_2$ nanofillers when the [Al]$_{dMMAO}$/[Zr]$_{cat}$ ratios was fixed at 2270 on the incorporation of LLDPE/TiO$_2$ nanocomposites.

Table 4.6

Triad distribution of LLDPE/TiO$_2$ nanocomposites obtained from ^{13}C NMR analysis.

Types of filler	EEE	HEE	HEH	EHE	EHH	HHH	1-hexene incorporation (%)
TiO$_2$(A)	0.438	0.174	0.053	0.120	0.215	0.000	33.5
TiO$_2$ (J)	0.536	0.183	0.014	0.097	0.171	0.000	26.8
TiO$_2$(D)	0.717	0.128	0.004	0.062	0.089	0.000	15.1
TiO$_2$(R)	0.674	0.152	0.006	0.071	0.097	0.000	16.8

E refers to ethylene and **H** refers to 1-hexene.

The resulted ^{13}C NMR spectra are shown in Appendix B for all LLDPE/TiO$_2$ samples, which were assigned typically to the LLDPE obtained from copolymerization of ethylene/1-hexene. The triad distribution was identified based on the method described by Randall [71]. It can be observed that all LLDPE/TiO$_2$ nanocomposites exhibited similar ^{13}C NMR patterns indicating similar molecular structure of polymer. Based on calculations described by Galland [75], the triad distributions of ethylene (E) and 1-hexene (H) incorporation are listed in Table 4.6. It indicated that all LLDPE/TiO$_2$ nanocomposites obtained from different TiO$_2$ nanoparticles were random copolymer having different degrees of 1-hexene incorporation. It was found that the incorporation of 1-hexene in LLDPE/TiO$_2$ (A) nanocomposites was the highest among other samples. This was due to the least steric hindrance due to the most dispersion of the TiO$_2$ (A) nanoparticles upon the smallest crystallite size.

4.2.6 Effects of the different TiO$_2$ nanofillers when the [Al]$_{dMMAO}$/[Zr]$_{cat}$ ratios was fixed at 2270 on the melting temperatures of LLDPE/TiO$_2$nanocomposites.

Table 4.7

Thermal properties of LLDPE/TiO$_2$ nanocomposites obtained from DSC measurement.

| Types of filler	T$_m$(K)	ΔH$_m$ (J/g)	Crystallinity (%)
TiO$_2$(A)	-[a]	-[a]	-[a]
TiO$_2$ (J)	351.7	5.16	1.8
TiO$_2$(D)	364.9	19.58	6.9
TiO$_2$(R)	354.9	17.98	6.3

[a] Value not be detected from the measurement.

The DSC results are shown in Table 4.7. It was found that the increased degree of 1-hexene incorporation basically decreased the crystallinity of samples. This was in agreement with the results obtained from ^{13}C NMR as mentioned before. Thus, the highest crystallinity for the LLDPE/TiO$_2$ (D) nanocomposites was evident. The crystallinity of LLDPE can be decreased with a higher degree of 1-olefin (1-hexene) insertion [76-78] along with the larger amount of TiO$_2$ being present [79-80]. As reported, when the larger amounts of the TiO$_2$ nanofillers are employed, they may locate themselves in the interlamellar spaces, which leave little room for additional crystallization. So, the presence of these nanofillers may even inhibit crystallization.

4.2.7 Characterization of LLDPE/TiO$_2$ nanocomposites with Scanning electron microscopy (SEM) and energy dispersive X-ray spectroscopy (EDX).

In order to study the morphologies and TiO$_2$ distribution inside the polymer matrix of LLDPE/TiO$_2$ nanocomposites, SEM/EDX were performed. The SEM micrographs and EDX mapping for Ti of all samples are shown in Figure 4.12. There was no significant change in morphologies for all samples upon the different TiO$_2$

nanoparticles employed. Based on the EDX mapping, it revealed good distribution of the TiO_2 nanofillers inside the polymer matrix.
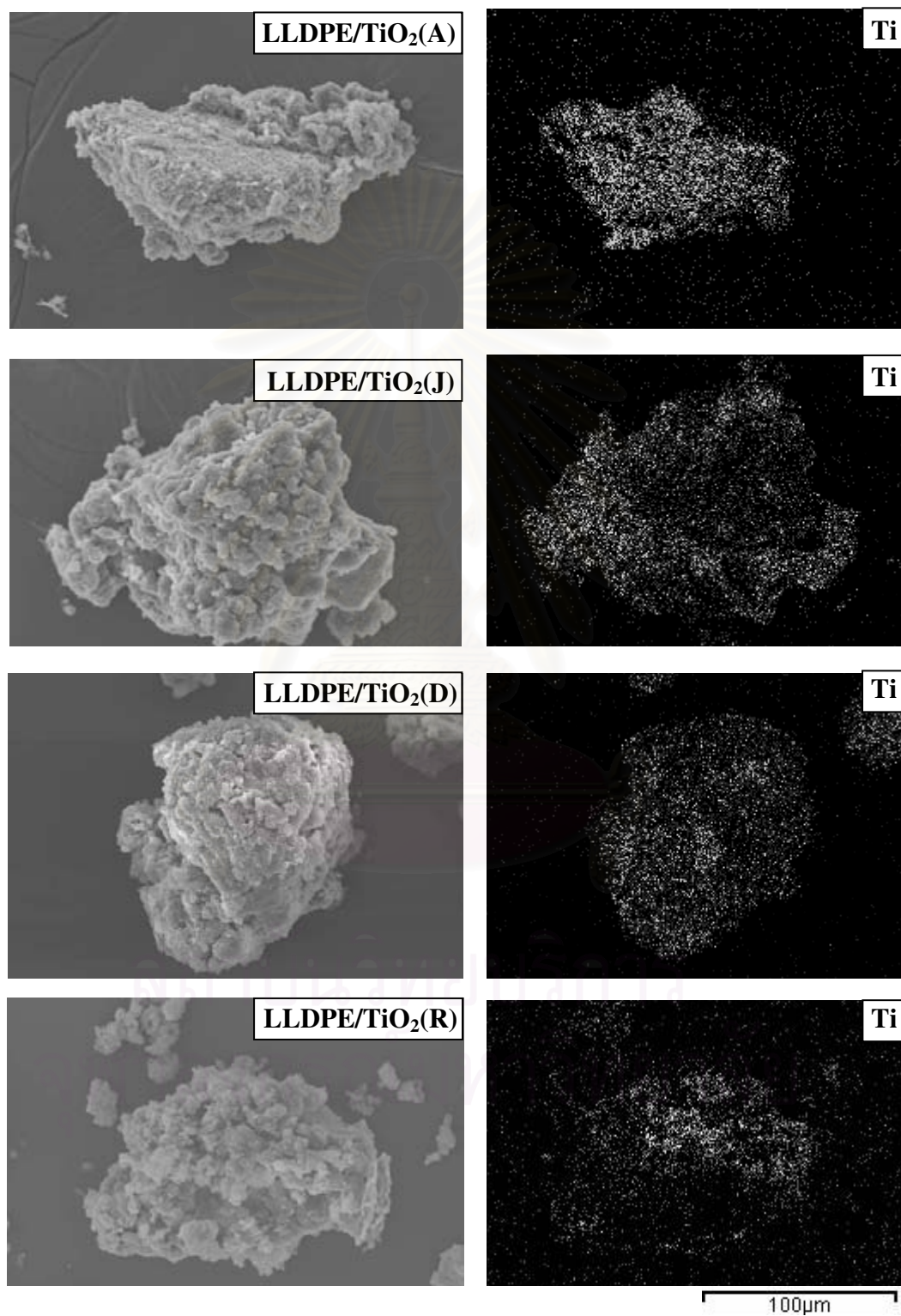
Figure 4.12 SEM micrographs of LLDPE/TiO_2 nancomposites and Ti distribution obtained from EDX upon different TiO_2 nanofillers.

4.2.8 Characterization of LLDPE/TiO$_2$ nanocomposites with Transmission electron microscope (TEM).

TEM was performed in order to determine the dispersion of TiO$_2$ nanofillers inside the polymer matrix. The TEM micrographs for the dispersion of TiO$_2$ in all LLDPE/TiO$_2$ samples are shown in Figure 4.13. In general, all TiO$_2$ nanofillers apparently exhibited good dispersion inside the polymer matrix without any changes in crystal morphologies. Figure 4.13 TEM micrographs of LLDPE/TiO$_2$ nancomposites having different TiO$_2$ nanofillers.
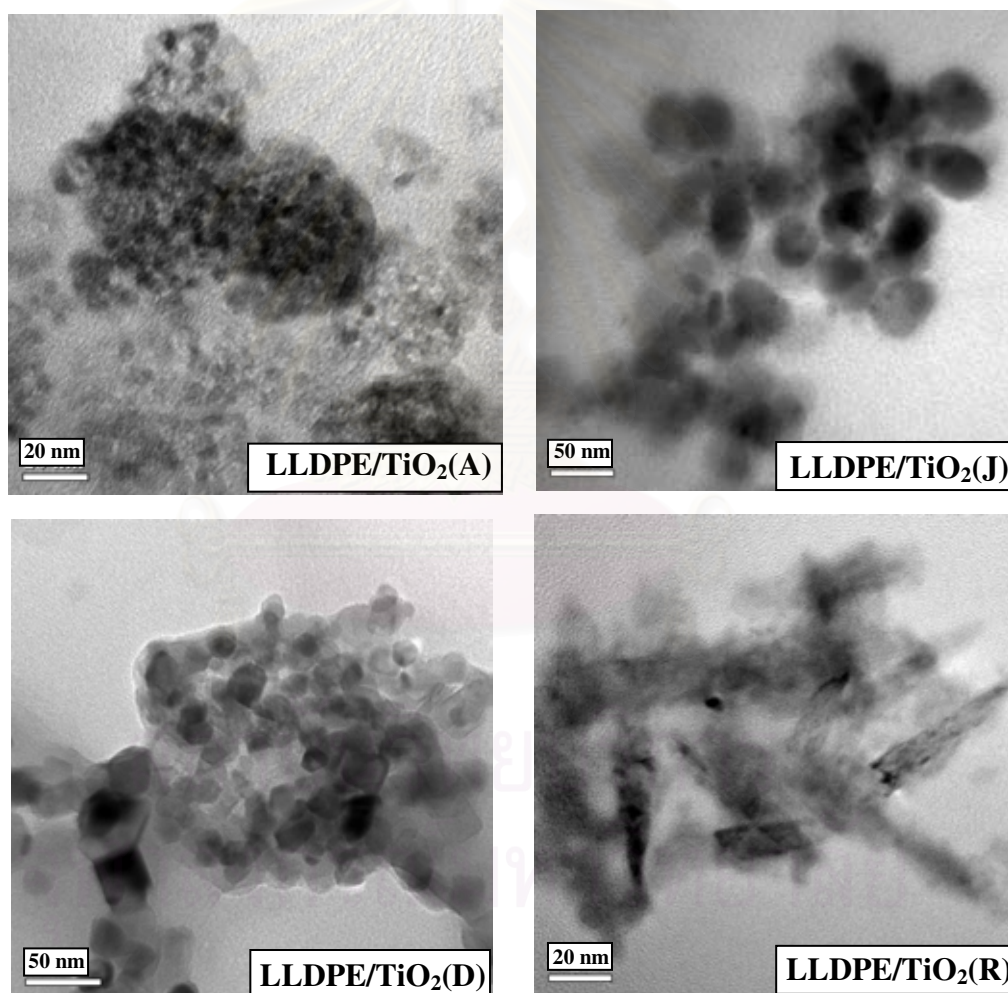
Figure 4.13 TEM micrographs of LLDPE/TiO$_2$ nancomposites having different TiO$_2$ nanofillers.

CHAPTER V

CONCLUSIONS AND RECOMMENTDATIONS

5.1 Conclusions

5.1.1 Effect of TiO_2 nanofillers having different phases and ratios of $[Al]_{dMMAO}/[Zr]_{cat}$

The LLDPE/TiO_2 nanocomposites were produced via *in situ* polymerization of ethylene/1-hexene with zirconocene/dMMAO catalyst using TiO_2 nanofillers having different phases. The polymerization activities obtained from the dMMAO/TiO_2 (A) containing anatase TiO_2 were higher than those from the dMMAO/TiO_2 (R) containing rutile TiO_2. This can be attributed to larger amount of dMMAO present on the TiO_2 (A) nanoparticles (identified by EDX measurement) coupled with weaker interaction (determined by TGA) between dMMAO and TiO_2 (A) nanoparticles. Increased $[Al]_{dMMAO}/[Zr]_{cat}$ ratios apparently resulted in increased polymerization activities. The LLDPE/TiO_2 nanocomposites obtained were random copolymer having different triad distribution and 1-hexene incorporation. In addition, the crystallinity of the LLDPE/TiO_2 (R) nanocomposites were higher due to less degree of 1-hexene insertion based on ^{13}C NMR and DSC measurements.

5.1.2 Effect of the different TiO_2 nanofillers when $[Al]_{dMMAO}/[Zr]_{cat}$ ratio was fixed at 2270

The LLDPE/TiO_2 nanocomposites were produced using different TiO_2 nanofillers with the same method above. The polymerization activities were in the order of TiO_2 (A) > TiO_2 (J) > TiO_2 (D) > TiO_2 (R). It was found that the presence of rutile phase can result in decreased activities due to the decreased adsorption ability of dMMAO on TiO_2 nanoparticles as seen by EDX. Besides the presence of rutile phase the strong interactions of dMMAO and TiO_2 were considered. Too strong interactions also caused the decreased activities. All LLDPE/TiO_2 nanocomposites obtained were

random copolymer having different triad distribution. The results obtained from ^{13}C NMR was in agreement with those from DSC where the higher degree of 1-hexene insertion apparently resulted in lower crystallinity of samples.

5.2 Recommendations

- Investigation of other fillers should be further studied.
- Interaction between fillers and dMMAO under reaction condition should be performed.

REFERENCES

[1] Turunen, J. P. J., and Pakkanen, T. T. Characterization of stepwise prepared, silica supported zirconocene catalysts designed for olefin polymerization. **Journal of Molecular Catalysis A: Chemical** 263 (2006): 1-8.

[2] Ribeiro, M. R., Deffieux, A., and Portela, M. F. Supported metallocene complexs for ethylene and propylene polymerizations: preparation and activity. **Industrial and Engineering Chemistry Research** 36 (1997): 1224-1237.

[3] Chien, J. C. W. Supported metallocene polymerization catalysis. **Topic in Catalysis** 7 (1999): 23-36.

[4] Kontou, E., and Niaouakis, M. Thermo-mechanical properties of LLDPE/SiO_2 nanocomposites. **Polymer** 47 (2006): 1267-1280.

[5] Li, K-T., Dai, C. L., and Kuo, C. W. Ethylene polymerization over a nano-sized silica supported Cp_2ZrCl_2/MAO catalyst. **Catalysis Communications** 8 (2007): 1209-1213.

[6] Nussbaumer, R. J., Caseri, W. R., and Tervoort, P. T. Polymer-TiO_2 nanocomposites: a route towards visually transparent broadband UV filters and high refractive index materials. **Macromolecular Materials and Engineering** 288 (2003): 44-49.

[7] Wang, Z., Li, G., and Zhang, X. Z. Dispersion behavior of TiO_2 nanoparticles in LLDPE/LDPE/TiO_2 nanocomposites. **Macromolecular Chemistry and Physics** 206 (2005): 258-262.

[8] Chen, X. D., Wang, Z., Liao, Z. F., Mai, Y. L., and Zhang, M. Q. Roles of anatase and rutile TiO_2 nanoparticles in photooxidation of polyurethane. **Polymer Testing** 26 (2007): 202-208.

[9] Kuo, M. C., Tsai, C. M., Huang, J. C., and Chen, M. PEEK coposites reinforced by nano-sized SiO_2 and Al_2O_3 particulates. **Materials chemistry and physics** 90 (2005): 185-195.

[10] Jongsomjit, B., Panpranot, J., Okada, M., Shiono, T., and Praserthdam, P. Characteristics of LLDPE/ZrO_2 nanocomposite synthesized by in-situ polymerization using a zirconocene/MAO catalyst. **Iranian Polymer Journal** 15 (2006): 431-437.

[11] Nawang, R., Danjaji, I. D., Ishiaku, U. S., Ismail, H., and Ishak, Z. A. M.

Mechanical properties of sago starch-filled linear low density polyethylene (LLDPE) composites. **Polymer Testing** 20 (2001): 167-172.

[12] Verbeek, C. J. R. Highly filled polyethylene/phlogopite composites. **Materials Letters** 52 (2002): 453-457.

[13] Haung, Y., Zhang, Y. Q., Hua,Y. Q. Studies on dynamic mechanical and rheological properties of LLDPE/nano-SiO_2 composites. **Journal Materials Science Letters** 22 (2003): 997-998.

[14] Rossi, G. B., Beaucage, G., Dang, T. D., Vaia, R. A. Bottom-up synthesis of polymer nanocomposites and molecular composites: ionic exchange with PMMA latex. **Nano Letters** 2 (2002): 319-323.

[15] Cheng, W., Wang, Z., Ren, C., Chen, H., Tang, T. Preparation of silica/polyacrylamide/polyethylene nanocomposite via in situ polymerization **Materials Letters** 61 (2007): 3193-3196.

[16] Jongsomjit, B., Panpranot, J., Praserthdam, P. Effect of nanoscale SiO_2 and ZrO_2 as the fillers on the microstructure of LLDPE nanocomposites synthesized via in situ polymerization with zirconocene. **Materials Letters** 61 (2007): 1376-1369.

[17] Jongsomjit, B., Ngamposri, S., Praserthdam, P. Catalytic activity during copolymerization of ethylene and 1-hexene via mixed TiO_2/SiO_2-supported MAO with rac-Et[Ind] $_2ZrCl_2$ metallocene catalyst. **Molecules** 10 (2005): 672-678.

[18] Kaminsky, W. and Laban, A. Metallocene catalysis. **Applied Catalysis A: General** 222 (2001): 47-61.

[19] Kaminsky, W. The discovery of metallocene catalysts and their present state of the art. **Journal Polymer Science Part A: Polymer Chemistry** 42 (2004): 3911-3921.

[20] Kristen, M. O. Supported metallocene catalysts with MAO and boron activators. **Topic in Catalysis** 7 (1999): 89-95.

[21] Mashima, K., Nakayama, Y., and Nakamura, A. Recent trends in the polymerization of α-olefins catalyzed by organometallic complexes of early transition metals. **Advances Polymer Science** 133 (1997): 1-51.

[22] Reichert, K. H., Meyer, K. R. **Macromolecule Chemistry** 169 (1973): 163-176.

[23] Andersen, A., Cordes, H.G., Herwig, J., Kaminsky, K., Merck, A., Mottweiler, R., Pein, J., Sinn, H., Vollmer, H.J. Halogen-free soluble ziegler catalysts for the polymerization of ethylene. control of molecular weight by choice of temperature. **Angewandte Chemie International Edition in English** 15 (1976): 630-632.

[24] Sinn, H., Kaminsky, W. Ziegler-Natta catalyst. **Advances in Organometallic Chemistry** 18 (1980): 99-149.

[25] Wild, F. R. W. P., Zsolnai, L., Huttner, G., and Brintzinger, H. H. *Ansa*-metallocene derivatives IV. synthesis and molecular structures of chiral *ansa*-titanocene derivatives with bridged tetrahydroindenyl ligands. **Journal of Organometallic Chemistry** 232 (1982): 233-247.

[26] Ewen, J. A., Jones, R. L., Razavi, A., and Ferrara, J. P. Syndiospecific propylene polymerizations with group 4 metallocenes. **Journal of the American Chemical Society** 110 (1988): 6255-6256.

[27] Alt, H. The heterogenization of homogeneous metallocene catalysts for olefin polymerization. **Journal of the Chemical Society, Dalton Transactions** (1999): 1703-1709.

[28] Coates, G. W. Precise control of polyolefin stereo chemistry using single-site metal catalysts. **Chemical Reviews** 100 (2000): 1223-1252.

[29] Long N. J. Metallocenes: An introduction to sandwich complexs London, Blackwell Science Ltd., 1998.

[30] Gupta, V. K.; Satish, S. and Bhardwaj, I. S. Metallocene complexes of group 4 elements in the polymerization of monoolefins. **Journal of Macromolecular Science - Reviews in Macromolecular Chemistry and Physics** C34, No.3 (1994): 439-514.

[31] Naga, N. and Imanishi, Y. Recent developments in olefin polymerizations with transition metal catalysts. **Progress in Polymer Science** 26 (2001): 1147-1198.

[32] Pédeutour, J. N., Radhakrishnan, K., Cramail, H., and Deffieux, A. Use of "TMA depleted" MAO for the activation of zirconocene in olefin polymerization. **Journal of Molecular Catalysis A: Chemical** 185 (2002): 119-125.

[33] Scheirs, J., and Kaminsky, W. **Metallocene-based Polyolefins.** vol. 1, West Sussex, :Wiley, 2000.

[34] Pédeutour, J.N., Radhakrishnan, K., Cramail, H., and Deffieux, A. Influence of X

ligand nature in the activation process of racEt(Ind)$_2$ZrX$_2$ by methylaluminoxane. **Journal of Molecular Catalysis A: Chemical** 176 (2001): 87-94.

[35] Cam, D., and Giannini, U. **Macromolecule Chemistry** 193 (1992): 1049-1055.

[36] Soga, K., Kim, H. J., and Shiono, T. Polymerization of ethylene with homogeneous metallocene catalysts activated by common trialkylaluminums and Si(CH$_3$)$_3$OH. **Macromolecular Chemistry Rapid Communication** 14 (1993): 765-770.

[37] Katayama, H., Shiraishi, H., Hino, T., Ogane, T., and Imai, A. The effect of aluminum compounds in the copolymerization of ethylene α-olefins. **Macromolecular Symposia** 97 (1995): 109-118.

[38] Jongsomjit, B., Ngamposri, S., and Preserthdam, P. Catalytic activity during copolymerization of ethylene and 1-hexene via mixed TiO$_2$/SiO$_2$-supported MAO with rac-Et[Ind]$_2$ZrCl$_2$ metallocene catalyst. **Molecules.** 10 (2005): 603-609.

[39] Ko, Y. S., and Woo, S. I. Copolymerization of Ethylene and α-Olefin Using Et(Ind)$_2$ZrCl$_2$ Entrapped inside the Regular and Small Pores of MCM-41. **Macromolecular Chemistry and Physics** 202 (2001): 739-744.

[40] Jongsomjit, B., Kaewkrajang, P., Shiono, T., and Praserthdam, P. Supporting effect of silica-supported methylaluminoxane (MAO) with zirconocene catalyst on ethylene/1-olefin copolymerization behaviors for linear low-density polyethylene (LLDPE) production. **Industrial and Engineering Chemistry Research** 43 (2004): 7959-7963.

[41] Przybyla, C., Tesche, B., and Fink, G. Ethylene hexane copolymerization with the heterogeneous catalyst system SiO$_2$/MAO/rac-Me$_2$Si[2-Me-4-Ph-Ind]$_2$ZrCl$_2$: the filter effect. **Macromolecular Rapid Communications** 20 (1999): 328-332.

[42] Harkki, O., Lehmus, P., Leino, R., Luttikhedde, H. J. G., Nasman, J. H., and Seppala, J. V. Copolymerzation of ethylene with 1-hexene or 1-hexadecene over siloxy-substituted. **Macromolecular Chemistry and Physics** 200 (1999): 1561-1565.

[43] Cheruvu, S. **US Pat 5608019** (1997).

[44] Albano, C., Sanchez, G., and Ismayel, A. Influence of a copolymer on the mechanical properties of a blend of PP and recycled and non-recycled HDPE. **Polymer Bulletin** 41 (1998): 91-98.

[45] Shan, C. L. P., Soares, J. B. P., and Penlidis, A. Ethylene/1-octene copolymerization studies with in situ supported metallocene catalysts: Effect of polymerization parameters on the catalyst activity and polymer microstructure. **Journal Polymer Science Part A: Polymer Chemistry** 40 (2002): 4426-4451.

[46] Pietikainen, P., and Seppala, J. V. Low molecular weight ethylene/propylene copolymers. Effect of process parameters on copolymerization with homogeneous Cp_2ZrCl_2 catalyst. **Macromolecules** 27 (1994): 1325-1328.

[47] Soga, K., and Kaminaka, M. Polymerization of propene with the heterogeneous catalyst system. **Macromolecular Chemistry Rapid Communications** 13 (1992): 221-224.

[48] Nowlin, T. E., Kissin, Y. V., and Wagner, K. P. High activity Ziegler-Natta catalyst for the preparation of ethylene copolymers. **Journal Polymer Science Part A: Polymer Chemistry** 26 (1988): 755-764.

[49] Quijada, R., Galland, G. B., and Mauler, R. S. The influence of the comonomer in the copolymerization of ethylene with α-olefins using $C_2H_4[Ind]_2ZrCl_2$/methylaluminoxane as catalyst system **Macromolecular Chemistry and Physics** 197 (1996): 3091-3098.

[50] Soga, K., Uozumi, T., Arai, T., and Nakamura, S. Heterogeneity of active species in metallocene catalysts. **Macromolecular Rapid Communications** 16 (1995): 379-385.

[51] de Fatima V. Marques, M., Conte, A. F., de Resende, C., and Chaves, E. G. Copolymerization of ethylene and 1-octene by homogeneous and different supported metallocenic catalysts. **Journal of applied polymer science** 82 (2001): 724-730.

[52] Kim, J. D., and Soares, J. B. P. Copolymerization of ethylene and 1-hexene with supported metallocene catalysts: Effect of support treatment. **Macromolecular Rapid Communications** 20 (1999): 347-350.

[53] Chu, K. J., Shan, C. L. P., Soares, J. B. P., and Penlidis, A. Copolymerization of

ethylene and 1-hexene with in-situ supported Et[Ind]$_2$ZrCl$_2$. **Macromolecular Chemistry and Physics** 200 (1999): 2372-2376.

[54] Chu, K. J., Soares, J. B. P., and Penlidis, A. Variation of molecular weight distribution (MWD) and short chain branching distribution (SCBD) of ethylene/1-hexene copolymers produced with different in-situ supported metallocene catalysts. **Macromolecular Chemistry and Physics** 201 (2000): 340-348.

[55] Shan, C. L. P., Chu, K. J., Soares, J. B. P., and Penlidis, A. Using alkylaluminum activators to tailor short chain branching distributions of ethylene/1-hexene copolymers produced with in-situ supported metallocene catalysts. **Macromolecular Chemistry and Physics** 201 (2000): 2195-2202.

[56] Kaminsky, W., and Renner, F. High melting polypropylenes by silica supported zirconocene catalysts. **Macromolecular Chemistry Rapid Communication** 14 (1995): 239-243.

[57] Chien, J. C., and He, D. Olefin copolymerization with metallocene catalysts. III. Supported metallocene/methylaluminoxane catalyst for olefin copolymerization. **Journal Polymer Science Part A: Polymer Chemistry** 29 (1991): 1603-1607.

[58] Chen, Y. X., Rausch, M. D., and Chien, J. C. Heptane soluble homogeneous zirconocene catalyst: Synthesis of a single diastereomer, polymerization catalysis, and effects of silica supports. **Journal Polymer Science Part A: Polymer Chemistry** 33 (1995): 2093-2108.

[59] Soga, K., and Kaminaka, M. Polymerization of propene with the heterogeneous catalyst system Et[IndH$_4$]$_2$ZrCl$_2$/MAO/SiO$_2$ combined with trialkylaluminium. **Macromolecular Chemistry Rapid Communication** 13 (1992): 221-224.

[60] Soga, K., and Kaminaka, M. Copolymerization of olefins with SiO$_2$-, Al$_2$O$_3$-, and MgCl$_2$-supported catalysts activated by trialkylaluminiums. **Macromolecular Chemistry and Physics** 195 (1994) 1369-1379.

[61] Soga, K., and Kaminaka, M. Polymerization of propene with a rac-(CH$_3$)$_2$Si(2,4-(CH$_3$)$_2$C$_5$H$_3$)(3′,5′-(CH$_3$)$_2$C$_5$H$_3$)ZrCl$_2$/MAO/SiO$_2$-Al-(iC$_4$H$_9$)$_3$ catalyst system. **Macromolecular Rapid Communications** 15 (1994): 593-600.

[62] Soga, K., Arai, T., Nozawa, H., and Uozomi, T. Recent development in

heterogeneous metallocene catalysts. **Macromolecular Symposia** 97 (1995): 53.

[63] Jin, J., Uozomi, T., Soga, K. Ethylene polymerization initiated by SiO_2-supported neodymocene catalysts. **Macromolecular Rapid Communications** 16 (1995): 317-322.

[64] Jordan, J., Jaco, K. I., Tannenbaum, R., Shara, M. A., and Jasiuk, I. Experimental trends in polymer nanocomposites. **Materials Science and Engineering A** 393 (2005): 1-11.

[65] Su, B., Liu, X., Peng, X., Xiao, T., and Su, Z. Preparation and characterization of the TiO_2/polymer complex nanomaterial. **Materials Science and Engineering A** 343 (2003): 59-62.

[66] Ma, D., Akpalu, Y. A., Li, Y., Siegel, R. W., and Schadler, L. S. Effect of titania nanoparticles on the morphology of low density polyethylene. **Journal of polymer science: Part B: Polymer Physics** 43 (2005): 488-497.

[67] Liu, G., Li, Y-F., Yan, F-Y., Zhao, Z-X., Zhou, L-C., and Xue, Q-J. Effect of nanoscale SiO_2 and TiO_2 as the fillers on the mechanical properties and aging behavior of linear low-density polyethylene/low-density polyethylene blends. **Journal of polymers and the environment** 13 (2005): 339-348.

[68] Chau, J. L. H., Lin, Y-M., Li, A-K., Su, W-F., Chang, K-S., Hsu, S. L-C., and Li, T-L. Transparent high refractive index nanocomposite thin films. **Materials letters** 61 (2007): 2908-2910.

[69] Nakayama, N., and Hayashi, T. Preparation and characterization of TiO_2 and polymer nanocomposite films with high refractive index. **Journal of applied polymer science** 105 (2007): 3662-3672.

[70] Hagimoto, H., Shiono, T., and Ikeda, T. Supporting effects of methylaluminoxane on the living polymerization of propylene with a chelating (diamide) dimethyltitanium complex. **Macromolecular Chemistry and Physics** 205 (2004): 19-26.

[71] Randall, J. C. A review of high resolution liquid ^{13}C nuclear magnetic resonance characterization of ethylene-based polymers. **Journal of Macromolecular**

Science, Reviews in Macromolecular Chemistry and Physics C29 (1989): 201.

[72] Desharun, D., Jongsomjit, B., and Praserthdam, P. Study of LLDPE/alumina nanocomposites synthesized by in situ polymerization with zirconocene/d-MMAO catalyst. **Catalysis communications** 9 (2008): 522-528.

[73] Severn, J. R., Chadwick, J. C., Duchateau, R., and Friederichs, N. "Bound but not gagged"-Immobilizing single-site α-olefin polymerization catalysts. **Chemical Reviews** 105 (2005): 4073-4147.

[74] Ketloy, C., Jongsomjit, B., and Praserthdam, P. Characteristics and catalytic properties of [t-BuNSiMe$_2$Flu]TiMe/dMMAO catalyst dispersed on various supports towards ethylene/1-octene copolymerization. **Applied Catalysis A: General** 327 (2007): 270-277.

[75] Galland, G. B., Quijada, P., Mauler, R. S., and de Menezes, R. S. Determination of reactivity ratios for ethylene/alpha-olefin copolymerization catalysed by the C$_2$H$_4$[Ind]$_2$ZrCl$_2$/methylaluminoxane system. **Macromolecular Rapid Communications** 17 (1996): 607-613.

[76] Alamo, R. G., and Mandelkern, L. Thermodynamic and structural properties of ethylene copolymers. **Macromolecules** 22 (1989): 1273-1277.

[77] Alamo, R. G., Viers, B.D., and Mandelkern, L. Phase structure of random ethylene copolymers: a study of counit content and molecular weight as independent variables. **Macromolecules** 26 (1993): 5740-5747.

[78] Simanke, A. G., Galland, G. B., Treitas, L. L., Jornada, J. A. H., and Quijada, R. Dynamic-mechanical properties of ethylene/alpha-olefin copolymers prepared by a metallocene catalyst. **Macromolecular Chemistry and Physics** 202 (2001): 172-179.

[79] Luyt, A. S., Molefi, J. A., and Krump H. Thermal, mechanical and electrical properties of copper powder filled low-density and linear low-density polyethylene composites. **Polymer Degradation and Stability** 91 (2006): 1629-1636.

[80] Chaichana, E., Jongsomjit, B., and Praserthdam, P. Effect of nano-SiO$_2$ particle size on the formation of LLDPE/SiO$_2$ nanocomposites synthesized via the in

situ polymerization with metallocene catalyst. **Chemical Engineering Science** 62 (2007): 899-905.

[81] Jongsomjit, B., Wongsalee, T., and Praserthdam, P. Characteristics and catalytic properties of Co/TiO$_2$ for various rutile:anantase ratios. **Catalysis Communications** 6 (2005): 705-710.

สถาบันวิทยบริการ

จุฬาลงกรณ์มหาวิทยาลัย
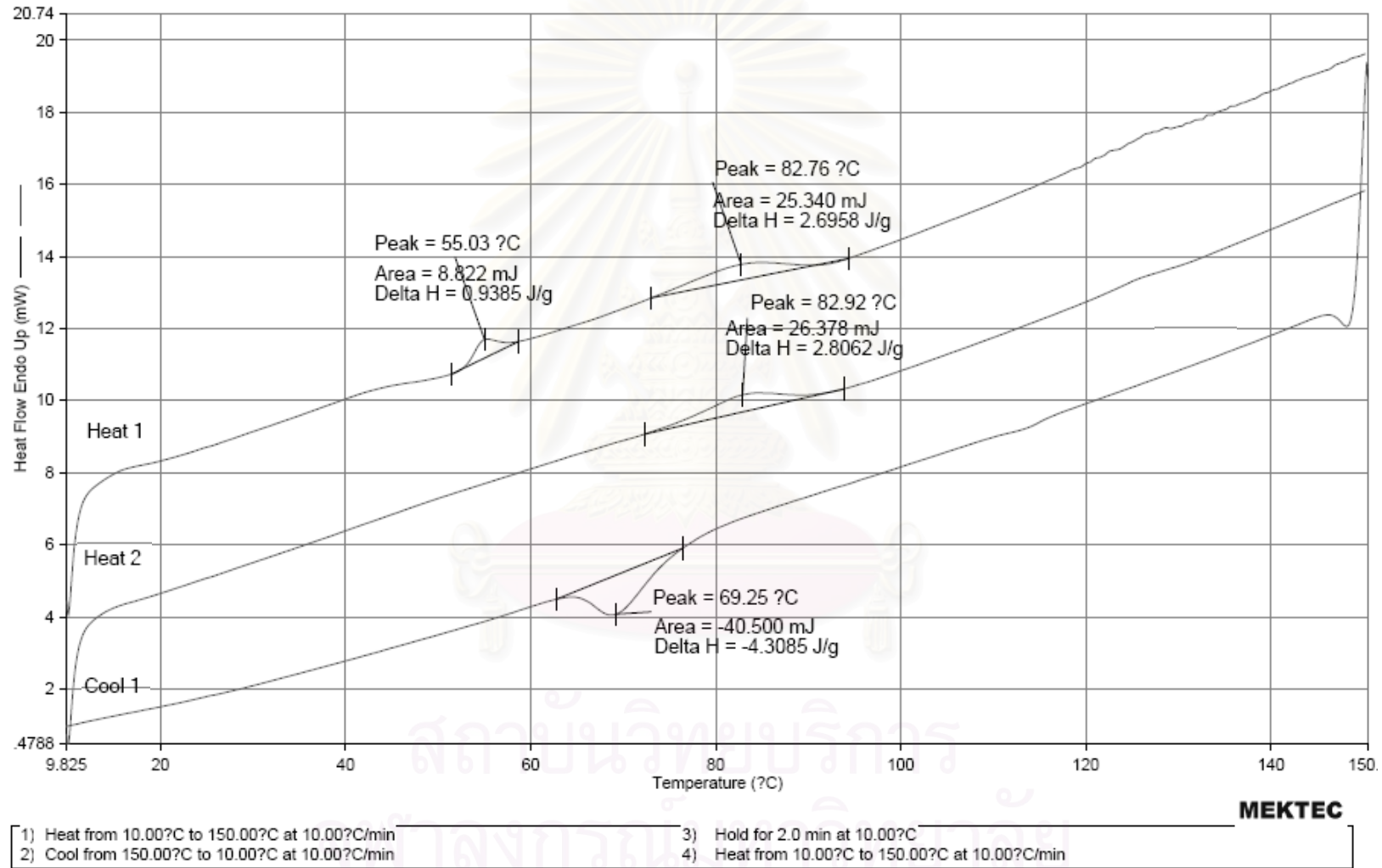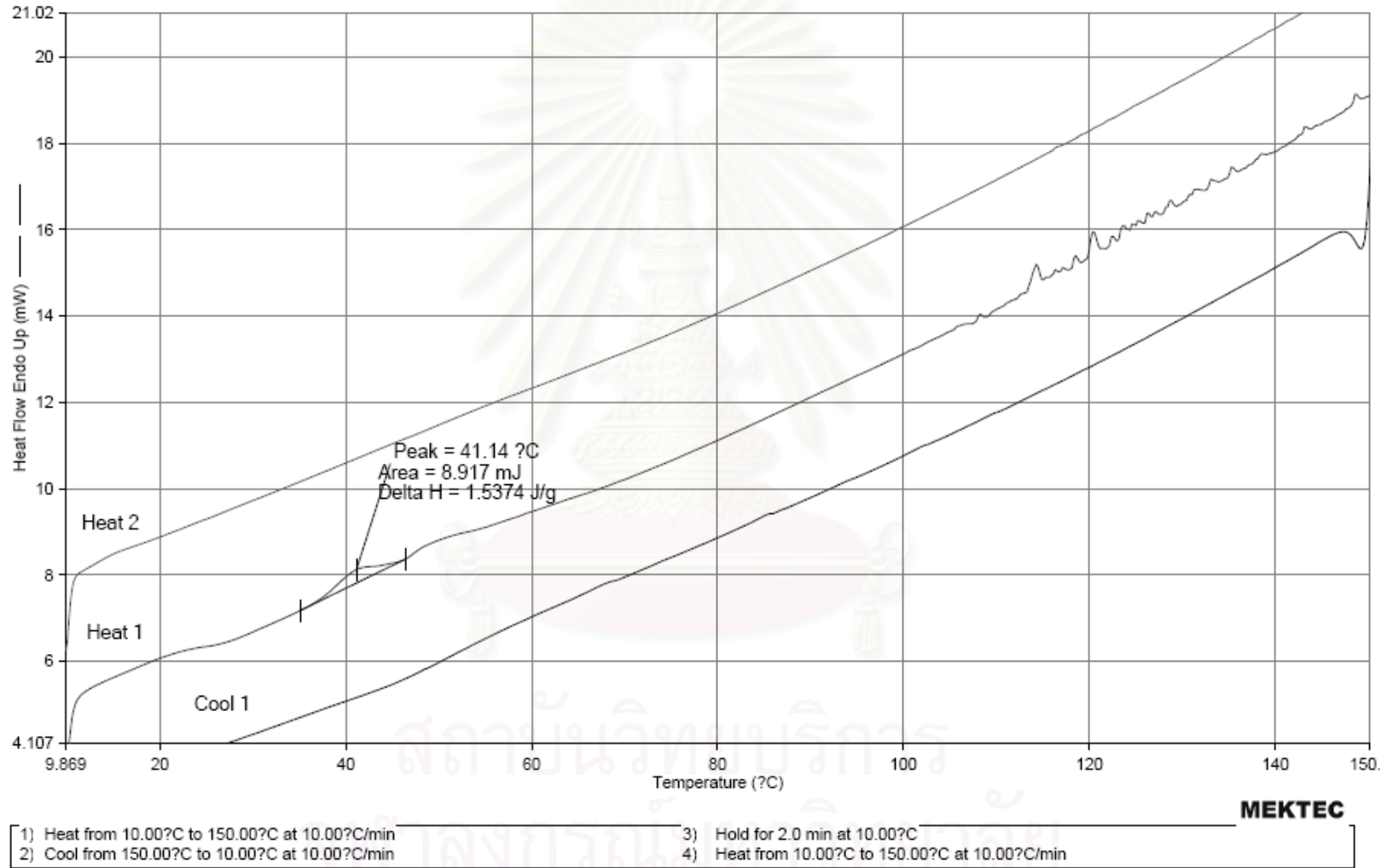
APPENDICES
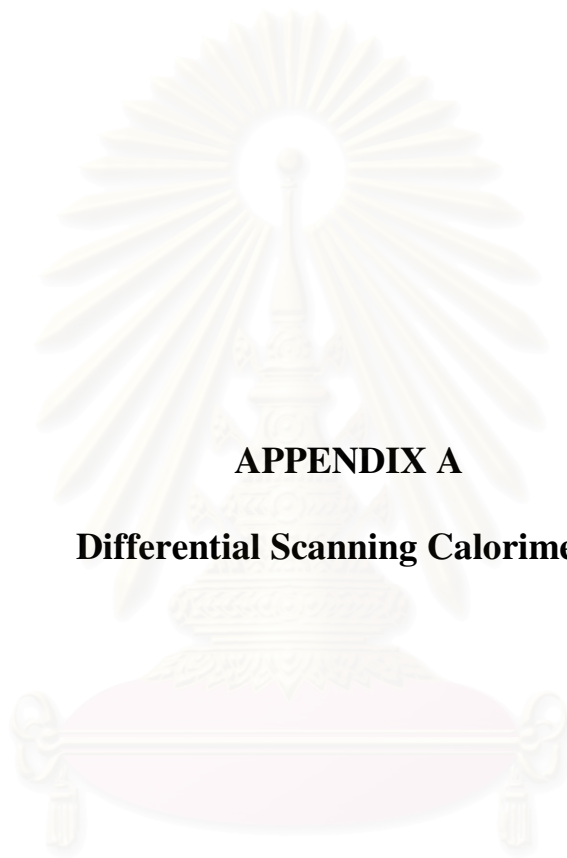
APPENDIX A

Differential Scanning Calorimeter
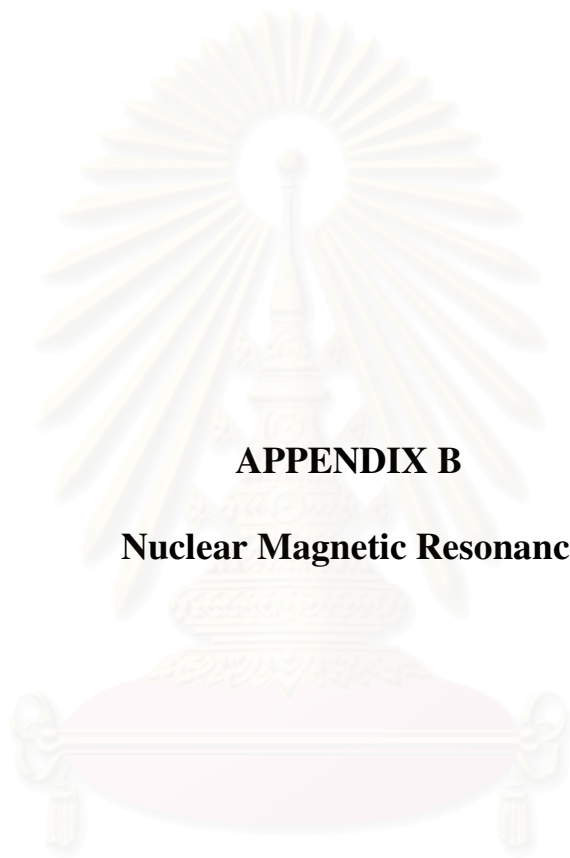
Figure A-1. DSC curve of LLDPE/TiO$_2$ (A) nanocomposites at Al/Zr = 1135

Figure A-2. DSC curve of LLDPE/TiO$_2$ (A) nanocomposites at Al/Zr = 2270
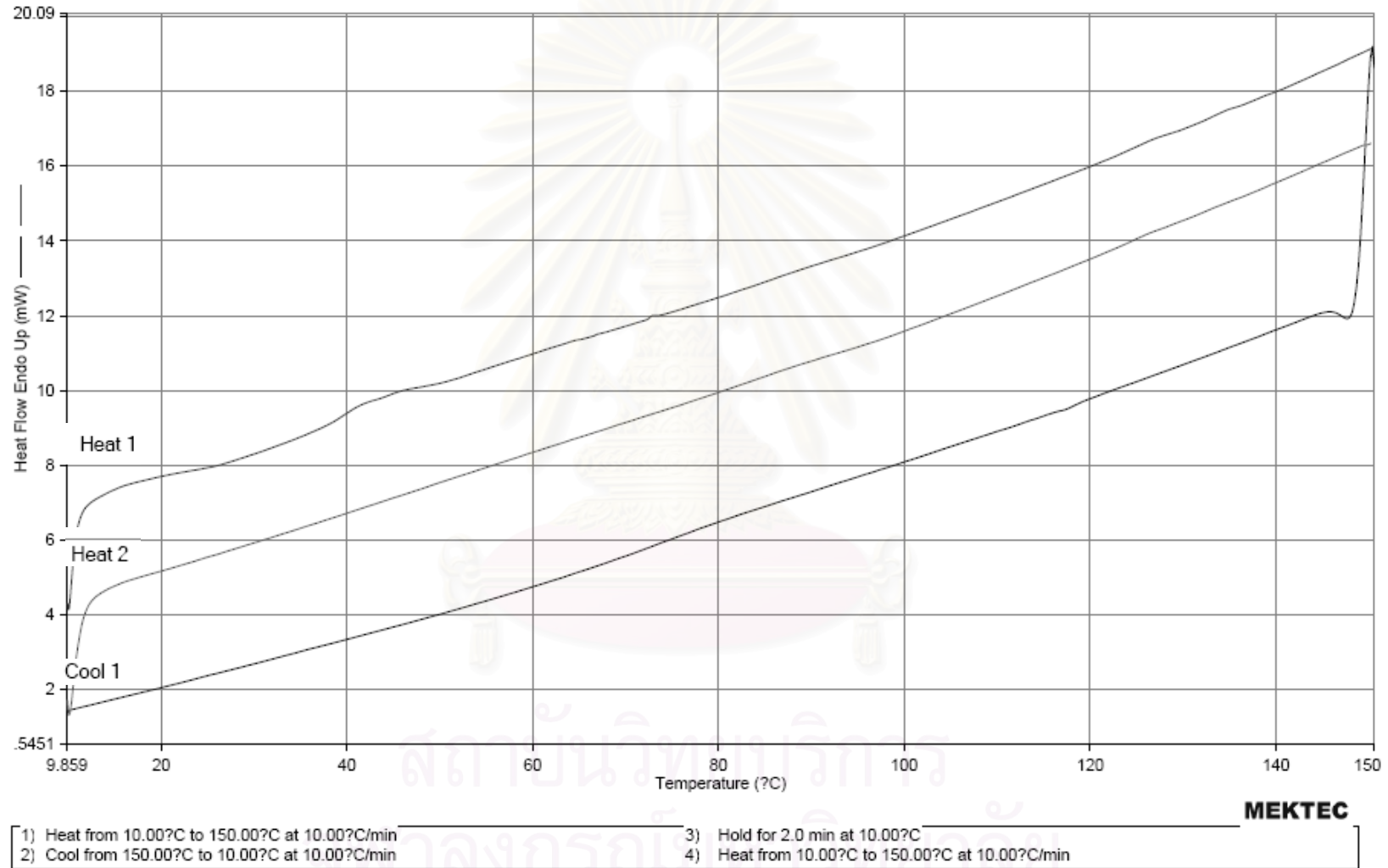
Figure A-3. DSC curve of LLDPE/TiO$_2$ (A) nanocomposites at Al/Zr = 3405
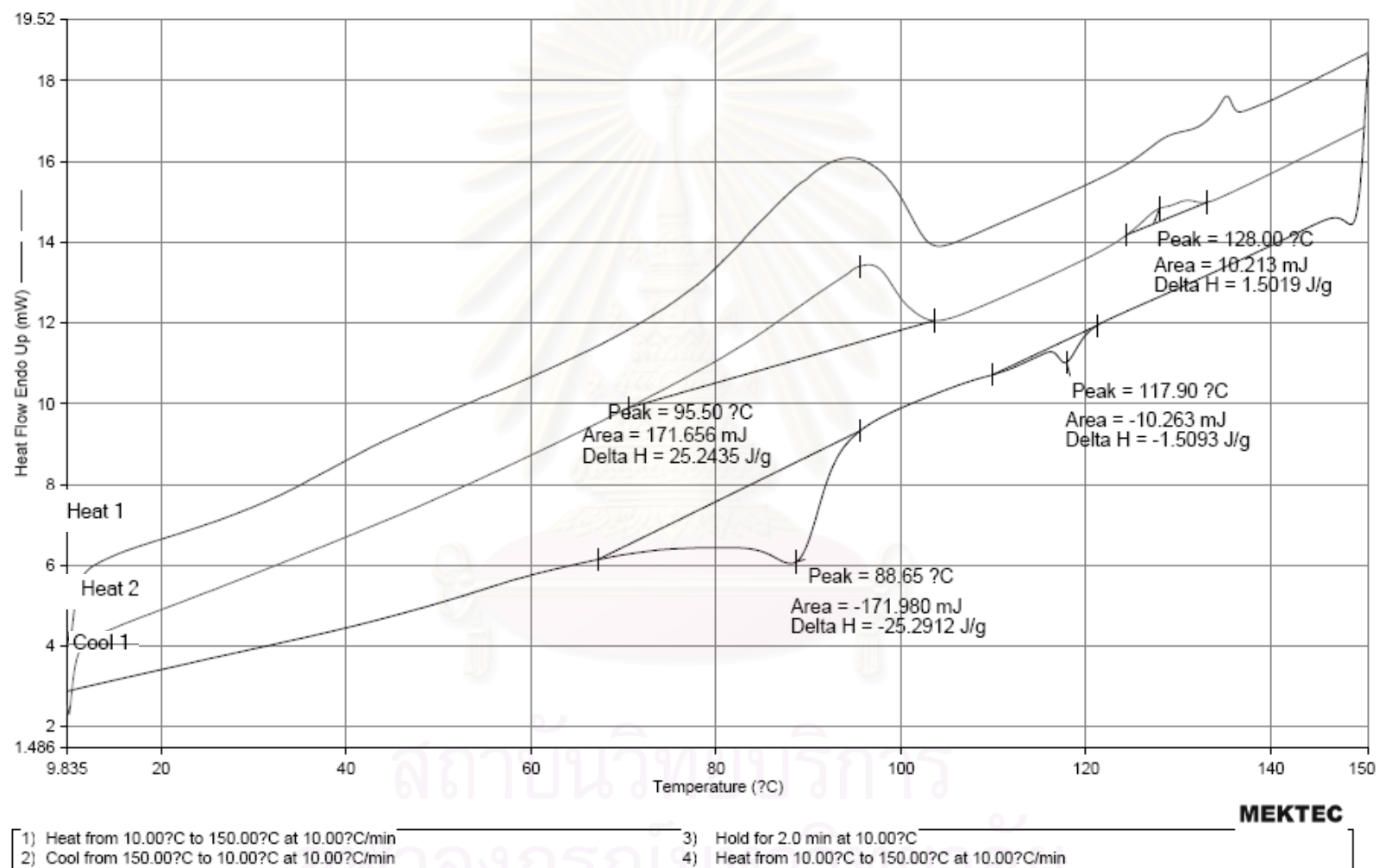
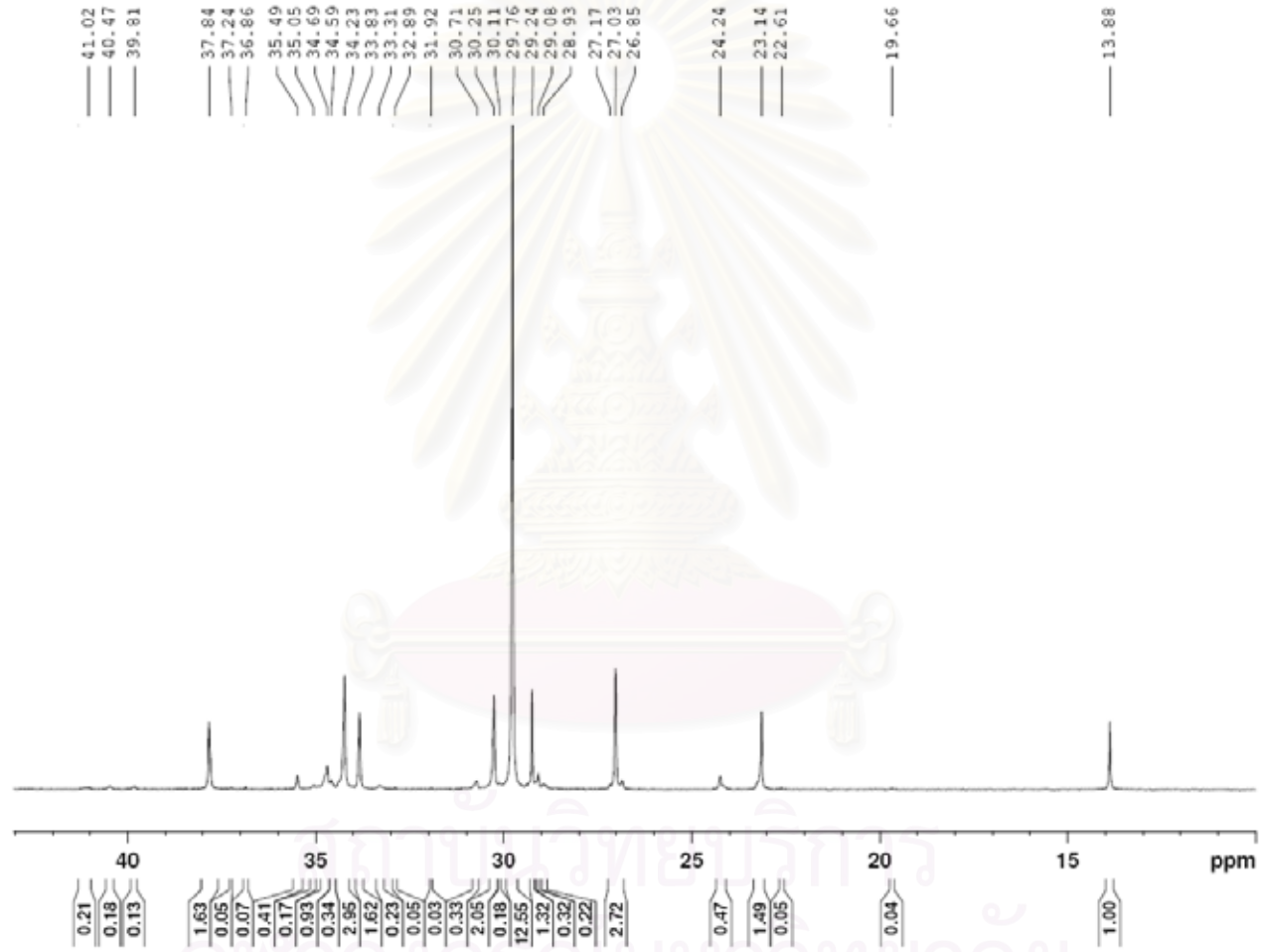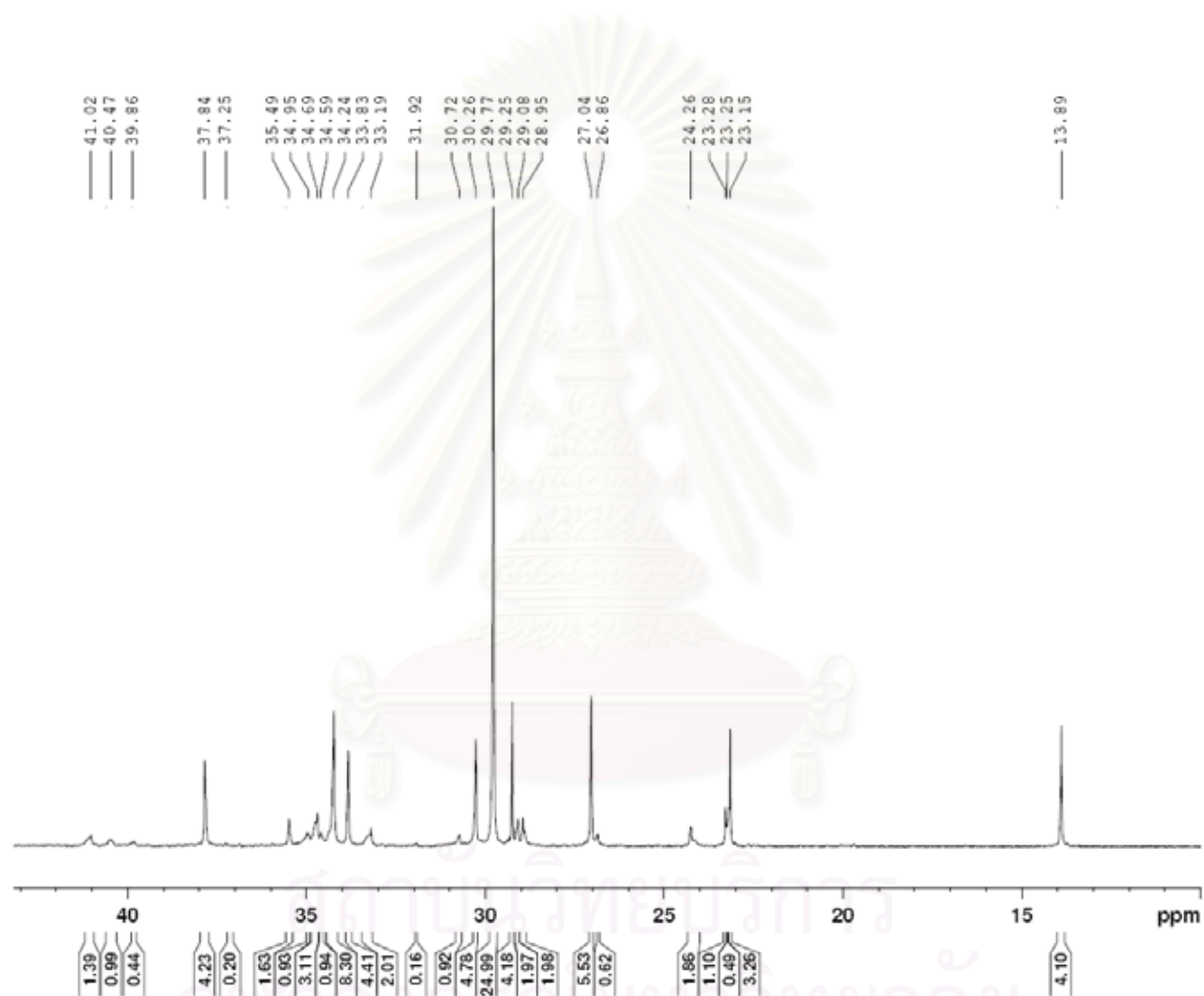**Figure A-4**. DSC curve of LLDPE/TiO$_2$ (R) nanocomposites at Al/Zr = 1135
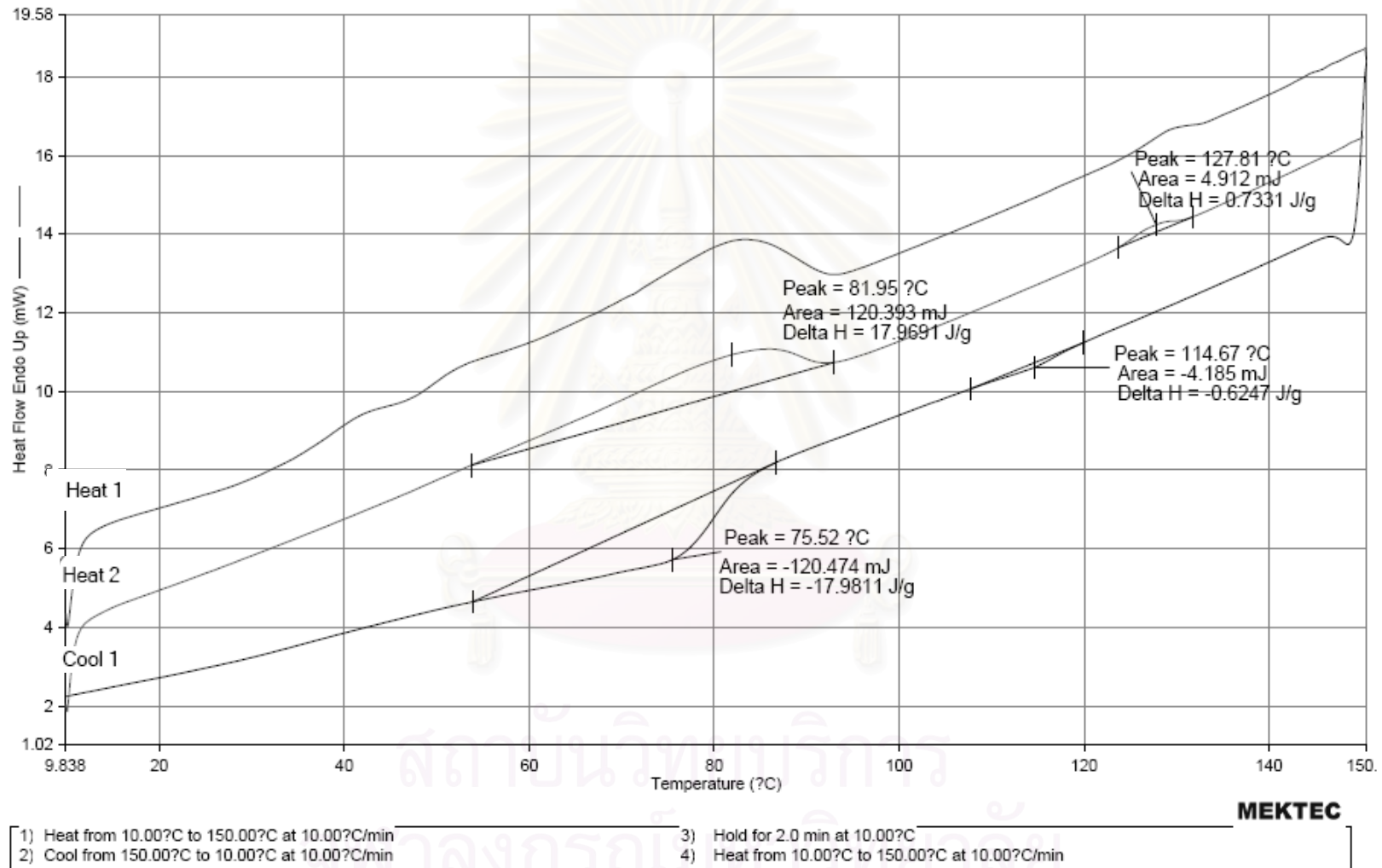
Figure A-5. DSC curve of LLDPE/TiO$_2$ (R) nanocomposites at Al/Zr = 2270
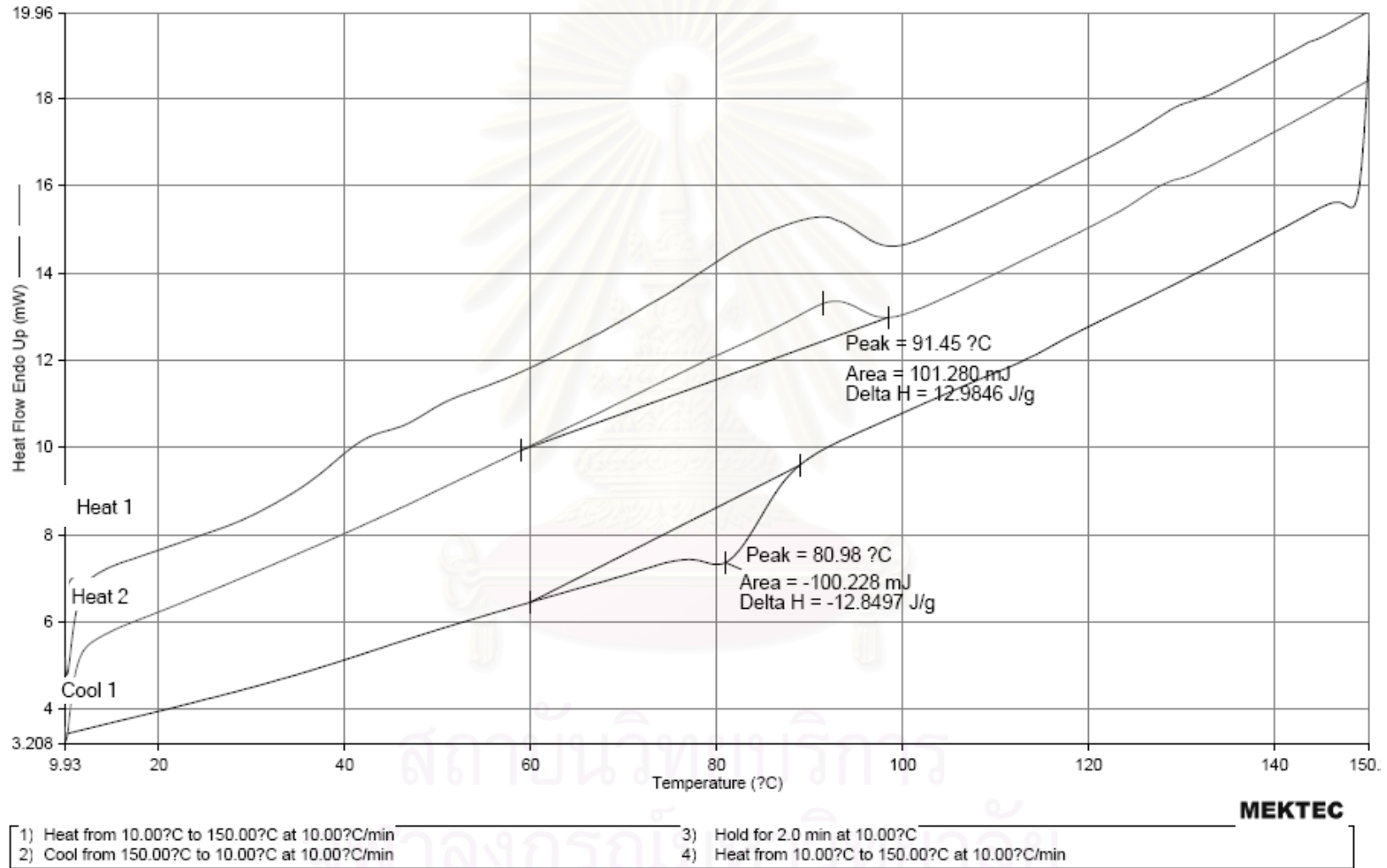
Figure A-6. DSC curve of LLDPE/TiO$_2$ (R) nanocomposites at Al/Zr = 3405
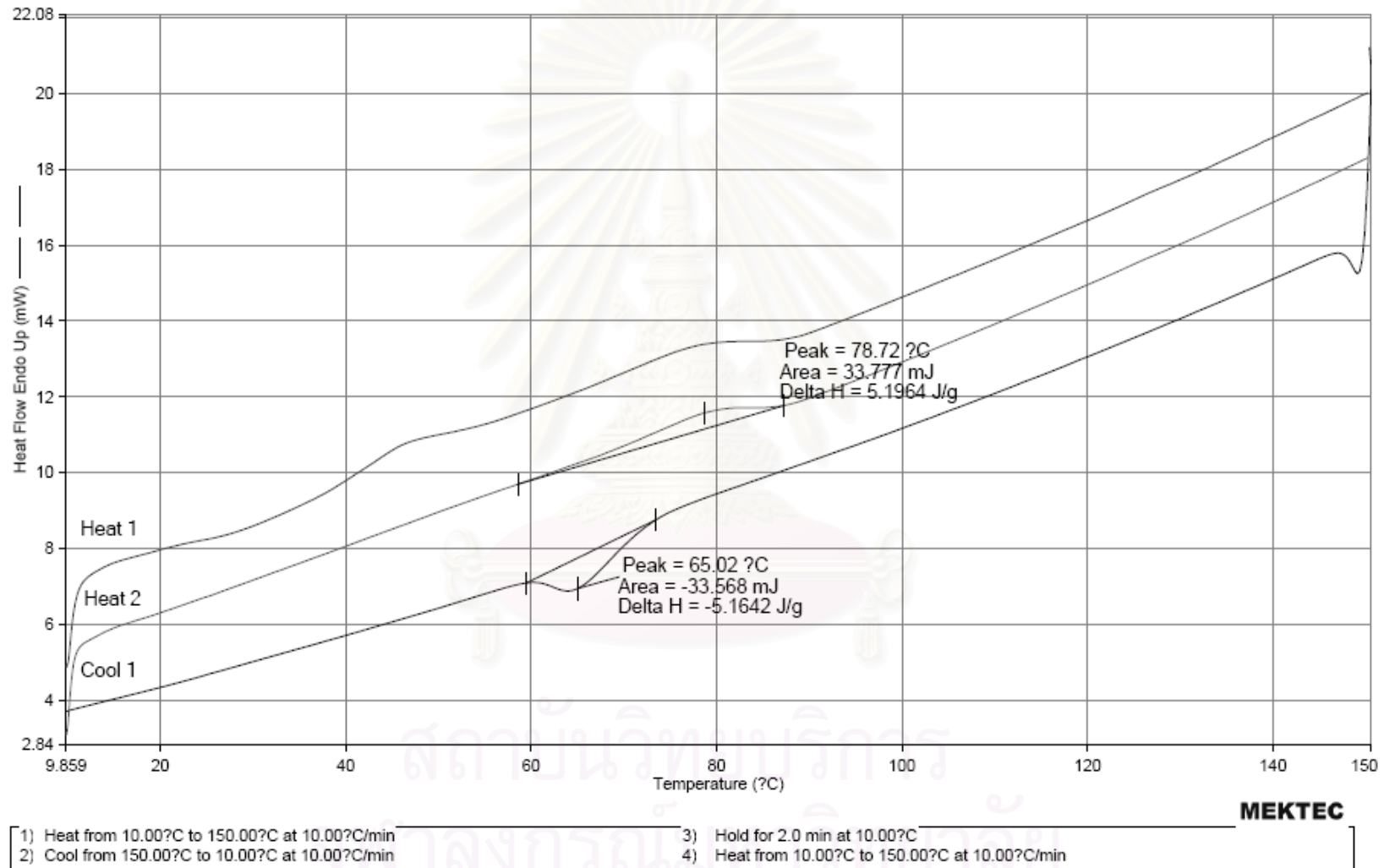
Figure A-7. DSC curve of LLDPE/TiO$_2$ (J) nanocomposites at Al/Zr = 2270
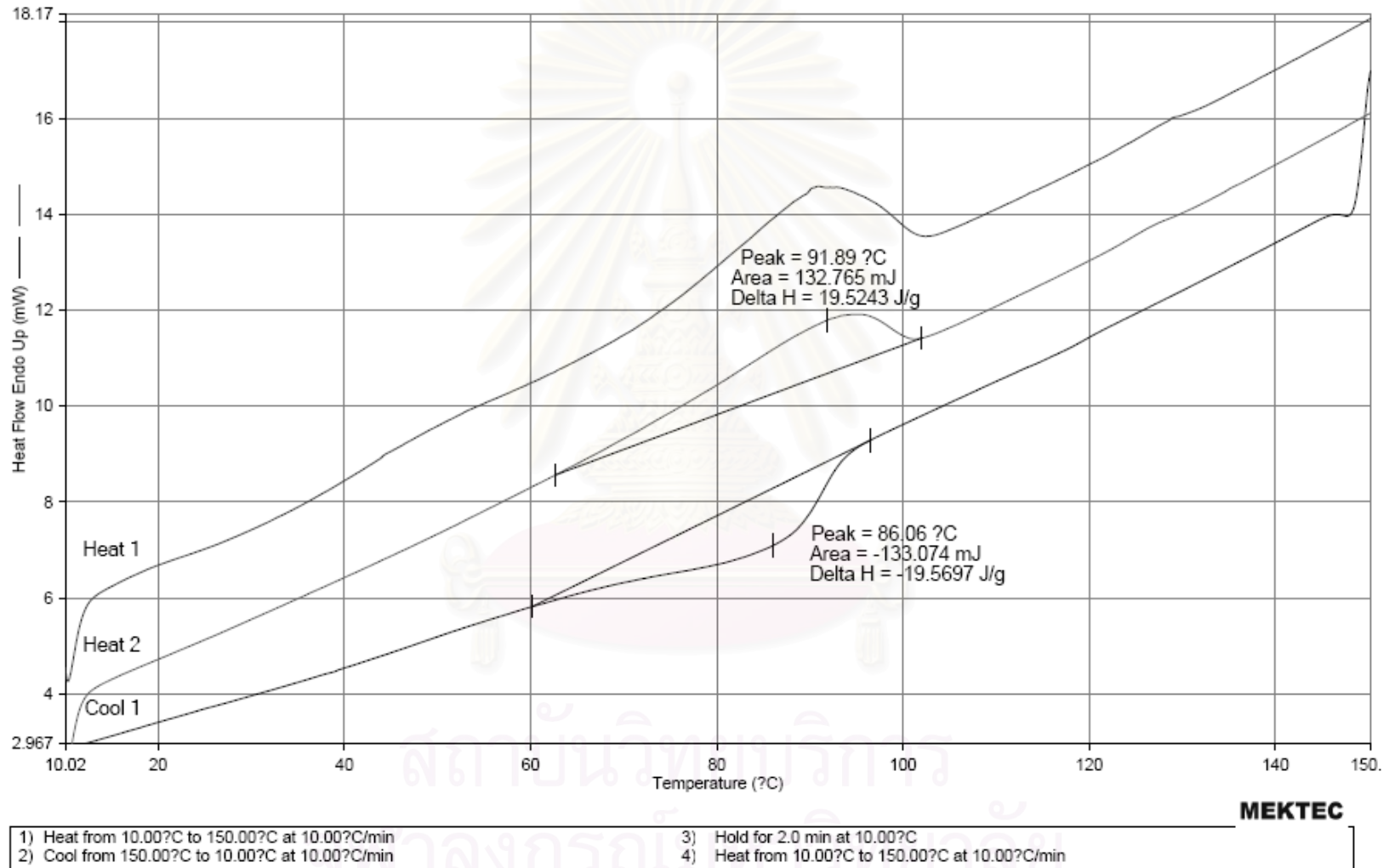
Figure A-8. DSC curve of LLDPE/TiO$_2$ (D) nanocomposites at Al/Zr = 2270

APPENDIX B

Nuclear Magnetic Resonance

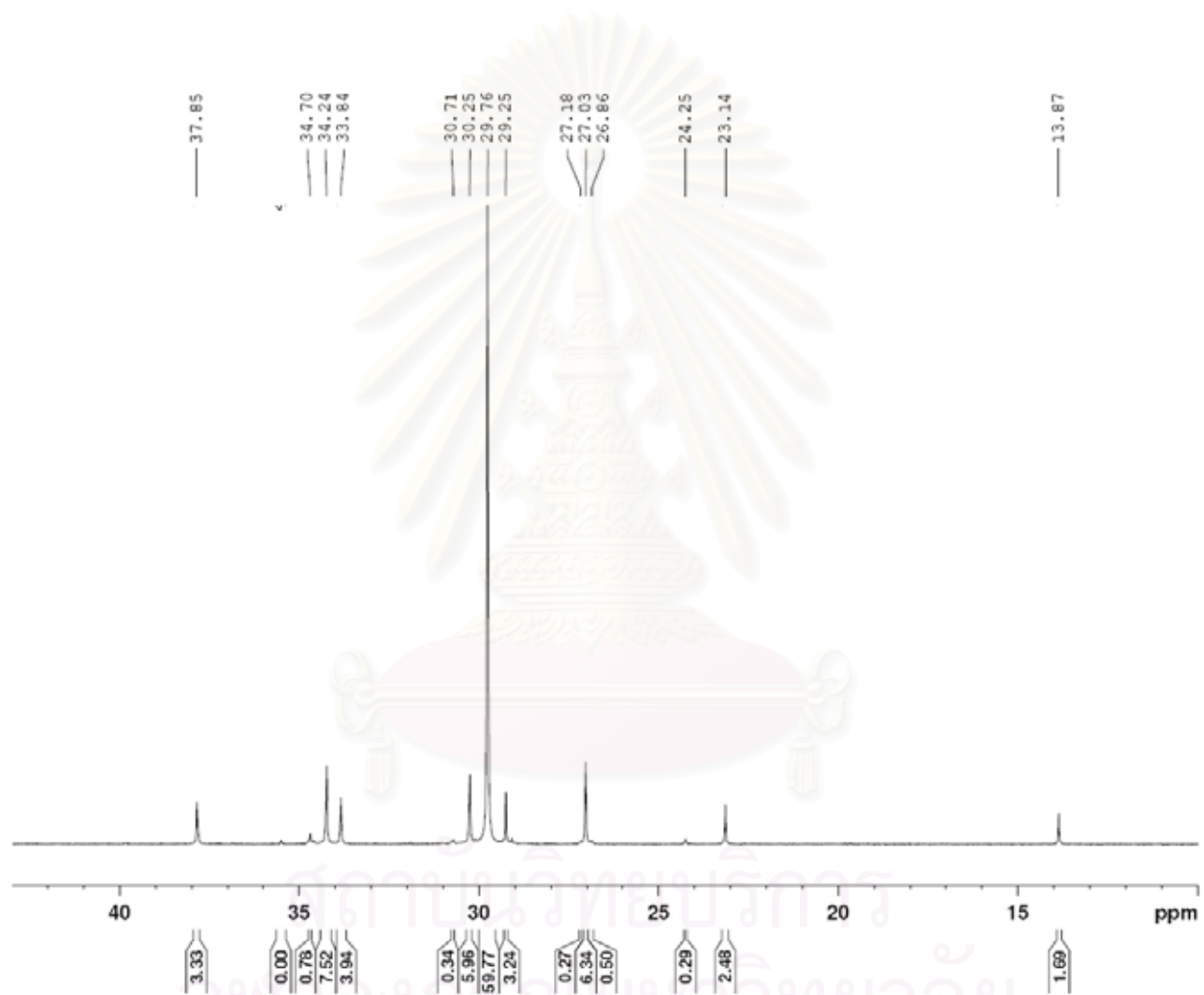**Figure B-1**. ^{13}C-NMR spectrum of LLDPE/TiO$_2$ (A) nanocomposites at Al/Zr = 1135

Figure B-2. ^{13}C-NMR spectrum of LLDPE/TiO$_2$ (A) nanocomposites at Al/Zr = 2270
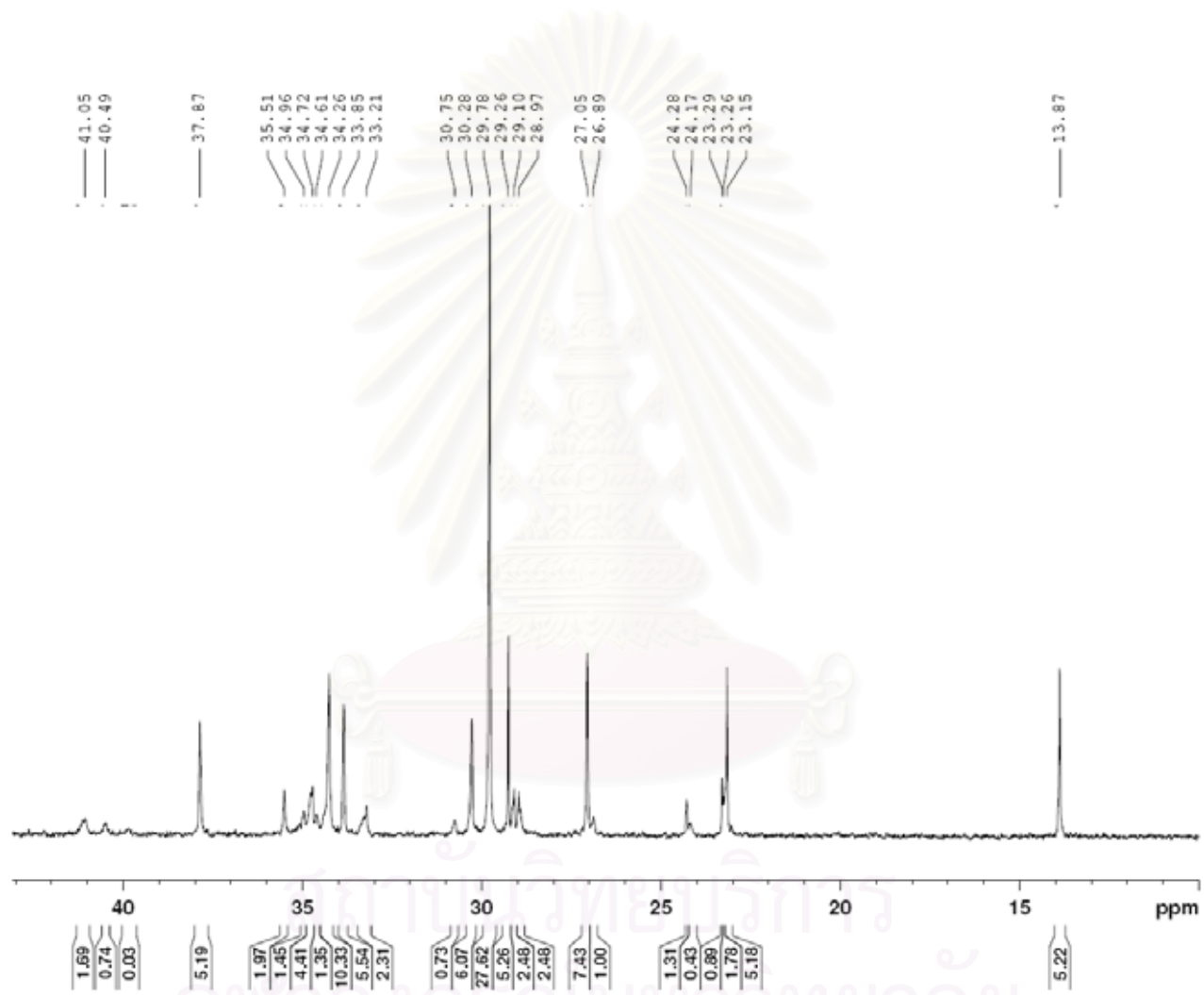
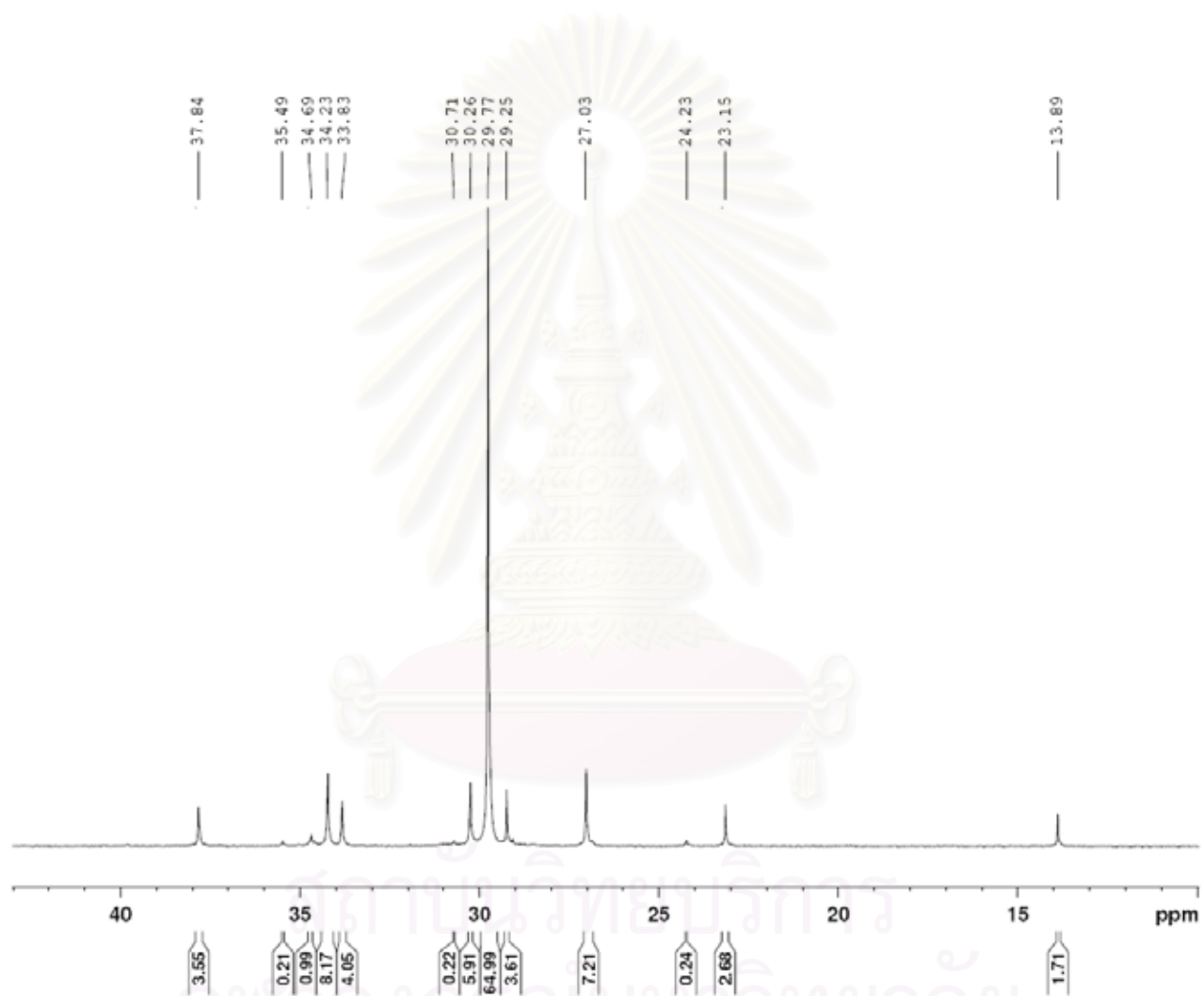**Figure B-3**. ^{13}C-NMR spectrum of LLDPE/TiO$_2$ (A) nanocomposites at Al/Zr = 3405
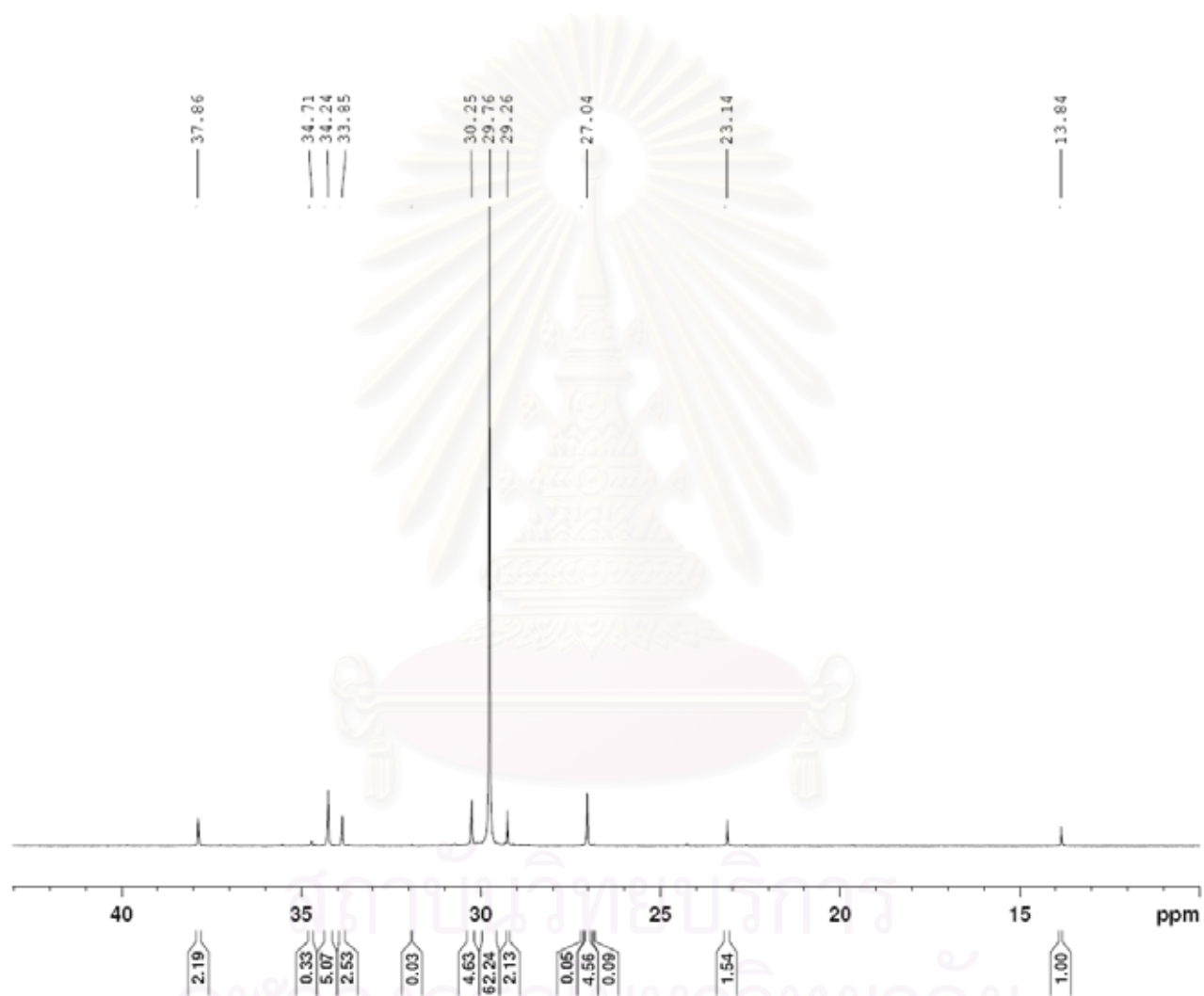
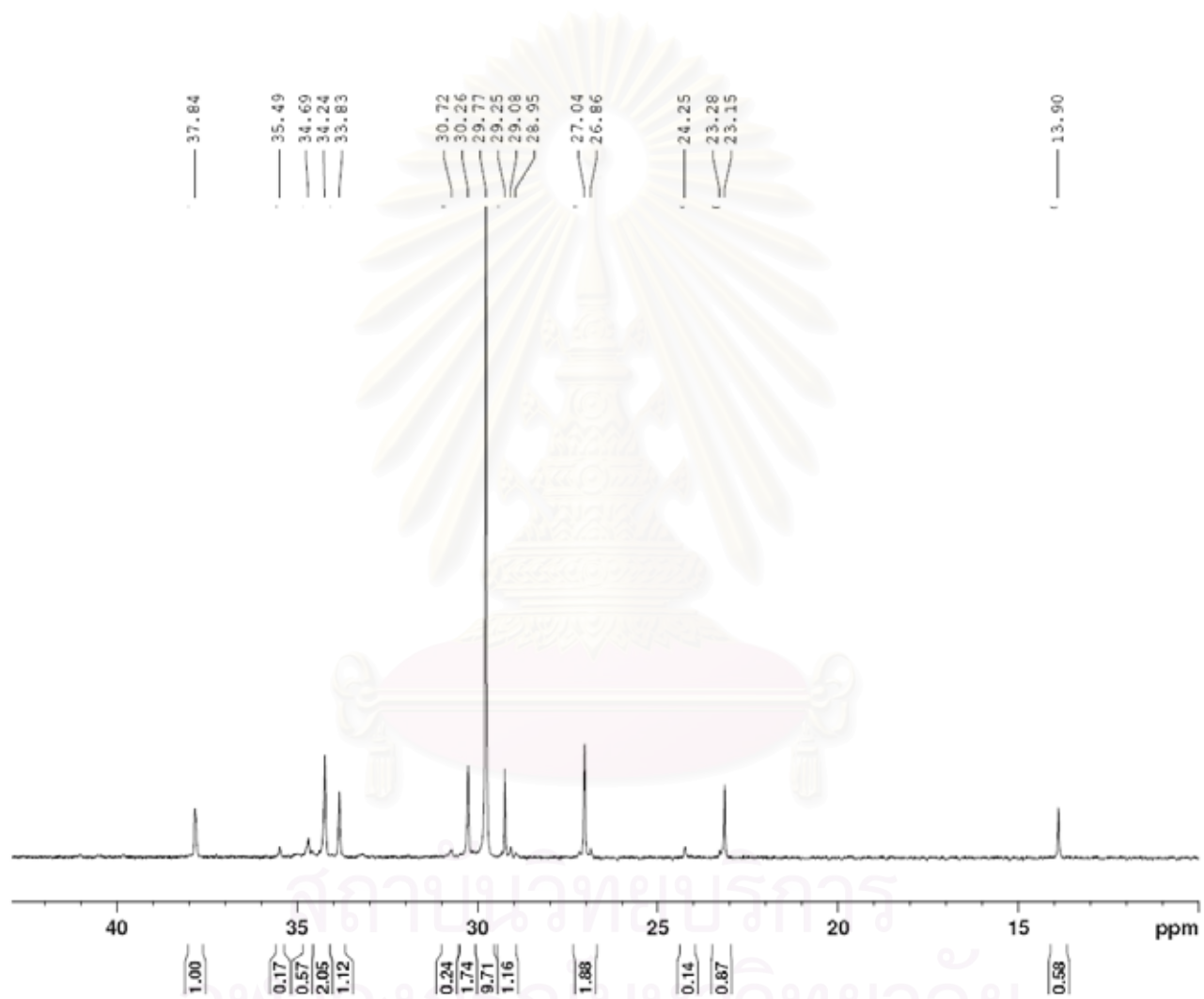**Figure B-4**. ^{13}C-NMR spectrum of LLDPE/TiO$_2$ (R) nanocomposites at Al/Zr = 1135

Figure B-5. ^{13}C-NMR spectrum of LLDPE/TiO$_2$ (R) nanocomposites at Al/Zr = 2270

Figure B-6. ^{13}C-NMR spectrum of LLDPE/TiO$_2$ (R) nanocomposites at Al/Zr = 3405

Figure B-7. ^{13}C-NMR spectrum of LLDPE/TiO$_2$ (J) nanocomposites at Al/Zr = 2270

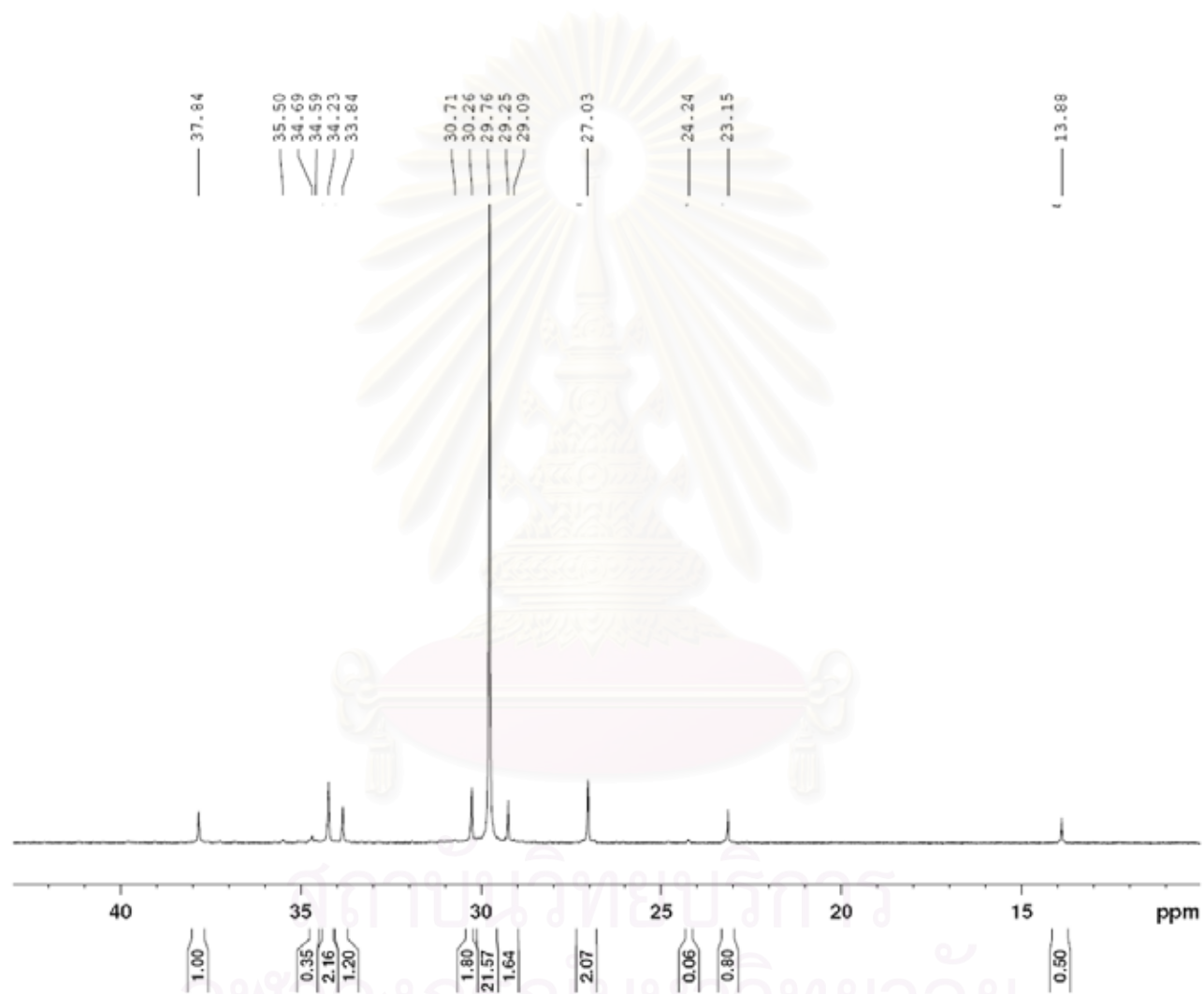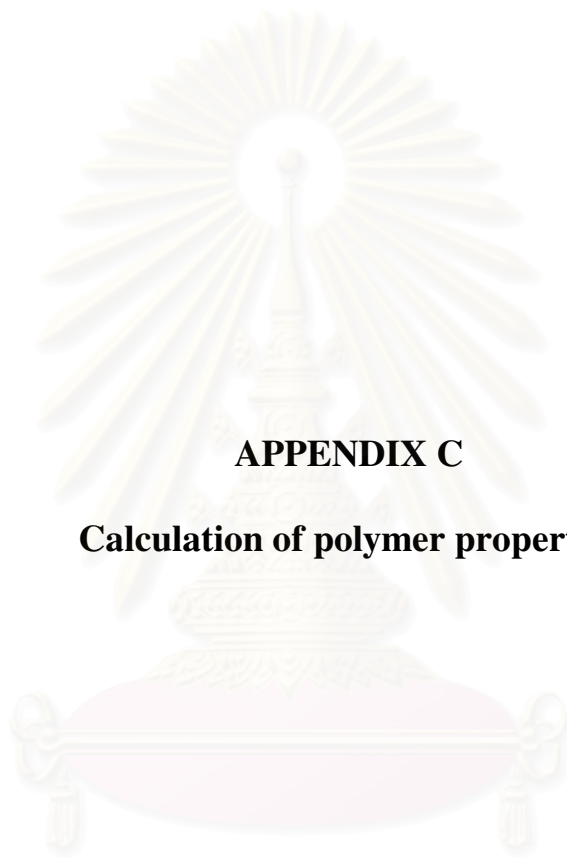**Figure B-8**. ^{13}C-NMR spectrum of LLDPE/TiO$_2$ (D) nanocomposites at Al/Zr = 2270

APPENDIX C

Calculation of polymer properties

Calculation of polymer microstructure

Polymer microstructure and also triad distribution of monomer can be calculated according to the Prof. James C. Randall as literature 75 in the list of reference. The detail of calculation was be interpreted as follow

Ethylene/1-hexene copolymer

The integral area of ^{13}C-NMR spectrum in the specify rage are listed.

T_A	=	39.5-42	ppm
T_B	=	38.1	ppm
T_C	=	33-36	ppm
T_D	=	26.5-27.5	ppm
T_F	=	24-25	ppm
T_G	=	23.4	ppm
T_H	=	14.1	ppm

Triad distribution was calculated as the followed formular

k[HHH]	=	$2T_A - T_C + T_G + 2T_F + T_E$
k[EHH]	=	$2T_C - 2T_G - 4T_F - 2T_E - 2T_A$
k[EHE]	=	T_B
k[EEE]	=	$0.5T_E - 0.5T_G - 0.25T_E$
k[HEE]	=	T_E
k[HEH]	=	T_F

Calculation of crystallinity for ethylene/1-olefin copolymer

The crystallinities of copolymers were determined by differential scanning calorimeter. % crystallynity of copolymers is calculated from equation.

$$\%Crystallinity = \frac{\Delta H_m}{\Delta H_m^o} \times 100$$

Where ΔH_m = the heat of fusion of sample (J/g)

ΔH_m^o = the heat of fusion of perfectly crystalline polyethylene

= 286 J/g

APPENDIX D

LIST OF PUBLICATION

1. Owpardit, W., Jongsomjit, B., and Praserthdam, P. "Synthesis of LLDPE/TiO$_2$ nanocomposites with ziconocene catalyst by *in situ* polymerization of ethylene/1-hexene" (The Proceeding of 17th Thailand Chemical Engineering and Applied Chemistry Conference, TIChE 2007).

2. Owpardit, W., Jongsomjit, B., and Praserthdam, P. "Characterization of LLDPE/TiO$_2$ nanocomposites synthesized by *in situ* polymerization with zirconocene/dMMAO catalyst" (The Submitted Paper to Applied Catalysis A: General).

3. Owpardit, W., and Jongsomjit, B. "A comparative study on synthesis of LLDPE/TiO$_2$ nanocomposites using different TiO$_2$ by *in situ* polymerization with zirconocene/dMMAO catalyst" (The Submitted Paper to Materials Chemistry and Physics).

VITA

Mr. Wathanyoo Owpradit was born in October 27th, 1983 in Bangkok, Thailand. He finished high school from Nawaminthrachinuthit Bodindecha school, Bangkok and received bachelor's degree in Science from the department of Chemical Technology, Faculty of Science, Chulalongkorn University, Bangkok, Thailand in 2006.